Design of an Unloader for Rotary Compressors

by

Danielle C. Tarraf

B.E., Mechanical Engineering
American University of Beirut (1996)

Submitted to the Department of Mechanical Engineering
in Partial Fulfillment of the Requirements for the Degree of
Master of Science in Mechanical Engineering

at the

Massachusetts Institute of Technology

June 1998

Signature of Author. . . . . .
Department of Mechanical Engineering
May 8, 1998

Certified by . . . . . .
Joseph L. Smith, Jr.
Collins Professor of Mechanical Engineering
Thesis Supervisor

Accepted by . . . . . .
Ain A. Sonin
Chairman, Department Committee on Graduate Students

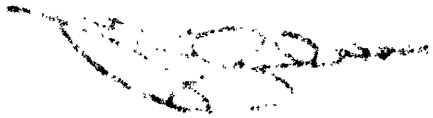

Design of an Unloader for Rotary Compressors

by

Danielle C. Tarraf

Submitted to the Department of Mechanical Engineering
on May 8, 1998 in partial fulfillment of the requirements
for the Degree of Master of Science in
Mechanical Engineering

Abstract

The capacity of rolling piston type rotary compressors is typically varied by using variable speed motor drives. That entails the use of high cost electronics. This study explores an alternative means of achieving variable capacity while keeping motor speed constant, by lifting the vane intermittently. The new technique should deliver comparable system performance and efficiency at lower initial costs in order to be competitive.

The thesis starts by analyzing the kinematics and dynamics of the vane motion using simplified working models of the system. Also, the interaction between the vane and the rolling piston is modeled, with focus on possible impact between the moving parts.

Next, the functional requirements for a vane lifting mechanism are set. The details of the design are worked out, and a complete set of engineering drawings is fully developed. A prototype of the mechanism was constructed; a brief description of the process is given.

The last part of the thesis presents the experimental work done to prove the success of the concept, to assess the mechanism, and to determine optimal operation modes. The prototype is shown to fulfill its goal of varying system capacity. The weaknesses of the design are pointed out. Some effort is made to single out the parameters that set optimal cycling times.

The main findings of the experiments are presented in a brief conclusion. Recommendations are made for second generation mechanism designs and for developing criteria for cycle time optimization.

Thesis Supervisor: Prof. Joseph L. Smith, Jr.
Title: Collins Professor of Mechanical Engineering

Acknowledgments

No matter how busy he was, my advisor, Prof. Joseph L. Smith, always made himself available to answer my frequent questions. He also made sure I got back on the right track on the numerous occasions that I wandered away. I thank him for his guidance and his patience.

My research experience was enriched by my frequent interaction with collaborating faculty members and researchers: Prof. Gerald Wilson, who gave me the opportunity to work on this project. His unique questions taught me to look at a given situation from a different perspective. Dr. Steve Umans and Prof. Peter Griffith offered many constructive comments and suggestions.

The hands-on part of the project would have been longer and more tedious without the help I got. Mike Demaree was my guide around unfamiliar shop territory. He made the various prototype parts and was always willing to lend a helping hand. David Otten was a tremendous help with instrumentation and data acquisition systems.

Doris Elsemiller gave a lot of help and advice. She added a bit of sunshine to the Cryogenics Lab.

I thank Carrier Corp. for financially supporting this project.

Finally, I wouldn't have had the courage to come to MIT and to do this work without my family's support. I am lovingly indebted to my parents and my brothers.

Table of Contents

Abstract **3**

Acknowledgements **5**

Table of Contents **6**

List of Figures **9**

List of Tables **12**

Nomenclature **13**

Introduction **19**

1.1 Basic Operation of a Rotary Compressor 20

1.2 The Need for Variable Capacity 21

1.3 Variable Capacity: Typical Methods 21

1.4 Variable Capacity: The New Concept 22

1.5 Overview of this Study 23

Analysis **25**

2.1 Motivation for the Analysis 25

2.2 The Carrier EDB240 Compressor 26

2.3 Kinematic Analysis 28

2.3.1 Model and Equations 28

2.3.2 Numerical Simulation 31

2.4 Dynamic Analysis 33

2.4.1 Model and Equations 33

2.4.2 Model for the Compression Process 46

2.4.3 Equations of Motion 50

2.4.4 Numerical Simulation of Vane Dynamics 51

2.5 Stress Analysis 55

2.5.1 Theory and Formulas 55

2.5.2 Numerical Simulation 56
2.6 Impact Analysis 57
Mechanism Design and Construction 61
3.1 Functional Requirements of the Design 61
3.2 Details of the Design 63
3.3 Construction of a Prototype Mechanism 93
Prototype Testing 95
4.1 Purpose of the Experiments 95
4.2 Preliminary Testing of the Components 96
4.3 Compressor Test Stand Experiments 96
4.3.1 Experimental Setup 96
4.3.2 Experimental Procedure 98
4.3.3 First Set of Experimental Data 101
4.3.4 Modified Experimental Setup 103
4.3.5 Second Set of Experimental Data 105
4.3.6 Variable Capacity Tests 105
4.4 System Experiments 106
4.4.1 Experimental Setup 106
4.4.2 First Set of Experiments and Results 107
4.4.3 Second Set of Experiments and Results 109
4.4.4 Third Set of Experiments and Results 116
4.4.5 Fourth Set of Experiments and Results 123
4.4.6 Fifth Set of Experiments and Results 128
4.4.7 Sixth Set of Experiments and Results 132
4.5 Summary of Findings and Results 134
4.5.1 Mechanism Design 134
4.5.2 Operating Scheme 135

Conclusion **137**

5.1 Project Achievements 137

5.2 Recommendations 137

References **130**

Appendices **131**

List of Figures

1.1 Typical construction features of a hermetic rolling piston type rotary compressor..... 19

1.2 Schematic of the compression mechanism in a rolling piston type rotary compressor..... 20

1.3 A complete compression cycle undergone by a rolling piston type rotary compressor..... 21

2.1 Graphic explanation of compression chamber and rolling piston dimensions..... 26

2.2 Graphic explanation of vane dimensions..... 26

2.3 Contact geometry between vane and rolling piston..... 28

2.4 Kinematic model of vane and rolling piston as a Slider Crank mechanism..... 29

2.5 Vane displacement from top dead center as a function of crank angle..... 32

2.6 Vane velocity as a function of crank angle..... 32

2.7 Vane acceleration as a function of crank angle..... 33

2.8 Free body diagram of the vane neglecting friction..... 34

2.9 Geometry relevant to spring force analysis..... 35

2.10 Equivalent pressure forces..... 36

2.11 Vane dimensions relevant to the pressure distributions on vane face..... 37

2.12 Vane tip geometry..... 37

2.13 A linear pressure distribution..... 39

2.14 Schematic of integration along curved vane tip..... 41

2.15 Orientation of pressure forces on curved vane tip..... 42

2.16 Contact force and geometry..... 45

2.17 Moment arms of the contact force to pivot points A_1 and A_2..... 45

2.18 Geometry of the suction and compression chambers..... 47

2.19 Spring force and inertia force versus crank angle..... 52
2.20 Pressure in the compression chamber versus crank angle..... 53
2.21 Magnitude of the contact force versus crank angle..... 53
2.22 Net unbalanced force acting on the vane along the y-direction..... 54
2.23 Net moment about pivot points A_1 and A_2..... 55
2.24 Subsurface shear stress due to Hertzian contact..... 57

3.1 Preliminary design of the vane lifting mechanism..... 62
3.14 Contact force for limiting case when pressure above vane is suction pressure..... 67
3.2 Assembled mechanism..... 69
3.3 Assembled mechanism (scaled 75%)..... 71
3.4 Cover plate..... 73
3.5 Cylinder..... 75
3.6 Piston liner..... 77
3.7 Mounting base..... 79
3.8 Piston..... 81
3.9 Lifting stem..... 83
3.10 Vane modifications..... 85
3.11 Compressor modifications..... 87
3.12 Variable Capacity Compressor shown in normal operation mode..... 89
3.13 Variable Capacity Compressor shown in unloaded mode..... 91
3.15 Sectional view of the compression mechanism and bearings..... 93
3.16 Top view of pump and one bearing after addition of sealing cover plate..... 94

4.1 Schematic diagram of the compressor test stand..... 97
4.2 Schematic diagram of the compressor test stand after modifications..... 104
4.3 Experimental system setup..... 106

4.4 Compressor suction and discharge pressure variation over two cycles (t_{cycle}=105s, R=1.18) 112

4.5 Compressor suction and discharge temperature variation over two cycles (t_{cycle}=105s, R=1.18) 113

4.6 Compressor instantaneous power consumption over two cycles (t_{cycle}=105s, R=1.18) 113

4.7 Compressor suction and discharge pressure variation over two cycles (t_{cycle}=59s, R=0.97) 114

4.8 Compressor suction and discharge temperature variation over two cycles (t_{cycle}=59s, R=0.97) 114

4.9 Compressor instantaneous power consumption over two cycles (t_{cycle}=59s, R=0.97) 115

4.10 Air temperatures at evaporator inlet and outlet (R=1, t_{cycle}=60s) 117

4.11 Air temperatures at evaporator inlet and outlet (R=1, t_{cycle}=40s) 117

4.12 Air temperatures at evaporator inlet and outlet (R=1, t_{cycle}=20s) 118

4.13 Air temperatures at evaporator inlet and outlet (R=1, t_{cycle}=10s) 118

4.14 Evaporator and condenser pressures (R=1, t_{cycle}=60s) 120

4.15 Evaporator and condenser pressures (R=1, t_{cycle}=40s) 120

4.16 Evaporator and condenser pressures (R=1, t_{cycle}=20s) 121

4.17 Evaporator and condenser pressures (R=1, t_{cycle}=10s) 121

4.18 Evaporator and condenser pressure variation over 40 seconds for 4 tests: Normal operation; R=1, t_{cycle}=10s; R=1, t_{cycle}=4s; R=0.33, t_{cycle}=8s 125

4.19 Compressor power consumption for various vane states 130

4.20 Voltage transient during motor start-up 133

4.21 Current transient during motor start-up 133

4.22 Instantaneous power transient during motor start-up 134

List of Tables

2.1 Numerical values of geometric parameters of the Carrier EDB240 compressor 27

2.2 CHEER, ARI and MAX. LOAD compressor testing conditions..... 52

4.1 Pre and post modification test results at ARI conditions..... 101

4.2 Modified compressor test results at ARI conditions, modified test stand used.. 105

4.3 Test data for variable capacity tests, 57s/48s and 29s/30s loaded and unloaded cycles..... 110

4.4 Characteristic cycle parameters for the two tests..... 111

4.5 Average evaporator and condenser pressures..... 123

4.6 Summary of system performance..... 126

4.7 Test characteristics..... 128

4.8 Test data and performance parameters..... 131

Nomenclature

$\mathbf{a(t)}$	Acceleration of the vane as a function of time [in./s^2]
$\mathbf{a(\theta)}$	Acceleration of the vane as a function of crank angle [in./s^2]
$\mathbf{A_d(\theta)}$	Instantaneous projected area of the discharge (compression) volume [in^2]
$\mathbf{A_s(\theta)}$	Instantaneous projected area of the suction volume [in^2]
$\mathbf{a_{mp}}$	Acceleration of the mechanism piston [in/s^2]
b	Half width of the rectangular area of elastic contact [in.]
B	Brinell hardness [psi]
c	Radial clearance between pump and compressor housing [in.]
$\mathbf{C_{cycle}}$	Average system capacity over one load/unload cycle [BTU/hr]
$\mathbf{C_l}$	Average system capacity during the loaded phase [BTU/hr]
COP	Coefficient of performance [ ]
$\mathbf{COP_n}$	System COP under normal operation [ ]
$\mathbf{C_p}$	Specific heat at constant pressure [BTU/lbm °F]
$\mathbf{d_{ch}}$	Inner diameter of cylindrical compressor chamber [in.]
$\mathbf{d_{rp}}$	Outer diameter of rolling piston [in.]
e	Rolling piston (shaft) eccentricity [in.]
EER	[BTU/W hr]
$\mathbf{E_i}$	Modulus of elasticity [psi]
$\mathbf{e_r}$	Coefficient of restitution [ ]
f	Frequency of rotation of the driving motor shaft [Hz]
F	Flowmeter frequency measurement [Hz]
F	Maximum contact force due to Hertzian contact [lbf]
$\mathbf{F_C}$	Contact force exerted by the rolling piston on the curved vane tip [lbf]
$\mathbf{F_I}$	Vane inertia force [lbf]

$\mathbf{F_{mp}}$	Differential pressure force on the mechanism piston [lbf]
$\mathbf{F_S}$	Spring force acting on the top edge of the vane [lbf]
$\mathbf{F_1}$	Force on top edge of the vane due to refrigerant at discharge conditions [lbf]
$\mathbf{F_2}$	Resultant pressure force on vane surface facing guide, discharge side [lbf]
$\mathbf{F_3}$	Resultant pressure force on vane surface facing guide, suction side [lbf]
$\mathbf{F_4}$	Resultant force on flat vane surface exposed to compression chamber [lbf]
$\mathbf{F_5}$	Resultant force on flat vane surface exposed to suction chamber [lbf]
$\mathbf{F_6}$	Resultant pressure force on curved vane tip in compression chamber [lbf]
$\mathbf{F_7}$	Resultant pressure force on curved vane tip in suction chamber [lbf]
G	Calibration factor
$\mathbf{h_{ch}}$	Depth of cylindrical compressor chamber [in.]
$\mathbf{h_n}$	Height of notch in vane [in.]
HRC	Rockwell Hardness [ ]
$\mathbf{h_1}$	Enthalpy of refrigerant at compressor suction [BTU/lbm]
$\mathbf{h_{2,S}}$	Enthalpy of refrigerant at compressor discharge, assuming isentropic compression [BTU/lbm]
$\mathbf{h_3}$	Enthalpy of refrigerant at condenser outlet [BTU/lbm]
$\mathbf{h_4}$	Enthalpy of refrigerant at evaporator inlet [BTU/lbm]
J	32.2 ft-lbm/lbf-ft^2
k	Spring constant [lb/in.]
K	Calibration factor
KE	Kinetic energy [lbf-in]
L	Distance between geometric center of rolling piston and center of curvature of vane tip. $L=r_v+r_{rp}$. [in.]
$\mathbf{l_o}$	Spring free length [in.]
$\mathbf{l_{min}}$	Minimum length of spring [in.]

$\mathbf{l_v}$	Length of vane [in.]
$\mathbf{l_{(\theta)}}$	Instantaneous spring length as a function of crank angle [in.]
$\mathbf{m}$	Mass flow rate of refrigerant [lbm/s]
$\mathbf{m_{air}}$	Mass flow rate of air across the evaporator [lbm/s]
$\mathbf{m_{mp}}$	Mass of the mechanism piston [lbm]
$\mathbf{m_v}$	Mass of vane [lb]
$\mathbf{n}$	Speed of rotation of the driving motor shaft [rpm]
$\mathbf{P}$	Pressure [psi]
$\mathbf{P_{avg,c}}$	Average compressor power consumption [kWatt]
$\mathbf{P_{avg,\ system}}$	Average system power consumption [kWatt]
$\mathbf{P_c}$	Condenser pressure [psig]
$\mathbf{P_{cycle}}$	Average compressor power consumption over one load/unload cycle [kWatt]
$\mathbf{P_d}$	Discharge pressure [psig]
$\mathbf{P_e}$	Evaporator pressure [psig]
$\mathbf{P_f}$	Fluid pressure at flowmeter (de-superheater loop experiments) [psig]
$\mathbf{P_{in}}$	Power input to compressor [kWatt]
$\mathbf{P_l}$	Average compressor power consumption during loaded phase [kWatt]
$\mathbf{P_s}$	Suction pressure [psig]
$\mathbf{P_{start}}$	Average compressor power consumption during motor start-up [kWatt]
$\mathbf{P_u}$, $\mathbf{P_U}$	Average compressor power consumption during unloaded phase [kWatt]
$\mathbf{P(\theta)}$	Instantaneous pressure in compression chamber as a function of crank angle [psig]
$\mathbf{q}$	Maximum Hertzian contact pressure [psi]
$\mathbf{Q_{cool}}$	Cooling load of the system (cooling rate) [BTU/hr]
$\mathbf{R}$	Ratio of loaded to unloaded cycle times (t_{on}/t_{off}) [ ]

$\mathbf{r_{ch}}$	Inner radius of cylindrical compressor chamber [in.]
$\mathbf{r_{rp}}$	Outer radius of rolling piston [in.]
$\mathbf{r_v}$	Radius of vane tip [in.]
s	Vane stroke [in.]
S	Motor slip (%) [ ]
t	Time [s]
$\mathbf{t_{cycle}}$	Cycle time (t_{on}+t_{off}) [s]
$\mathbf{t_{on}}$	Time duration of loaded phase [s]
$\mathbf{t_{off}}$	Time duration of unloaded phase [s]
$\mathbf{t_{off, critical}}$	Critical time duration of the unloaded phase beyond which it is energy efficient to shut motor off [s]
$\mathbf{t_p}$	Thickness of pump wall [in.]
$\mathbf{t_v}$	Thickness of vane [in.]
U	Internal strain energy [lbf-in.]
V	Volume [in^3]
v(t)	Velocity of the vane as a function of time [in./s]
v(θ)	Velocity of the vane as a function of crank angle [in./s]
$\mathbf{V_D}$	Displacement volume [in^3]
$\mathbf{V_{ms}}$	Volume of the mechanism lifting stem [in^3]
$\mathbf{v_{rp}}$	Velocity of the rolling piston along the line of impact [in./s]
$\mathbf{v_v}$	Velocity of the vane along the line of impact [in./s]
$\mathbf{V_v}$	Volume of the vane [in^3]
$\mathbf{v_{v/rp}}$	Vane velocity relative to the rolling piston along the line of impact [in./s]
$\mathbf{w_n}$	Average width of notch in vane [in.]
$\mathbf{w_v}$	Width of vane [in.]
x(t)	Displacement of the vane as a function of time [in.]

x(θ)	Displacement of the vane as a function of crank angle [in.]
x,y; X,Y	Rectangular coordinates
θ	Crank angle of the rolling piston (θ=0 <=> Top dead center) [rad]
ω	Angular speed of rotation of the rolling piston center about the center of the compression chamber. ω=dθ/dt. [rad/s]
ω_n	Natural Frequency of the vane/lifting stem/spring system [Hz]
δ	Maximum deflection due to Hertzian contact [in.]
ΔP	Pressure difference between the evaporator and condenser (P_c-P_e) [psig]
ρ,ψ	Polar coordinates
θ_o	Crank angle at which a sealed compression chamber forms [rad]
γ	Specific heat ratio (C_p/C_v) [ ]
η	Motor efficiency [ ]
σ_u	Ultimate tensile strength [psi]
τ_{max}	Maximum allowable shear stress [psi]
υ_i	Poisson's ratio [ ]
μ	Dynamic viscosity of refrigerant [micro poise]
ρ	Density of refrigerant [lbm/ft^3]
$\Delta T_{air, evap}$	Average temperature difference of air across the evaporator [°F]
ϕ	Connecting rod angle [rad]
%Cap	Percentage of normal operation capacity

Subscripts

ch	Cylindrical compressor chamber
d	Discharge
des	Desired operating state

i	Initial
f	Final
n	Vane notch
p	Pump
rev	Reversible process
rp	Rolling Piston
s	Suction
test	Actual testing conditions
v	Vane
1	State at compressor suction
2	State at compressor discharge
3	State at condenser outlet
4	State at evaporator inlet

Chapter 1

Introduction

The compressor examined in this study is the rolling piston type rotary compressor. The typical construction features of a hermetic type rotary compressor are shown in Figure 1.1.

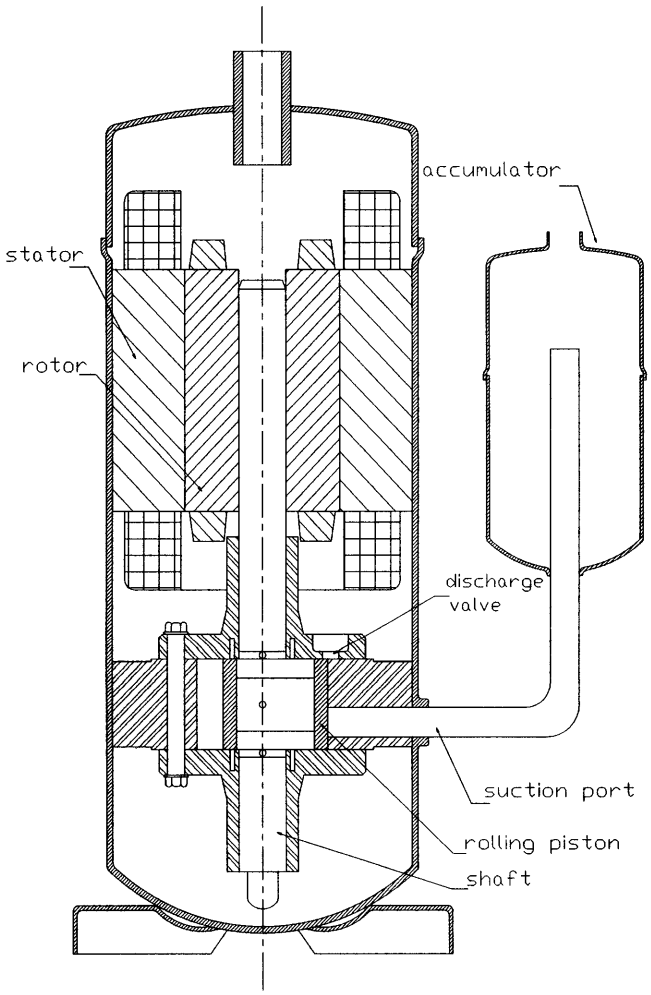

Figure 1.1: Typical construction features of a hermetic rolling piston type rotary compressor

1.1 Basic Operation of a Rotary Compressor

Some familiarity with the basic operation of this type of compressor is essential to the understanding of the work presented in this thesis. A simple schematic of the compression device in a rolling piston type rotary compressor is shown in Figure 1.2.

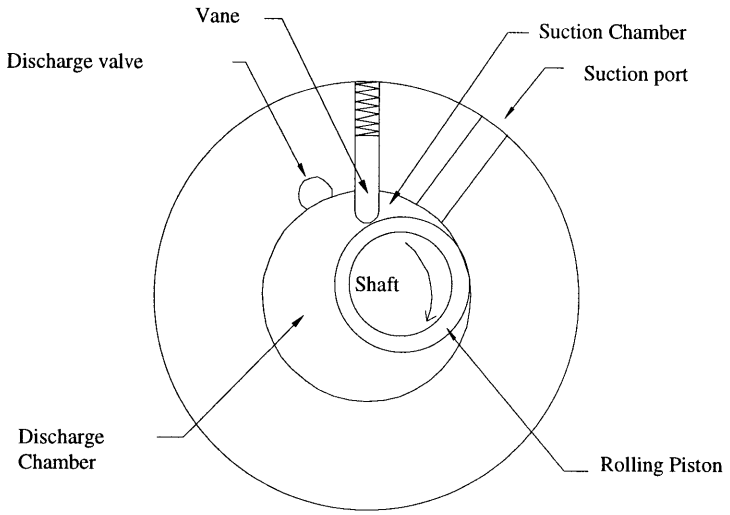

Figure 1.2: Schematic of the compression mechanism in a rolling piston type rotary compressor

The major components of the compression mechanism are: the cylindrical chamber, which includes the suction and discharge chambers. Within this chamber are the rolling piston, the eccentric shaft, and the reciprocating vane. The chamber is in contact with refrigerant at suction and discharge conditions via the inlet (suction) port and the pressure activated discharge valve, respectively.

The shaft is driven by the motor and rotates eccentrically about the center of the cylindrical chamber. The rolling piston rotates eccentrically with the shaft. It also slides relative to the shaft, thus rotating about its axis. As it rolls, the rolling piston contacts the wall of the cylindrical chamber thus forming a sealing point. During normal operation, the vane is mainly pressure loaded by the fluid at discharge pressure which acts on its top surface. It pushes against the rolling piston. Hence, a second sealing point is maintained under normal operation. The position of the rolling piston as the system goes through one complete revolution of the shaft is illustrated in Figure 1.3. The suction chamber (s) is always in contact with fluid at suction pressure via the inlet port. As soon as the piston / chamber wall sealing point crosses the inlet port, a closed discharge chamber (d) is formed. Fluid at suction conditions is trapped within it. Further rotation of the piston causes this discharge chamber to decrease in volume continuously, thus building up fluid pressure in the chamber. Once the chamber pressure exceeds the compressor discharge pressure, the pressure unbalance activates the discharge valve causing it to open, thus discharging the high pres-

sure fluid. When the piston reaches top dead center of its travel, the two sealing points merge into one. A single chamber exists at this instant, and the cycle repeats itself. The spring shown in Figure 1.2 is important during system start-up. That is, before the pressure on the discharge side builds up sufficiently to hold the vane down against the rolling piston. During normal operation, it contributes only mildly to the force acting on the top side of the vane, as will be shown in a later chapter.

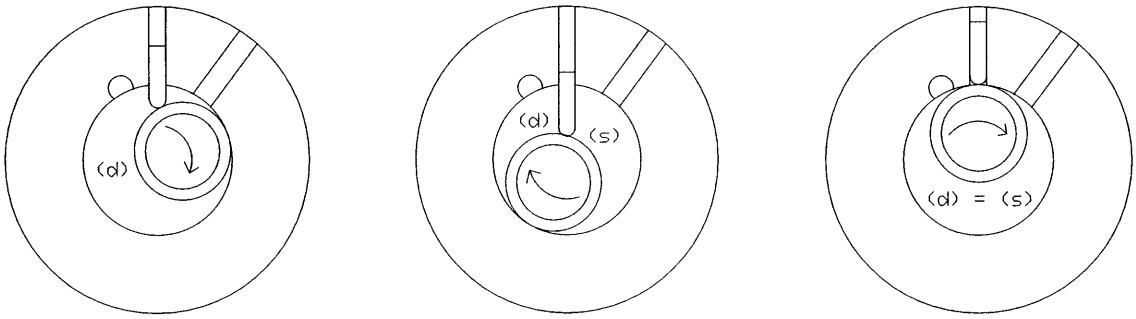

Figure 1.3: A complete compression cycle undergone by a rolling piston type rotary compressor.

1.2 The Need for Variable Capacity

Rolling piston type rotary compressors have a number of advantages, namely: High efficiency and reliability, low noise, relatively light weight and small size compared to other compressors having the same capacity [1]. Thus, this type of compressor is widely used in domestic air-conditioning and refrigeration units. Constantly changing environmental conditions impose varying loads and operating conditions on the system. Hence the need for variable capacity operation, to ensure the comfort of the user and especially as the requirements of energy saving and conservation of resources grow more stringent.

1.3 Variable Capacity: Typical Methods

Vapor compression systems are the most commonly employed systems in domestic refrigeration and air-conditioning applications. Variable capacity is generally achieved in these systems by varying the mass flow rate of refrigerant in the system. This, in turn, requires varying the average mass flow rate of fluid through the compressor driving the system. Typically, that is done by using a variable speed drive for the pump. As a result, the speed of rotation of the eccentric rolling piston changes. Hence, the frequency at which the compressor releases a charge of high pressure fluid changes, and thus the average mass flow rate of the fluid changes as well. Usually, some electronics are used to excite the motor driving the pump at various frequencies. The cost of the electronics can be quite high, at

least of the order of $100/kW. This contributes considerably to the initial cost of the system.

1.4 Variable Capacity: The New Concept

It seems advantageous to devise a method for varying the capacity of rolling piston type rotary compressors without having to resort to variable speed motors. This would eliminate the need for high cost electronics. In turn, that would lower the initial cost of the system. Obviously, the advantage is only real provided the new technique provides comparable performance during operation. Otherwise, the savings in initial costs would be lost in operating costs over the life of the compressor. This study attempts to explore and develop a new concept for varying compressor capacity. The new technique should perform as efficiently as the typical variable speed motor method used in order to be truly competitive.

Looking at reciprocating positive displacement compressors for ideas; The most common method for varying compressor capacity is by holding the suction valve open for a certain number of cycles. When the suction valve is open, the fluid in the compressor remains in contact with the suction side. Hence, as the piston travels, the fluid is pushed in and out of the compression space, without ever reaching a high enough pressure to activate the discharge valve. This decreases the average mass flow rate of refrigerant through the compressor, thus decreasing its capacity. By controlling the number of cycles during which the suction valve is held open and those in which it is closed, the capacity of the system can be controlled. If a similar idea were to be implemented to the rotary compressor at hand, the first obvious problem is that no suction valve exists. Instead, a suction (or inlet) port is used, and this connects the suction volume to fluid at suction conditions at all times. Further examination of the situation reveals that in a reciprocating compressor:
i. The suction chamber and the discharge chamber are identical.
ii. Holding the suction valve open opens up the otherwise sealed compression (discharge) chamber to suction. Hence, the upwards piston motion can no longer sufficiently pressurize the now large mass of fluid to a pressure higher than discharge.

Based on the above, two scenarios come to mind for the rotary compressor. The first is the addition of a suction valve, which would be kept open all through normal operation, and which will be closed intermittently during lower capacity operation. As a result, after an "initial" lost cycle, the discharge volume can no longer be replenished with fresh refrigerant at suction conditions. Hence, the volume ratio characteristic of the compressor will no longer suffice to raise the pressure of the small amount of remaining refrigerant. The other scenario consists of lifting the vane for some number of cycles, thus breaking the discharge chamber's seal. As a result, as the piston rotates, the fluid is in contact with suction and is just moved around in a space that is invariant in volume. Hence, its pressure does not rise significantly and the discharge valve remains closed during this time.

Although the above two scenarios are quite different in concept and implementation, they both achieve the same end result: varying the average mass flow rate of fluid through the compressor. A colleague, Dr. Greg Nellis [2], carried out a preliminary analysis to compare the relative advantages of the two methods. The results seemed quite decisive: Scenario two, the Vane Lifting Technique, seemed clearly superior in terms of higher efficiency, as reflected by the EER value. This conclusion holds assuming that:

i. The vane lifting mechanism can be properly controlled, that is, activated and deactivated at the optimum piston position.

ii. The vane lifting mechanism could operate at the required speed (achieve full reversal in ~16.$\overline{6}$ milliseconds, equivalent to the time required by the piston to undergo a complete revolution if motor slip is 0).

1.5 Overview of this Study

The purpose of this investigation is twofold. First, to investigate the feasibility of designing and constructing a satisfactory vane lifting mechanism. Second, to assess the technical soundness of the new concept. Stated simply, it aims at answering the following two questions: Can this idea be implemented to really achieve variable capacity? Can a suitable mechanism be devised and constructed?

The approach taken is largely practical and experimental. Analysis and modeling are kept to a strict minimum given the limits imposed by time constraints for the project.

In the next chapter, a simple model is developed to study the kinematics and dynamics of the vane motion. The interaction between the vane and the rolling piston is also studied and the resulting stresses are calculated. Finally, given the possibility of impact between the vane and the rolling piston, such a situation is modeled and analyzed. The resulting impact stresses are determined and the possibility of failure is evaluated.

Chapter 3 follows the evolution of the design from a concept to its final form. It includes detailed working drawings of the various components of the mechanism, as well as an assembly drawing. It also contains a description of the modifications made to the existing compressor to fit and mount the mechanism. The construction of a prototype mechanism is described in this chapter as well.

A series of tests were done on the modified compressor. These ranged from simple tests on a compressor test stand to testing the operation of the compressor in an actual system. This is the subject of Chapter 4. The experimental apparatus and test conditions are described, the test data is presented and then analyzed for the various tests.

The final chapter wraps up the topic: Based on the test results, the concept is evaluated, and so is the actual mechanism design. Recommendations are made for further work.

Chapter 2

Analysis

2.1 Motivation for the Analysis

As the name indicates, the vane lifting mechanism's function is to lift the vane. The mechanism should be able to provide enough force for that purpose. Also, it should be able to lift the vane fast enough so that it doesn't interfere with the motion of the rolling piston. To translate "enough force" and "fast enough" into quantitative terms, a knowledge of the dynamics and kinematics of the vane motion is required. Once the above are determined, another important question arises: How critical is proper timing to the success of the vane lifting mechanism? In other words, can we tolerate having the mechanism let go of the vane when the crank angle[1] is non zero? Answering that involves modeling of the resulting impact, determining the corresponding impact stresses, and evaluating their effect on the system components.

The motivation for this part of the thesis is to seek answers for all the above questions. This chapter contains a kinematic analysis, a dynamic analysis, a stress analysis and an impact analysis of the vane and rolling piston. The models used for the analysis are described in the coming sections. The simplifying assumptions are stated. The relevant equations are derived and then implemented. Although the theory and models hold for any size rolling piston type rotary compressor, the numerical values of various parameters, and consequently the dimensions of the mechanism depend on the size of the compressor. In this work, the focus is on the Carrier EDB240 rolling piston type rotary compressor. The numerical values of all parameters and the results given pertain to this particular compressor. Thus, section 2.2 overviews the main construction features and the relevant dimensions of the compression device in the EDB240 compressor.

A note on units: In spite of the author's preference for SI Units, the bulk of the work is done in US Customary Units. The equivalent SI measurements are provided in certain instances. That is due to the apparent preference of advisors and collaborators on this project for English units.

---

1. Crank angle is defined and illustrated in section 2.2.

2.2 The Carrier EDB240 Compressor

The Carrier EDB240 is a rolling piston type rotary compressor; It is used in domestic vapor compression air-conditioning systems of 24,000 BTU/hr capacity (2 Tons of refrigeration). The working fluid is Freon (Refrigerant R-22).

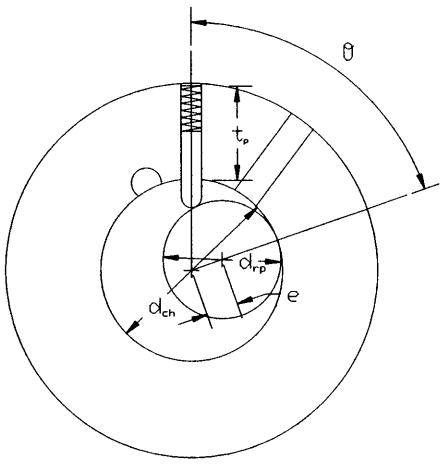

Figure 2.1: Graphic explanation of compression chamber and rolling piston dimensions

Figure 2.1 illustrates the nomenclature for the relevant geometry of the compression chamber and the rolling piston. d_{ch} is the diameter of the cylindrical compression chamber, and d_{rp} is the outside diameter of the rolling piston. r_{ch} and r_{rp} are the corresponding radii. The rolling piston is a hollow cylinder that mounts on a shaft. This detail is not shown in the figure because it is irrelevant in this context. e is the eccentricity of the shaft, and hence the rolling piston, to the axis of the compression chamber. h_{ch} is not shown in the figure. It represents the height of the compression chamber (perpendicular to the page). θ is the crank angle of the rolling piston: $\theta=0$ corresponds to the piston being at top dead center. t_p is the thickness of the pump wall in the vicinity of the vane (the thickness varies slightly at some other locations due to minor details).

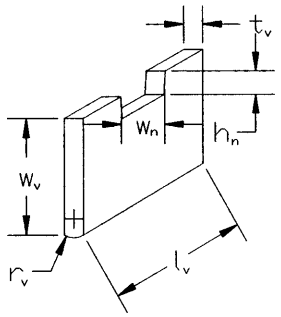

Figure 2.2: Graphic explanation of vane dimensions

Figure 2.2 shows the vane and the nomenclature of the relevant vane dimensions. The figure is self explanatory. The notch on the top edge of the vane seats the loading spring. Note that w_n represents the average width (the notch is tapered). The relevant dimensions of the spring are its original length, l_o, and its minimum length, l_{min}. The spring constant is denoted by k.

A note about materials: The vane is made of M2 tool steel, through hardened to Rockwell hardness 60C - 65 C. The rolling piston is made of gray cast iron, through hardened to 45C - 55C.

The numerical values of all relevant dimensions are listed for convenient reference in Table 2.1 below. The compressor was designed using metric units, hence the values of some parameters are taken off company production drawings in millimeters and then converted to inches for use in this work.

Table 2.1: Numerical values of geometric parameters of the Carrier EDB240 compressor

Parameter	**Measurement (SI units)**	**Measurement (US Customary Units)**
d_{ch}	59.004 mm	2.323 in.
d_{rp}	48.889 mm	1.925 in.
e	5.048 mm	0.199 in.
h_{ch}	38.993 mm	1.535 in.
h_n	-	0.119 in.
k	-	8.29 lb/in.
l_o	36.000 mm	1.417 in.
l_{min}	-	0.56 in.
l_v	38.976 mm	1.534 in.
m_v	-	0.083 lb
r_{ch}	-	1.162 in.
r_{rp}	-	0.963 in.
r_v	4.500 mm	0.177 in.

Parameter	Measurement (SI units)	Measurement (US Customary Units)
t_p	-	1.580 in.
t_v	4.647 mm	0.183 in.
w_n	-	0.375 in.
w_v	28.300 mm	1.114 in.

2.3 Kinematic Analysis

2.3.1 Model and Equations

The motion of the vane is analyzed in this section. Equations for the displacement, velocity and acceleration of the vane are developed, both as functions of crank angle and of time (with a suitably defined time origin). The analysis is purely geometric, based on the assumption that the vane remains in contact with the rolling piston at all time. This assumption is necessarily true if there is no leakage. The only exception is during the first few cycles after initial start-up, when the vane may bounce on the rolling piston.

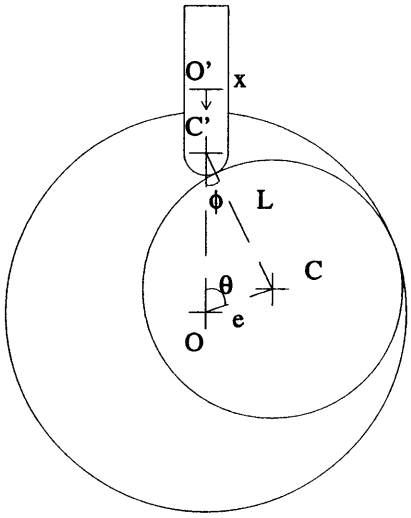

Figure 2.3: Contact geometry between vane and rolling piston

A simple two-dimensional diagram of the contact geometry between the vane and the rolling piston is presented in Figure 2.3. O is the geometric center of the cylindrical compres-

sion chamber. C is the center of the rolling piston, and C' is the center of curvature of the vane tip. Define a coordinate axis, x, which tracks point C' as the vane moves. The origin of this axis, O', corresponds to the location of point C' when the vane is at top dead center of its travel. Thus, x represents the displacement of the vane from top dead center. A is the point of contact of the rolling piston and vane. A travels back and forth along the vane tip. The crank angle θ, defined in the previous section, is the clockwise angle that OC makes with OC'. Let ϕ be the angle between C'O and C'C. ϕ will be referred to as the connecting rod angle, for reasons that will become clear as we proceed. The eccentricity, e, is shown, as well as a new parameter L. L is the distance between C' and C. A simplifying assumption is made: no deformation occurs at either vane or rolling piston surfaces. That is, the contact remains a line contact, and hence distance L is constant, equal to the sum of the radii of curvature of the two contacting surfaces.

The rolling piston is driven by the motor shaft. The shaft is cylindrical and rotates off-center. The axis of rotation of the shaft is parallel to its axis of symmetry and passes through point O. Hence, point C follows a circular path centered at O. The rolling piston may also slide circumferentially around the shaft. The motion is a rotation about C, and hence does not affect the location of this point. Therefore, this motion will not be considered in the analysis because it is irrelevant.

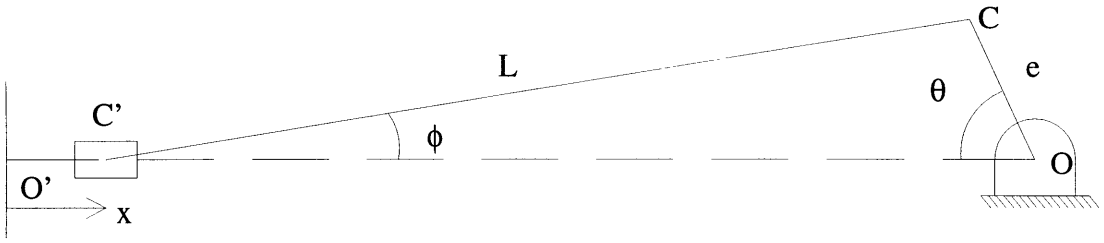

Figure 2.4: Kinematic model of vane and rolling piston as a Slider Crank mechanism.

Assume that the rolling piston orbits in the clockwise sense in Figure 2.3. The system consisting of the vane and the rolling piston can be modeled as a Slider Crank mechanism, as shown in Figure 2.4. C'C and OC are analogous to the connecting rod and the crank, respectively, of a slider crank mechanism. Hence, the names of the corresponding angles, ϕ and θ. Distance OO' ($\overline{OO'}$) is fixed. When the vane is at top dead center, both angles θ and ϕ are 0. Hence;

$$\overline{OO'} = e + L \tag{2.1}$$

When the vane is at any other position,

$$\overline{OO'} = x + L\cos\phi + e\cos\theta \tag{2.2}$$

Equating the right hand sides of equations 2.1 and 2.2 and rearranging, we get:

$$x = e(1 - \cos\theta) + L(1 - \cos\phi) \tag{2.3}$$

Sine Law applied to triangle OCC' gives:

$$\sin\phi = \frac{e}{L}\sin\theta \tag{2.4}$$

Hence:

$$\cos\phi = \sqrt{1 - (\sin\phi)^2} = \sqrt{1 - \left(\frac{e}{L}\sin\theta\right)^2} \tag{2.5}$$

Replacing the value of $\cos\phi$ from equation 2.5 in equation 2.3, we get an expression for vane travel from top dead center as a function of crank angle.

$$x_{(\theta)} = e + L - e\cos\theta - \sqrt{L^2 - (e\sin\theta)^2} \tag{2.6}$$

The velocity and acceleration of the vane as a function of crank angle are the first and second time derivative, respectively, of the above expression. Using the chain rule of differentiation:

$$v_{(\theta)} = \frac{dx_{(\theta)}}{dt} = \frac{dx_{(\theta)}}{d\theta} \cdot \frac{d\theta}{dt} \tag{2.7}$$

$$a = \frac{d^2x_{(\theta)}}{dt^2} = \frac{d}{dt}\left[\frac{dx_{(\theta)}}{d\theta} \cdot \frac{d\theta}{dt}\right] = \frac{d^2x_{(\theta)}}{d\theta^2} \cdot \left(\frac{d\theta}{dt}\right)^2 + \frac{d^2\theta}{dt^2} \cdot \frac{dx_{(\theta)}}{d\theta} \tag{2.8}$$

$d\theta/dt$ is the angular speed of rotation (ω) of point C about point O. ω is set by the rotational speed of the motor shaft, and is constant for a constant speed drive (which is the case for the EDB240 compressor). Thus, $\frac{d^2\theta}{dt^2} = \frac{d\omega}{dt} = 0$, and the second part of the right hand expression in equation 2.8 goes to zero. Equations 2.7 and 2.8 reduce to:

$$v_{(\theta)} = \omega \cdot \frac{dx_{(\theta)}}{d\theta} \tag{2.9}$$

$$a_{(\theta)} = \omega^2 \cdot \frac{d^2x_{(\theta)}}{d\theta^2} \tag{2.10}$$

Carrying out the differentiations, we get the expressions for vane speed and acceleration as a function of the crank angle of the rolling piston:

$$v_{(\theta)} = e\omega \cdot \sin\theta + \frac{e^2\omega \cdot \sin 2\theta}{2\sqrt{L^2 - (e\sin\theta)^2}} \tag{2.11}$$

$$a_{(\theta)} = e\omega^2 \cdot \cos\theta + \frac{e^2\omega^2 \cdot \cos 2\theta}{\sqrt{L^2 - (e\sin\theta)^2}} + \frac{e^4\omega^2 \cdot (\sin 2\theta)^2}{4[L^2 - (e\sin\theta)^2]^{3/2}} \tag{2.12}$$

Starting from the definition of $\omega = \frac{d\theta}{dt}$. Integrate to get an equation for the crank angle as a function of time:

$$\theta_{(t)} = \int_0^t \omega dt + \theta_o \tag{2.13}$$

Taking the origin of the time axis to be when the vane is at top dead center. From geometry, the corresponding angle θ, θ_o, is zero. Replacing θ by ωt in equations 2.6, 2.11 and 2.12. We get expressions for the displacement, velocity and acceleration of the vane as a function of time.

$$x_{(t)} = e + L - e \cdot \cos\omega t - \sqrt{L^2 - (e \cdot \sin\omega t)^2} \tag{2.14}$$

$$v_{(t)} = e\omega \cdot \sin\omega t + \frac{e^2\omega \cdot \sin 2\omega t}{2\sqrt{L^2 - (e \cdot \sin\omega t)^2}} \tag{2.15}$$

$$a_{(t)} = e\omega^2 \cdot \cos\omega t + \frac{e^2\omega^2 \cdot \cos 2\omega t}{\sqrt{L^2 - (e \cdot \sin\omega t)^2}} + \frac{e^4\omega^2 \cdot (\sin 2\omega t)^2}{4[L^2 - (e \cdot \sin\omega t)^2]^{3/2}} \tag{2.16}$$

Finally, the stroke of the vane, s, is by definition the total distance covered by the vane as it travels between top and bottom dead centers. When the vane is at bottom dead center, the distance $\overline{OO'}$ is:

$$\overline{OO'} = (L-e)+s \tag{2.17}$$

Equating the right hand sides of equations 2.1 and 2.17, we get that the stroke $s = 2e$.

Let the frequency of rotation of the motor shaft be f. The corresponding angular speed of rotation of the rolling piston about center O is:

$$\omega = 2\pi f \tag{2.18}$$

2.3.2 Numerical Simulation

The Carrier EDB240 compressor is driven by a single phase induction motor. If motor slip is zero, it drives the shaft at a rotational speed n=3600 rpm. In practice, motor slip (S) at full load is around 1.5%. Due to this, the rotational speed of the motor drops to about 3546 rpm.

For the purpose of the simulation, the assumption is that S=0. Hence, n=3600 rpm equivalent to a frequency of rotation f of 60 Hz. Thus, ω=377 rad/s. The equations of motion were plotted versus crank angle using Matlab. The resulting graphs are shown in Figures 2.5, 2.6 and 2.7.

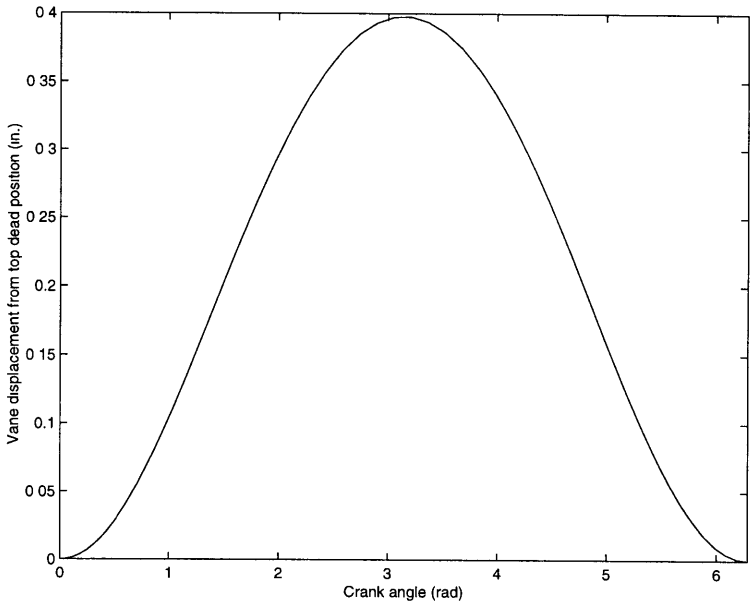

Figure 2.5: Vane displacement from top dead center as a function of crank angle

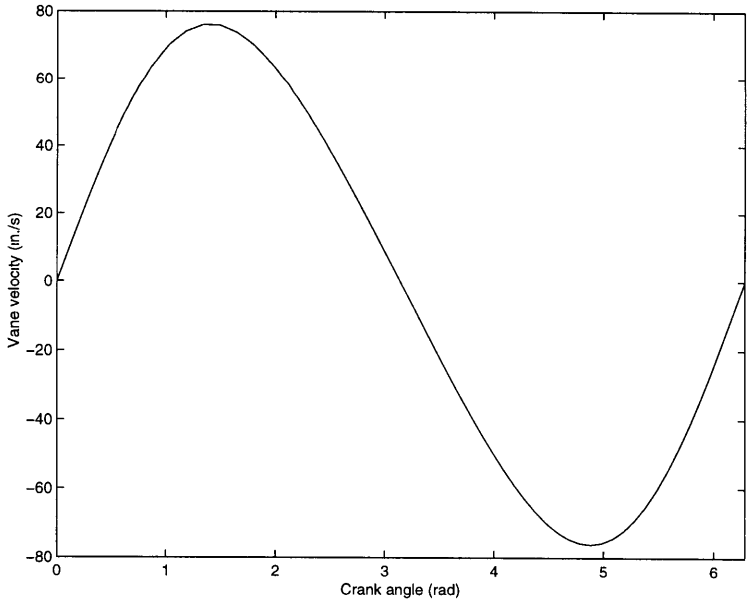

Figure 2.6: Vane velocity as a function of crank angle

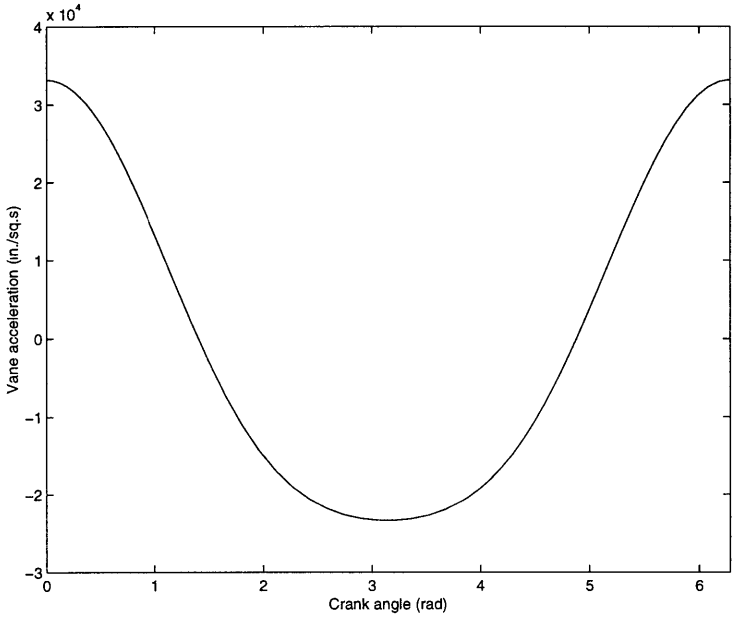

Figure 2.7: Vane acceleration as a function of crank angle

The maximum displacement is found to be 0.398 in., as expected (twice the eccentricity). Negative velocity corresponds to the vane being in the upwards stroke, moving towards top dead center. Negative acceleration signifies either a decceleration (between $\theta=\pi/2$ and $\theta=\pi$)or an acceleration in the negative x direction (between $\theta=\pi$ and $\theta=3\pi/2$).

The maximum speed at which the vane moves is found to be 76.16 in./s. The maximum acceleration/decceleration the vane encounters during its travel is 33,250 in./s^2.

2.4 Dynamic Analysis

This section presents a very simple dynamic model of the vane. The forces considered in the analysis are the spring force and the various contact and pressure forces. Frictional effects are completely neglected. The assumption is that all moving surfaces are adequately lubricated. (Namely the contact surface between the vane tip and the rolling piston, and the sliding surface between the faces of the vane and the vane guide). Hence, the resulting friction coefficients should be small and the corresponding frictional forces minimal in effect.

2.4.1 Model and Equations

A free body diagram of the vane (neglecting friction) is shown in Figure 2.8. F_s is the spring force. F_1 is the resultant force due to the refrigerant at discharge pressure acting on

the top edge of the vane. F_c is the contact force exerted by the rolling piston on the curved vane tip at the line of contact. The direction and point of application of F_c vary continuously throughout a cycle. F_5 is the resultant load on the flat section of the vane surface exposed to refrigerant in the suction chamber. F_4 is the resultant load on the flat surface due to refrigerant in the compression chamber. The pressure in this chamber cyclically varies between suction and discharge. The corresponding resultant forces on the curved vane tip due to contact with fluid at same conditions are F_7 and F_6 respectively. The pressure distribution of the fluid within the small clearance space between the vane and its guide on either side of the vane is assumed to be linear. The resultant pressure forces are denoted by F_2 and F_3 as shown. The inertia force is not shown in Figure 2.8 but will be considered in the analysis of course.

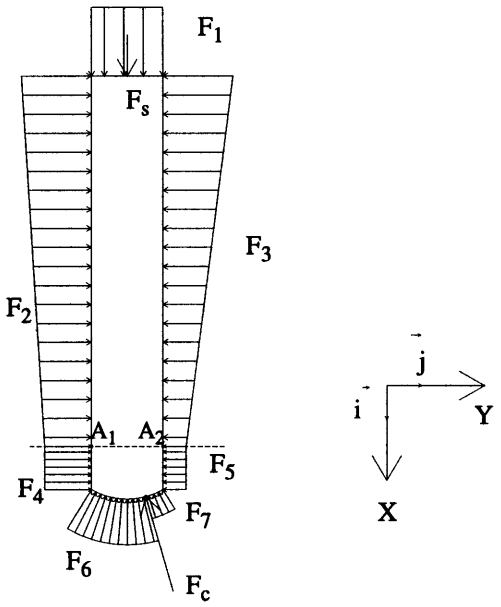

Figure 2.8: Free body diagram of the vane neglecting friction

Call the point of contact between the vane and the rolling piston point A. Consider an imaginary line that connects the edges of the vane guides. Let the intersection of this imaginary line with the vane be points A_1 and A_2 on the discharge and suction sides, respectively. The location of these three points varies with crank angle.

The moments caused by all the forces about points A_1 and A_2 need to be determined. The sign convention adopted is that clockwise moments and counterclockwise moments are considered positive about points A_1 and A_2 respectively. The purpose of these moment calculations and the choice of sign convention is not immediately obvious, and will be explained in detail in the following section.

Spring Force

The spring rests in the vane notch and pushes against the compressor housing. The clearance c between the outer edge of the pump and the housing is very small, of the order of a few thousands of an inch. Hence, it will be neglected.

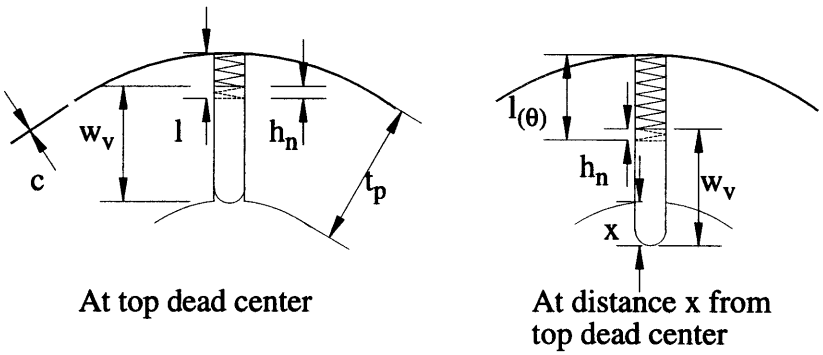

Figure 2.9: Geometry relevant to spring force analysis

When the vane is at top dead center, from geometry as shown in Figure 2.9:

$$t_p = l_{(0)} + w_v - h_n \tag{2.19}$$

$l_{(0)}$ denotes the length of the spring when the vane is at top dead center. When the vane moves a distance x from top dead center, the spring correspondingly elongates by the same distance x.

$$t_p = l_{(\theta)} + (w_v - x_{(\theta)}) - h_n \tag{2.20}$$

Hence, the instantaneous spring length as a function of crank angle is:

$$l_{(\theta)} = t_p + h_n - w_v + x_{(\theta)} \tag{2.21}$$

The resulting instantaneous spring force is:

$$F_{S(\theta)} = k \cdot \Delta l_{(\theta)} = k \cdot (l_o - l_{(\theta)}) \tag{2.22}$$

Replacing equation 2.6 for $x_{(\theta)}$ in equation 2.21 and then equation 2.21 for $l_{(\theta)}$ in equation 2.22, we get an expression for the magnitude of the spring force on the vane as a function of crank angle.

$$F_{S(\theta)} = k \cdot [l_o - t_p - h_n + w_v - e - L + e\cos\theta + \sqrt{L^2 - (e\sin\theta)^2}] \tag{2.23}$$

The spring is always in compression. Hence, the resulting spring force can be represented vectorially as:

$$\vec{F}_{S(\theta)} = F_{S(\theta)} \cdot \vec{i} \tag{2.24}$$

The moment caused by the spring force about points A1 and A2 is always positive for both

cases (due to the sign convention adopted). It is given by:

$$\overline{M}_{S,\,A_1(\theta)} = \overline{M}_{S,\,A_2(\theta)} = F_{S(\theta)} \cdot \frac{t_v}{2} \tag{2.25}$$

Pressure Forces

The vane is in contact with fluid at all points on its surface except for points along the line of contact with the rolling piston. Boundary lubrication at that location allows for some metal to metal contact. Hence, the vane is subjected to pressure forces on all its surfaces. The pressure forces acting on its sides are not shown in Figure 2.8 (If they were, they would be perpendicular to the plane of the diagram). The reason being that they should be equal and opposite due to similar conditions, and thus would balance out. All other pressure distributions acting on the vane surfaces are shown in Figure 2.8. The task undertaken in this section is to reduce these pressure distributions into equivalent point forces, denoted by F_i, i going from 1 to 7, with suitably determined points of application. The resulting pressure force diagram is shown in Figure 2.10

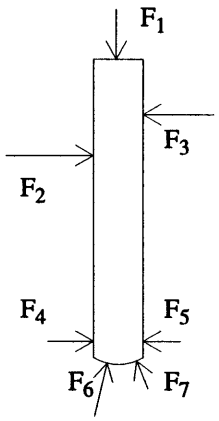

Figure 2.10: Equivalent pressure forces

Force F_1 is the resultant of a uniformly distributed load on the top edge of the vane. Hence, it acts at the midpoint of the edge (It has the same point of application as the spring force). In magnitude, it is equal to the product of the fluid pressure and the area subjected to it. Hence:

$$\vec{F_1} = P_d \cdot (l_v \cdot t_v) \cdot \hat{i} \tag{2.26}$$

The moment caused by this force about both points A1 and A2 is always positive and is given by:

$$\overline{M}_{1,\,A_1(\theta)} = \overline{M}_{1,\,A_2(\theta)} = \frac{1}{2} P_d \cdot l_v \cdot t_v^2 \tag{2.27}$$

Determining equivalent forces F_2 through F_5 is a little bit trickier. That is mainly because the area upon which a given fluid pressure profile acts is a function of vane position with respect to its guide.

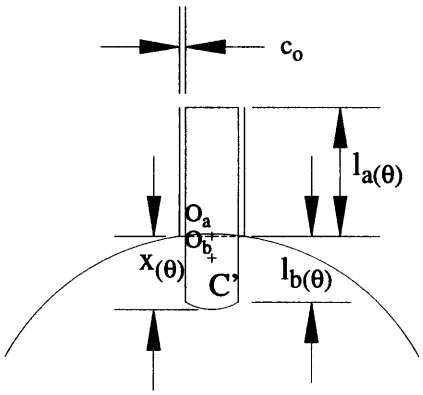

Figure 2.11: Vane dimensions relevant to the pressure distributions on vane face

Forces F_2 and F_3 are due to a linear distribution of pressure acting on an area $A_{a(\theta)}=l_{a(\theta)}.l_v$. Forces F_4 and F_5 are due to a uniform pressure distribution acting on area $A_{b(\theta)}=l_{b(\theta)}.l_v$. In Figure 2.11, the dotted straight line connects the two edges of the vane guide. Note that the clearance c_o between the vane and its guide is highly exaggerated in this diagram. Also, it is shown to be symmetric, which is generally not the case. O_b denotes the midpoint of this straight line. O_a is the midpoint of the dotted arc shown. This arc is the extension of the pump chamber wall circular profile. Thus, O_a also coincides with the location of the vane tip when the vane is at top dead center. In the analysis that follows, points O_a and O_b are assumed to coincide. This assumption should not introduce much error given that the vane thickness is much smaller than the radius of the cylindrical chamber. That is, $t_v<<r_{ch}$.

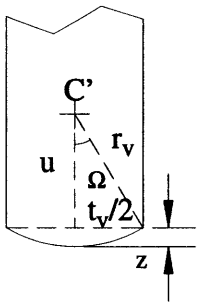

Figure 2.12: Vane tip geometry

Now refer to Figure 2.12 for a closer look at the vane tip geometry. Pythagora's Law gives that:

$$u = \sqrt{r_v^2 - \left(\frac{t_v}{2}\right)^2} \tag{2.28}$$

Hence,

$$z = r_v - u = r_v - \sqrt{r_v^2 - \left(\frac{t_v}{2}\right)^2} \tag{2.29}$$

and angle Ω:

$$\Omega = \text{asin}\left(\frac{t_v}{2r_v}\right) \tag{2.30}$$

From Figure 2.11, it is obvious that, with the assumption made regarding O_a and O_b:

$$l_{b(\theta)} = x_{(\theta)} - z; (x_{(\theta)} \geq z) \quad \text{and} \quad = 0; (x_{(\theta)} < z) \tag{2.31}$$

$$w_v = l_{a(\theta)} + l_{b(\theta)} + z \Rightarrow l_{a(\theta)} = w_v - z - l_{b(\theta)} \tag{2.32}$$

Replacing for x(θ) and z from equations 2.6 and 2.29 respectively, we get that:

$$l_{b(\theta)} = e + L - r_v + \sqrt{r_v^2 - \left(\frac{t_v}{2}\right)^2} - e\cos\theta - \sqrt{L^2 - (e\sin\theta)^2}; 0 \tag{2.33}$$

$$x_{(\theta)} \geq z; x_{(\theta)} < z$$

$$l_{a(\theta)} = w_v - e - L + e\cos\theta + \sqrt{L^2 - (e\sin\theta)^2} \tag{2.34}$$

Thus, equivalent pressure force F_5 acts at a distance 1/2 $l_{b(\theta)}$ from point A_2 (defined earlier) and is given by:

$$\vec{F}_{5(\theta)} = -P_s \cdot (l_{b(\theta)} \cdot l_v) \cdot \vec{j} \tag{2.35}$$

Its moment about points A_1 and A_2 is the same in magnitude, but varies from positive to negative respectively for the sign convention defined earlier:

$$\overline{M}_{5, A_1(\theta)} = -\overline{M}_{5, A_2(\theta)} = \frac{1}{2} P_s \cdot l_v \cdot l^2_{b(\theta)} \tag{2.36}$$

Following similar reasoning:

$$\vec{F}_{4(\theta)} = P_{(\theta)} \cdot l_v \cdot l_{b(\theta)} \cdot \vec{j} \tag{2.37}$$

$$\overline{M}_{4, A_1(\theta)} = -\overline{M}_{4, A_2(\theta)} = -\frac{1}{2} P_{(\theta)} l_v l^2_{b(\theta)} \tag{2.38}$$

$P_{(\theta)}$ is the pressure in the compression chamber. As mentioned previously, it varies during each cycle from suction to discharge pressure. The compression process is modeled, and an expression for $P_{(\theta)}$ is determined later in section 2.4.2.

The pressure distribution on either face of the vane within the vane guide is assumed to be linear. On the discharge side, it varies from P_d to $P_{(\theta)}$ over a length $l_{a(\theta)}$. On the suction side, it varies from P_d to P_s over the same length.

To avoid going over the same derivation twice, consider in general a linear pressure distribution acting on an area of length Δ and of unit width, as shown in Figure 2.13. f is a variable that represents distance from the origin O. Let the pressure at f=0 be P_i and at f=Δ be P_f.

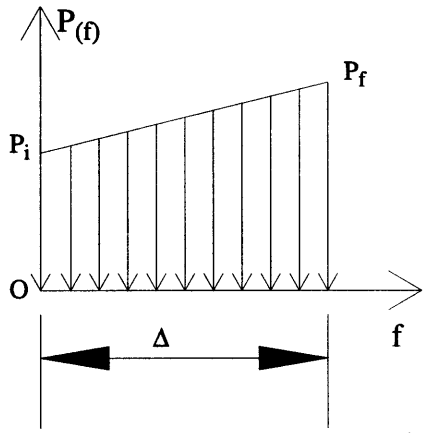

Figure 2.13: A linear pressure distribution.

The effect of this pressure distribution can be modeled by one equivalent force, F, applied at a specific distance δ to be determined. The pressure distribution can be expressed mathematically as:

$$P_{(f)} = \frac{P_f - P_i}{\Delta} \cdot f + P_i \tag{2.39}$$

The equivalent force per unit width is the infinitesimal sum of the elements of force acting on infinitesimally small areas.

$$F = \int_0^{\Delta} P_{(f)} df = \frac{P_f - P_i}{\Delta} \int_0^{\Delta} f df + P_i \int_0^{\Delta} df = \left(\frac{P_f - P_i}{\Delta}\right)\frac{\Delta^2}{2} + P_i \Delta$$

$$\therefore F = \frac{1}{2}(P_f + P_i)\Delta \tag{2.40}$$

This force should be applied at a distance δ from point O such that the moment caused by the linear pressure distribution and that by the equivalent force about point O are equal.

$$M = \int_0^{\Delta} P_{(f)} f df = F\delta \tag{2.41}$$

Thus,

$$\frac{P_f - P_i}{\Delta}\int_0^{\Delta} f df + P_i \int_0^{\Delta} f df = F\delta$$

$$\frac{1}{3}\left(\frac{P_f - P_i}{\Delta}\right)\Delta^3 + \frac{1}{2}P_i\Delta^2 = \frac{1}{2}(P_f + P_i)\Delta\delta$$

$$\therefore \delta = \frac{(2P_f + P_i)}{3(P_f + P_i)}\Delta \tag{2.42}$$

Applying the results given by equations 2.40 and 2.42 to determine forces $F_{2(\theta)}$ and $F_{3(\theta)}$ is simple. The corresponding variables P_i, P_f and Δ have to be identified and substituted for in each case. Let f=0 to correspond to the top edge of the vane. P_d corresponds to P_i and $l_{a(\theta)}$ to Δ for both pressure distributions. For the discharge side pressure distribution, $P_{(\theta)}$ corresponds to P_i while for the suction side pressure distribution, P_s corresponds to P_i. Substituting in the relevant equations, and keeping in mind that the equations were derived per unit width, we get:

$$\vec{F}_{2(\theta)} = \frac{1}{2} l_v (P_{(\theta)} + P_d) l_{a(\theta)} \cdot \hat{j} \tag{2.43}$$

$$\vec{F}_{3(\theta)} = -\frac{1}{2} l_v (P_s + P_d) l_{a(\theta)} \cdot \hat{j} \tag{2.44}$$

$$\delta_{2(\theta)} = \frac{(2P_{(\theta)} + P_d)}{3(P_{(\theta)} + P_d)} l_{a(\theta)} \tag{2.45}$$

$$\delta_{3(\theta)} = \frac{(2P_s + P_d)}{3(P_s + P_d)} l_{a(\theta)} \tag{2.46}$$

The moments caused by these forces about A_1 and A_2 are:

$$\overline{M}_{2,A_1(\theta)} = -\overline{M}_{2,A_2(\theta)} = \frac{1}{2} l_v (P_{(\theta)} + P_d) l_{a(\theta)} [l_{a(\theta)} - \delta_{2(\theta)}]$$

$$= \frac{1}{2} l_v (P_{(\theta)} + P_d) l^2_{a(\theta)} \left[\frac{P_{(\theta)} + 2P_d}{3(P_{(\theta)} + P_d)}\right]$$

$$= \frac{1}{6} l_v (P_{(\theta)} + 2P_d)[w_v - e - L + e\cos\theta + \sqrt{L^2 - (e\sin\theta)^2}]^2 \tag{2.47}$$

$$M_{3,A_1(\theta)} = M_{3,A_2(\theta)} = -\frac{1}{6} l_v (P_s + 2P_d)[w_v - e - L + e\cos\theta + \sqrt{L^2 - (e\sin\theta)^2}]^2 \quad (2.48)$$

The forces due to pressure on the curved edge of the vane, F_6 and F_7, can be determined by integrating the elemental pressure forces along the curved surface. The integration is done vectorially, to take into account that the direction of the infinitesimal force at any point changes so as to remain perpendicular to the surface. For that purpose, consider an infinitesimally thin surface strip that extends along the length of the vane and of width ds as shown in Figure 2.14. Define angle γ to be the counterclockwise angle that the perpendicular $\hat{n}$ to this area makes with the line of symmetry of the vane through point O'.

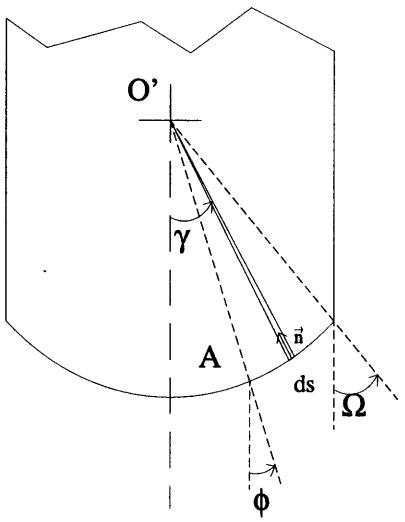

Figure 2.14: Schematic of integration along curved vane tip

The area of this strip, represented vectorially in terms of the inwards normal to the surface at that location, is:

$$\overrightarrow{dA} = l_v \cdot ds\hat{n}_{(\gamma)} = l_v \cdot ds[-\cos\gamma \cdot \hat{i} - \sin\gamma \cdot \hat{j}] \quad (2.49)$$

Correspondingly, the infinitesimal force due to pressure on that strip is:

$$\overrightarrow{dF}_{(\gamma)} = P \cdot \overrightarrow{dA}_{(\gamma)} \quad (2.50)$$

Thus, keeping in mind that $ds=r_v.d\theta$, the total pressure force along a section of the vane tip extending from $\gamma=\gamma_0$ to $\gamma=\gamma_f$ is:

$$\vec{F} = \int_{\gamma_o}^{\gamma_f} (P \cdot \overrightarrow{dA_{(\gamma)}}) = Pl_v \int_{\gamma}^{\gamma_f} [-\cos\gamma \cdot \vec{i} - \sin\gamma \cdot \vec{j}] r_v d\gamma$$

$$\vec{F} = Pl_v r_v [\sin\gamma_o - \sin\gamma_f]\vec{i} + Pl_v r_v [\cos\gamma_f - \cos\gamma_o]\vec{j} \qquad (2.51)$$

Equation 2.51 can be used to determine forces F_6 and F_7, by substituting the proper values for γ_o and γ_f. Adhering to the sign convention for γ: on the discharge side, γ_o=-Ω and γ_f=ϕ. On the suction side, γ_o=ϕ and γ_f=Ω. Hence,

$$\vec{F}_6 = -P_{(\theta)} l_v r_v (\sin\Omega + \sin\phi)\vec{i} + P_{(\theta)} l_v r_v (\cos\phi - \cos\Omega)\vec{j}$$

$$\vec{F}_{6(\theta)} = -P_{(\theta)} l_v r_v \left[\frac{t_v}{2r_v} + \frac{e}{L}\sin\theta\right]\vec{i} + P_{(\theta)} l_v r_v \left[\sqrt{1-\left(\frac{e}{L}\sin\theta\right)^2} - \sqrt{1-\left(\frac{t_v}{2r_v}\right)^2}\right]\vec{j} \qquad (2.52)$$

$$\vec{F}_7 = P_s l_v r_v (\sin\phi - \sin\Omega)\vec{i} + P_s l_v r_v (\cos\Omega - \cos\phi)\vec{j}$$

$$\vec{F}_{7(\theta)} = P_s l_v r_v \left[\frac{e}{L}\sin\theta - \frac{t_v}{2r_v}\right]\vec{i} + P_s l_v r_v \left[\sqrt{1-\left(\frac{t_v}{2r_v}\right)^2} - \sqrt{1-\left(\frac{e}{L}\sin\theta\right)^2}\right]\vec{j} \qquad (2.53)$$

Both forces F_6 and F_7 cause a non-zero moment about pivot points A_1 and A_2. The moment arms are hard to calculate explicitly as a function of the crank angle because of the complicated geometry. The point of application of force F_6 is along the curved edge of the vane, at an angle of $\frac{\phi+\Omega}{2}$, due to symmetry. Similarly, F_7 acts along the edge of the vane at an angle of $\frac{\phi-\Omega}{2}$, as shown in Figure 2.15.

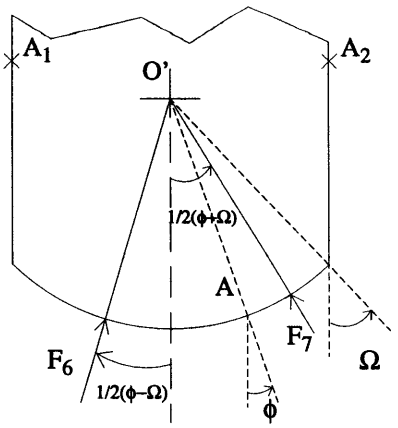

Figure 2.15 : Orientation of pressure forces on curved vane tip

Consider first force F_6. It can be decomposed into two components along the coordinate axis defined, F_{6x} and F_{6y}. The moment arm of F_{6y} about points A_1 and A_2 is the same, given by: $l_{b(\theta)} + \left[r_v \cos\left(\frac{\phi - \Omega}{2}\right) - u\right] = x_{(\theta)} + r_v\left[\cos\left(\frac{\phi - \Omega}{2}\right) - 1\right]$. The moment arm of F_{6x} about A_1 is: $\frac{t_v}{2} - r_v \sin\left(\frac{\phi - \Omega}{2}\right)$ and about A_2 is: $\frac{t_v}{2} + r_v \sin\left(\frac{\phi - \Omega}{2}\right)$. Hence, the moment of F_6 about points A_1 and A_2 is given by:

$$\overline{M}_{6,A_1} = -P_{(\theta)} l_v r_v \left[\frac{t_v}{2r_v} + \frac{e}{L}\sin\theta\right]\left[\frac{t_v}{2} - r_v \sin\left(\frac{\phi - \Omega}{2}\right)\right] -$$

$$P_{(\theta)} l_v r_v \left[\sqrt{1 - \left(\frac{e}{L}\sin\theta\right)^2} - \sqrt{1 - \left(\frac{t_v}{2r_v}\right)^2}\right]\left\{x_{(\theta)} + r_v\left[\cos\left(\frac{\phi - \Omega}{2}\right) - 1\right]\right\}$$

$$\overline{M}_{6,A_2} = -P_{(\theta)} l_v r_v \left[\frac{t_v}{2r_v} + \frac{e}{L}\sin\theta\right]\left[\frac{t_v}{2} + r_v \sin\left(\frac{\phi - \Omega}{2}\right)\right] +$$

$$P_{(\theta)} l_v r_v \left[\sqrt{1 - \left(\frac{e}{L}\sin\theta\right)^2} - \sqrt{1 - \left(\frac{t_v}{2r_v}\right)^2}\right]\left\{x_{(\theta)} + r_v\left[\cos\left(\frac{\phi - \Omega}{2}\right) - 1\right]\right\}$$

$$\overline{M}_{6,A_1} = -P_{(\theta)} l_v r_v \left\{\left[\frac{t_v}{2r_v} + \frac{e}{L}\sin\theta\right]\left[\frac{t_v}{2} - r_v \sin\left(\frac{\phi - \Omega}{2}\right)\right] + \left[\sqrt{1 - \left(\frac{e}{L}\sin\theta\right)^2} - \sqrt{1 - \left(\frac{t_v}{2r_v}\right)^2}\right]\left\{x_{(\theta)} + \left[r_v \cos\left(\frac{\phi - \Omega}{2}\right) - 1\right]\right\}\right\} \quad (2.54)$$

$$\overline{M}_{6,A_2} = -P_{(\theta)} l_v r_v \left\{\left[\frac{t_v}{2r_v} + \frac{e}{L}\sin\theta\right]\left[\frac{t_v}{2} + r_v \sin\left(\frac{\phi - \Omega}{2}\right)\right] - \left[\sqrt{1 - \left(\frac{e}{L}\sin\theta\right)^2} - \sqrt{1 - \left(\frac{t_v}{2r_v}\right)^2}\right]\left\{x_{(\theta)} + r_v\left[\cos\left(\frac{\phi - \Omega}{2}\right) - 1\right]\right\}\right\} \quad (2.55)$$

No effort will be made to analytically reduce the above equations to explicit functions of the crank angle θ. The variation of ϕ with θ will be simulated numerically and used in the equations in the next section.

Following a similar procedure, the moment of force F_7 can be calculated about points A_1 and A_2:

$$\overline{M}_{7,A_1} = P_s l_v r_v \left\{ -\left[\frac{e}{L}\sin\theta - \frac{t_v}{2r_v}\right]\left[\frac{t_v}{2} + r_v \sin\left(\frac{\phi+\Omega}{2}\right)\right] + \left[\sqrt{1-\left(\frac{t_v}{2r_v}\right)^2} - \sqrt{1-\left(\frac{e}{L}\sin\theta\right)^2}\right]\left[x_\theta + r_v\left(\cos\left(\frac{\phi+\Omega}{2}\right) - 1\right)\right]\right\} \tag{2.56}$$

$$\overline{M}_{7,A_2} = -P_s l_v r_v \left\{ \left[\frac{e}{L}\sin\theta - \frac{t_v}{2r_v}\right]\left[\frac{t_v}{2} - r_v \sin\left(\frac{\phi+\Omega}{2}\right)\right] + \left[\sqrt{1-\left(\frac{t_v}{2r_v}\right)^2} - \sqrt{1-\left(\frac{e}{L}\sin\theta\right)^2}\right]\left(x_{(\theta)} + r_v\cos\left(\frac{\phi+\Omega}{2}\right) - 1\right)\right\} \tag{2.57}$$

Inertia Force

The inertia of the vane may be represented as a force acting in the direction opposite to the acceleration of the vane, according to D'Alembert's principle. Thus,

$$\vec{F}_{I(\theta)} = -\frac{m}{J} A_{(\theta)} \hat{i} \tag{2.58}$$

J is required as a conversion factor in this equation because English units are used. $J = 32.2\frac{ft \cdot lbm}{lbf \cdot s^2} = 386.4\frac{in \cdot lbm}{lbf \cdot s^2}$.

The moment of the inertia force is either positive about both pivot points A_1 and A_2 or negative about both, depending on whether the vane is accelerating or deccelerating. It is given by:

$$M_{I,A_1(\theta)} = M_{I,A_2(\theta)} = -\frac{m}{J} \cdot \frac{t_v}{2} \cdot A_{(\theta)} \tag{2.59}$$

Contact Force

Let the magnitude of the contact force as a function of crank angle be $F_{C(\theta)}$. An expression for $F_{C(\theta)}$ cannot be written at this stage: The contact force varies such as to keep the forces acting on the vane balanced along the direction of motion as the vane moves. Based on the assumption of perfect line contact between the vane and rolling piston, the direction of the contact force is necessarily along the line of centers CC'. (Keep in mind that the friction forces are neglected).

The components of the contact force along the X and Y directions are, respectively:

$$\overline{F}_{C,x(\theta)} = -F_{C(\theta)} \cdot \cos\phi \tag{2.60}$$

$$\bar{F}_{C,y(\theta)} = -F_{C(\theta)} \cdot \sin\phi \tag{2.61}$$

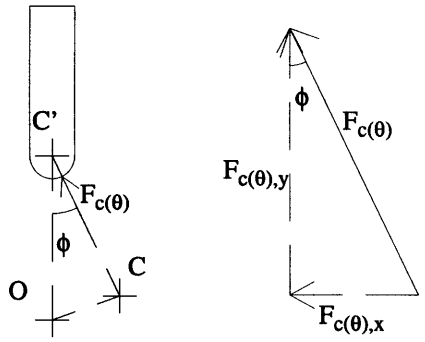

Figure 2.16: Contact force and geometry

Replacing cosϕ and sinϕ by their values from equations 2.5 and 2.4 respectively, we get the expression for the contact force:

$$\vec{F}_{C(\theta)} = \bar{F}_{C,x(\theta)} \cdot \hat{i} + \bar{F}_{C,y(\theta)} \cdot \hat{j}$$

$$\vec{F}_{C(\theta)} = -F_{C(\theta)} \cdot \cos\phi \cdot \hat{i} - F_{C(\theta)} \cdot \sin\phi \cdot \hat{j} \tag{2.62}$$

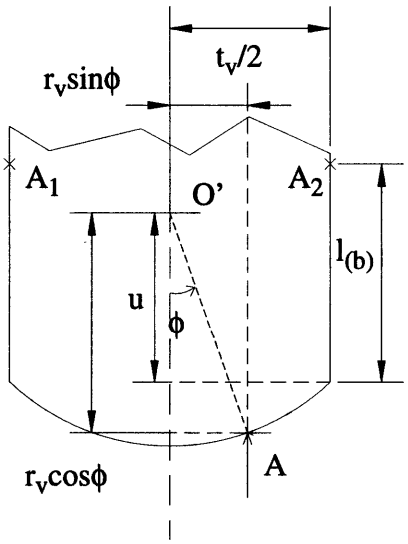

Figure 2.17: Moment arms of the contact force to pivot points A_1 and A_2

The relevant geometry is shown in Figure 2.17. The moment arm of $\vec{F}_{C,y(\theta)}$ about A_1 or A_2 is $r_v\cos\phi - u + l_{b(\theta)}$. The moment arm of $\vec{F}_{C,x(\theta)}$ about A_1 is $\frac{t_v}{2} + r_v\sin\phi$ and about

A_2 is $\frac{t_v}{2} - r_v \sin\phi$. Hence, the moment caused by the contact force about A_1 is:

$$\overline{M}_{C,A_1(\theta)_1} = -F_{C(\theta)} \cdot \cos\phi \cdot \left(\frac{t_v}{2} + r_v \sin\phi\right) + F_{C(\theta)} \cdot \sin\phi \cdot (r_v \cos\phi - u + l_{b(\theta)})$$

$$= F_{C(\theta)}\left[-\frac{t_v}{2}\cos\phi + (l_{b(\theta)} - u)\sin\phi\right]$$

using equations 2.28 and 2.41: $= F_{C(\theta)}\left[-\frac{t_v}{2}\cos\phi + (x_{(\theta)} - r_v)\sin\phi\right]$

The moment caused by the contact force about A_2 is:

$$\overline{M}_{C,A_2(\theta)} = -F_{C(\theta)} \cdot \cos\phi \cdot \left(\frac{t_v}{2} - r_v \sin\phi\right) - F_{C(\theta)} \cdot \sin\phi \cdot (r_v \cos\phi - u + l_{b(\theta)})$$

$$= F_{C(\theta)}\left[-\frac{t_v}{2}\cos\phi + (u - l_{b(\theta)})\sin\phi\right]$$

$$\overline{M}_{C,A_1} = F_{C(\theta)}\left[-\frac{t_v}{2}\sqrt{1 - \left(\frac{e}{L}\sin\theta\right)^2} + (x_{(\theta)} - r_v)\frac{e}{L}\sin\theta\right] \tag{2.63}$$

$$\overline{M}_{C,A_2(\theta)} = F_{C(\theta)}\left[-\frac{t_v}{2}\sqrt{1 - \left(\frac{e}{L}\sin\theta\right)^2} + (r_v - x_{(\theta)})\frac{e}{L}\sin\theta\right] \tag{2.64}$$

2.4.2 Model for the Compression Process

The compression chamber is that sealed chamber formed between the vane, the rolling piston, and the inner wall of the cylindrical chamber which is in contact with the discharge valve. The compression chamber starts to exist in a cycle as soon as the rolling piston passes over the suction port. Thereafter, as the crank angle increases, the volume of the compression chamber decreases, thus pressurizing the fluid.

Analysis of the system dynamics requires knowledge of the variation in pressure with crank angle within the compression space. That, in turn, requires knowledge about the instantaneous volume of the compression space, at any given crank angle. Hence, that will be the next task.

Define as the suction volume that volume within the cylindrical chamber that is in contact with fluid at suction conditions. The geometry of the compression volume is complicated by the presence of certain details, namely the vane and the discharge valve. The geometry of the suction volume is also complicated by the presence of the vane. However, if the causes of the various complications are removed, the problem reduces to a simple geometric exercise.

Figure 2.18 shows a simplified representation of the compression mechanism (also referred to as the pump). The vane is assumed to be infinitely thin. The extra "pocket" of fluid near the discharge valve is neglected. The larger circle represents the wall of the cylindrical chamber. The smaller circle represents the outer surface of the rolling piston. A rectangular (X,Y) coordinate system is chosen, centered at O. The X axis is chosen to pass through point C, and thus the coordinate system rotates with the rolling piston. A polar coordinate system (ρ,ψ) is also defined. The location of any point can be specified in terms of its distance, ρ, from point O and the angle ψ it makes with the X axis. The rolling piston is assumed to rotate clockwise.

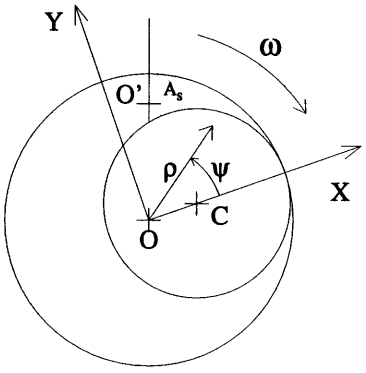

Figure 2.18: Geometry of the suction and compression chambers

The relation between the rectangular and polar coordinates is:

$$X = \rho\cos\psi \tag{2.65}$$

$$Y = \rho\sin\psi \tag{2.66}$$

The equations of the two circles in the X-Y coordinate system are:

$$\text{Cylindrical Chamber:} \quad X^2 + Y^2 = r_{ch}^2 \tag{2.67}$$

$$\text{Rolling Piston:} \quad (X-e)^2 + Y^2 = r_{rp}^2 \tag{2.68}$$

The corresponding equations in the polar coordinate system (ρ,ψ) can be written. Because the origin of the axis coincides with the center of the cylindrical chamber, the equation for the chamber can be written simply as:

$$\rho_{ch} = \pm r_{ch} \tag{2.69}$$

Starting from the rectangular coordinate axis equation (equation 2.68) and using equations 2.65 and 2.66, the equation for the rolling piston can be derived in polar coordinates. The resulting second order equation can then be solved[1]:

$$X^2 - 2eX + e^2 + Y^2 = r_{rp}^2$$

$$X^2 - 2eX + e^2 + Y^2 - r_{rp}^2 = 0$$

$$(\rho\cos\psi)^2 - 2e\rho\cos\psi + e^2 + (\rho\sin\psi)^2 - r_{rp}^2 = 0$$

$$\rho^2 - 2e\cos\psi \cdot \rho + e^2 - r_{rp}^2 = 0$$

Solve the second order equation: $\Delta = 4(e\cos\psi)^2 - 4(e^2 - r_{rp}^2)$

$$= 4e^2[(\cos\psi)^2 - 1] + 4r_{rp}^2 = 4[r_{rp}^2 - (e\sin\psi)^2]$$

$$\text{Hence: } \rho_{rp} = \frac{2e\cos\psi \pm 2\sqrt{r_{rp}^2 - (e\sin\psi)^2}}{2}$$

Practically, only the larger value (corresponding to +) constitutes a valid solution. Thus,

$$\rho_{rp} = e\cos\psi + \sqrt{r_{rp}^2 - (e\sin\psi)^2} \tag{2.70}$$

The suction volume at any angle θ is the difference between the areas enclosed between the vane, the X axis, and each of the two circles.Therefore, the projected area of the suction volume is:

$$A_{s(\theta)} = \frac{1}{2}\int_0^\theta \rho_{ch}^2 d\psi - \frac{1}{2}\int_0^\theta \rho_{rp}^2 d\psi$$

$$= \frac{1}{2}\int_0^\theta r_{ch}^2 d\psi - \frac{1}{2}\int_0^\theta [e\cos\psi + \sqrt{r_{rp}^2 - (e\sin\psi)^2}]^2 d\psi$$

$$= \frac{1}{2}\left\{(r_{ch}^2 - r_{rp}^2)\cdot\psi\Big|_0^\theta - e^2\int_0^\theta[(\cos\psi)^2 - (\sin\psi)^2]d\psi - \right.$$

$$\left. 2e\int_0^\theta \cos\psi\sqrt{r_{rp}^2 - (e\sin\psi)^2}d\psi\right\}$$

$$= \frac{1}{2}\left\{(r_{ch}^2 - r_{rp}^2)\cdot\theta - \frac{1}{2}e^2\sin 2\theta - 2e^2\int_0^{\sin\theta}\sqrt{\left(\frac{r_{rp}}{e}\right)^2 - (\sin\psi)^2}d(\sin\psi)\right\}$$

---

1. Given a second order equation in x: $ax^2 + bx + c = 0$. The solution is $x = \frac{-b \pm \sqrt{\Delta}}{2a}$, where $\Delta = b^2 - 4ac$

$$= \frac{1}{2}\left\{ (r_{ch}{}^2 - r^2{}_{rp}) \cdot \theta - \frac{1}{2}e^2 \sin 2\theta - 2e^2 \left[\frac{\sin\psi}{2} \sqrt{\left(\frac{r_{rp}}{e}\right)^2 - (\sin\psi)^2} \right]_0^{\theta} \right.$$

$$\left. + \frac{1}{2}\left(\frac{r_{rp}}{e}\right)^2 \operatorname{asin}\frac{e\sin\psi}{r_{rp}}\Bigg|_0^{\theta} \right\}$$

$$A_{s(\theta)} = \frac{1}{2}\left\{ (r_{ch}{}^2 - r^2{}_{rp}) \cdot \theta - \frac{1}{2}e^2 \sin 2\theta - e^2 \left(\sin\theta \sqrt{\left(\frac{r_{rp}}{e}\right)^2 - (\sin\theta)^2} \right.\right.$$

$$\left.\left. - \frac{r_{rp}{}^2}{e^2} \operatorname{asin}\frac{e\sin\theta}{r_{rp}} \right) \right\} \tag{2.71}$$

The difference between the areas of the two circles is the projected area of the total space occupied by fluid inside the pump. That space consists of the suction and the discharge volume. Thus, the projected area of the discharge volume is:

$$A_{d(\theta)} = (\pi r^2{}_{ch} - \pi r^2{}_{rp}) - A_{s(\theta)} \tag{2.72}$$

The discharge volume as a function of crank angle can be approximated as:

$$V_{d(\theta)} = h_{ch} A_{d(\theta)}$$

$$= h_{ch}\left\{ \left(\pi - \frac{1}{2}\theta\right)(r^2{}_{ch} - r^2{}_{rp}) + \frac{1}{4}e^2 \sin 2\theta + \frac{1}{2}e^2 \sin\theta \sqrt{\left(\frac{r_{rp}}{e}\right)^2 - (\sin\theta)^2} \right. \tag{2.73}$$

$$\left. + \frac{1}{2} r_{rp}{}^2 \operatorname{asin}\frac{e\sin\theta}{r_{rp}} \right\}$$

This equation is only valid once the point of contact between the rolling piston and the cylindrical chamber passes beyond the suction port. The corresponding crank angle, θo, is determined by the compressor geometry; $\theta o = 0.61$ rad. The volume of the compression chamber is then at its largest, $V_{d(\theta o)}$. For crank angles below that threshold value, there is no sealed compression space at all.

Consider the closed system consisting of the fluid trapped within the compression chamber. The system undergoes a compression process during each cycle of the compressor. The motor shaft rotates at approximately 3600 rpm (if S=0), which means that the time for one motor cycle is only $16.\overline{6}$ milliseconds. The compression cycle begins and ends before

the motor cycle does; Hence, a compression cycle is completed in less than $16.\overline{6}$ ms. Given the very short duration of the compression process, it can be modeled as adiabatic. To further simplify the problem, assume the fluid is superheated enough so that it behaves as an ideal gas. Thus, the process can be modeled as an isentropic compression process. If we further assume that the specific heat ratio, γ, does not vary significantly during the process, the fluid pressure and the volume it occupies are related by:

$$PV^{\gamma} = cst \tag{2.74}$$

At the start of the compression process, the fluid pressure is at its suction value. The crank angle is then θo, as discussed previously. Thus, the instantaneous pressure in the compression chamber can be easily determined by:

$$P_{(\theta)} = P_s\left(\frac{V_{(\theta_o)}}{V_{(\theta)}}\right)^{\gamma} \tag{2.75}$$

2.4.3 Equations of Motion

So far, expressions have been developed for the various forces that act on the vane. The spring force, the inertia force, and all the pressure forces can be calculated independently, using these expressions and results from the compression process model. The only unknown that remains is the magnitude of the contact force.

Dynamic equilibrium of the vane during its motion requires, according to D'Alembert's Law of Motion:

$$\sum \vec{F}_{(\theta)} = \vec{0}$$

$$\vec{F}_{S(\theta)} + \vec{F}_{I(\theta)} + \vec{F}_{C(\theta)} + \vec{F}_1 + \vec{F}_{2(\theta)} + \vec{F}_{3(\theta)} + \vec{F}_{4(\theta)} + \vec{F}_{5(\theta)} + \vec{F}_{6(\theta)} + \vec{F}_{7(\theta)} = \vec{0} \tag{2.76}$$

That is, the vector sum of all forces acting on the vane, including the inertia force, has to be null for dynamic equilibrium. This vector equation can be projected along two axes to yield two scalar equations. Let subscripts x and y denote the components of a vector along the x and y axes respectively. That is, $\vec{F} = F_x\vec{i} + F_y\vec{j}$ The corresponding scalar equations for the vane are:

$$F_S + F_I + F_{Cx} + F_1 + F_{6x} + F_{7x} = 0 \tag{2.77}$$

$$F_{C,y} + F_2 + F_3 + F_4 + F_5 + F_{6,y} + F_{7,y} = 0 \tag{2.78}$$

As mentioned earlier, the only unknown is the magnitude of the contact force, F_C. If, for any reason, the forces are unbalanced along the x-direction, the vane either loses contact with the piston, causing leakage or digs into it, causing damage. Thus, proper operation of the compression mechanism requires that the forces be balanced along the x-direction.

Unless yielding and failure occur, the magnitude of the contact force F_C varies such as to preserve equilibrium along this direction. This might create an unbalance of forces that will push the vane against its guide, along the y-direction. (The value of F_C which satisfies equation 2.77 will not satisfy equation 2.78 in general). If the vane is pushed towards the suction side, it may, under the action of an unbalanced moment, rotate counterclockwise about its point of contact with the sharp edge of the vane guide (A_2). On the other hand, if the vane is driven sideways towards the discharge side, its point of contact with the edge of the vane guide (A_1) may act as a pivot point about which it can rotate in the clockwise sense.

It is important to predict if the vane cocks anytime during a cycle. The reason being that the extent of cocking, if any, affects the compliance requirements of whatever link is designed to join the vane and the vane lifting mechanism. For that purpose, the resultant moment about pivot points A_1 and A_2 is calculated:

$$\sum \overline{M}_{A_1} = \overline{M}_{S,A_1} + \overline{M}_{I,A_1} + \overline{M}_{C,A_1} + \overline{M}_{1,A_1} + \overline{M}_{2,A_1} + \overline{M}_{3,A_1} + \overline{M}_{4,A_1} + \overline{M}_{5,A_1} + \overline{M}_{6,A_1} + \overline{M}_{7,A_1} \tag{2.79}$$

$$\sum \overline{M}_{A_{21}} = \overline{M}_{S,A_{21}} + \overline{M}_{I,A_{21}} + \overline{M}_{C,A_2} + \overline{M}_{1,A_2} + \overline{M}_{2,A_2} + \overline{M}_{3,A_2} + \overline{M}_{4,A_2} + \overline{M}_{5,A_2} + \overline{M}_{6,A_2} + \overline{M}_{7,A_2} \tag{2.80}$$

The sign convention for moments requires that the moment be positive about a given point, which acts as a pivot point, for the vane to cock. Note that a given point (A_1 or A_2), only acts as a pivot point if the vane is in contact with the "proper" side of the vane guide.

What has been discussed qualitatively in this section is explored quantitatively in the next section. The results from the previous section are used. The relevant forces are plotted and discussed in the context of their effect on the mechanism design.

2.4.4 Numerical Simulation of Vane Dynamics

The spring force and the inertia force are expected to depend only on the kinematics of the vane. They should be independent of the pressure anywhere in the system. Equations 2.23 and 2.58 confirm this. Matlab was used to plot these two forces over a complete cycle, as shown in Figure 2.19. Negative forces tend to push the vane away from the rolling piston. Apparently, the magnitude of the spring force is quite low in general, barely balancing the inertial force when the vane nears top dead center. Clearly, the spring cannot be what keeps the vane in contact with the rolling piston during normal operation. The role of the spring is probably restricted to the first few cycles after initial start-up. Later on, after some pressure buildup, the pressure force probably forces the two components to remain in contact.

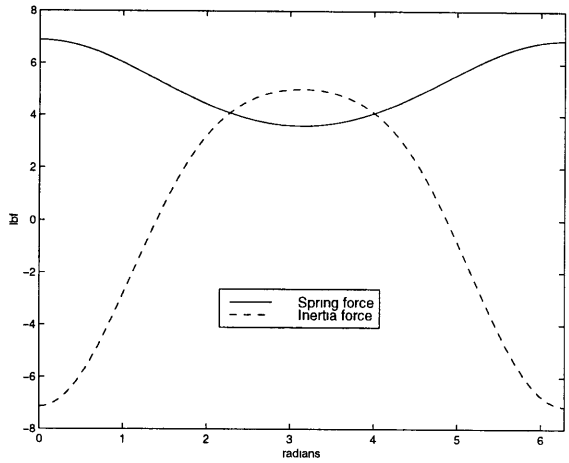

Figure 2.19: Spring force and inertia force versus crank angle

The magnitudes of the various pressure forces, and consequently of the contact force, depend on the suction and discharge pressure. So does the pressure profile in the compression chamber over a cycle. In this analysis, all parameters are evaluated for three standardized compressor testing conditions. These conditions are referred to as CHEER, ARI and MAX. LOAD testing conditions. They cover the range over which the compressor is expected to operate. Table 2.2 quantitatively describes these testing conditions.

Table 2.2: CHEER, ARI and MAX. LOAD compressor testing conditions

	$T_{suction}$	$T_{sat.\ suction}$	$T_{sat.\ discharge}$	$P_{suction}$	$P_{discharge}$
CHEER	65 °F	45 °F	100 °F	90.8 psia	210.9 psia
ARI	65 °F	45 °F	130 °F	90.8 psia	311.9 psia
MAX. LOAD	75 °F	55 °F	155 °F	107.4 psia	419.6 psia

The pressure force acting on the top edge of the vane, F_1, was calculated for the 3 conditions. Its value was found to be: 55.1, 83.4, and 113.7 lbf for CHEER, ARI and MAX. LOAD respectively. This confirms the statement made earlier that the spring's function is mainly during start-up.

Figure 2.20 shows the variation in pressure in the compression chamber versus crank angle over a complete cycle, evaluated for the three conditions above. An average value of γ was used (γ=1.187). This plot covers only the range of crank angles where a sealed dis-

charge chamber exists ($\theta > \theta_0$). The pressure increases until it exceeds the discharge pressure for any given condition. At that point, the discharge valve opens, and fluid leaves the compression chamber. This discharge process is assumed to occur at constant pressure.

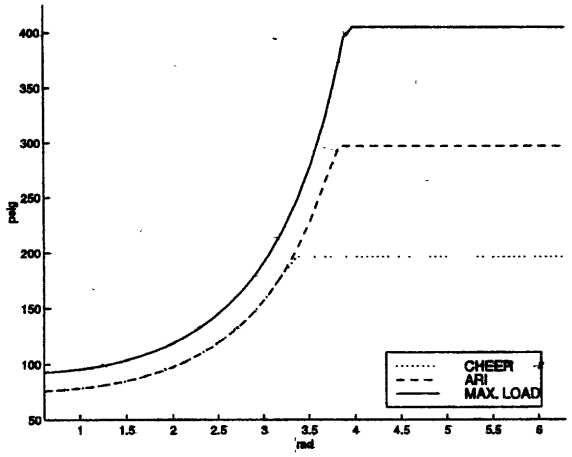

Figure 2.20: Pressure in the compression chamber versus crank angle

The various pressure forces on the sides and curved edge of the vane were calculated for the 3 testing conditions. These forces, each taken individually, do not affect the vane lifting mechanism's design. Thus, they will not be plotted here. However, their combined effect, in conjunction with the inertia and spring forces, determines the magnitude of the contact force.

The contact force creates stress fields near the contact interface. Hence, knowledge about the contact force quantifies the vane/rolling piston interaction. The magnitude of the contact force, F_C, was calculated as a function of the crank angle using equation 2.77. Figure 2.21 is a plot of the contact force as it varies over one cycle for the 3 testing conditions.

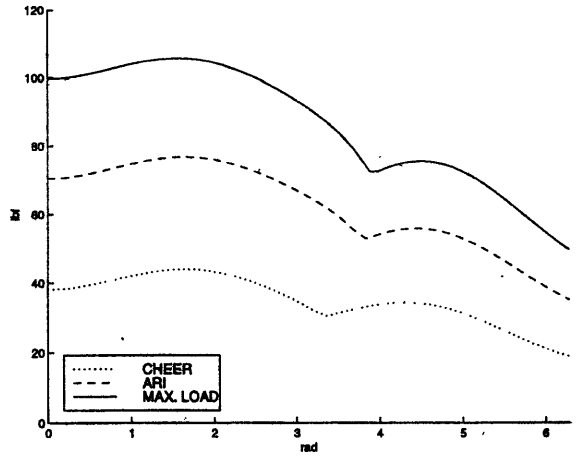

Figure 2.21: Magnitude of the contact force versus crank angle

Having thus determined the magnitude of the contact force, the left hand side of equation 2.78 can be used to evaluate the net force acting on the vane along the y-direction, ΣF_y. Figure 2.22 shows the variation in ΣF_y over a complete cycle for the 3 standard tests conditions considered. As expected, the net force is unbalanced for most of the cycle. This will push the vane sideways against its guide. During the first portion of the cycle, ΣF_y is negative. Thus, the vane is pushed towards the discharge (compression) chamber. Later on, when ΣF_y becomes positive, the vane moves sideways towards the suction chamber.

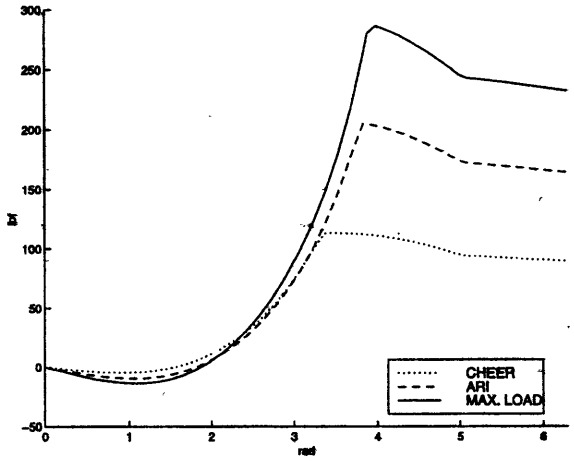

Figure 2.22: Net unbalanced force acting on the vane along the y-direction

A remark is in order about Figures 2.21 and 2.22. At first glance, one might think the simulation is in error; that the values of a given parameter at $\theta=0$ and $\theta=2\pi$ should match for a given set of conditions. Upon further reflection, it becomes apparent that there should be a large step change in the vicinity of top dead center. The cause of this step change will become clear shortly.

The pressure in the compression chamber reaches its discharge value sometime after bottom dead center. The crank angle at which that occurs depends on the operating conditions. At that point, the discharge valve opens and high pressure fluid leaves the compressor. As the sealing point crosses the discharge valve, however, a large change occurs. Low pressure fluid is now in contact with the discharge valve. As a result, a blow back process occurs in which some high pressure fluid leaks back into the cylindrical chamber. A large step change is expected to accompany this effect.

The simulation model does not take into account this blow back process. That is why the large step change seems to occur at top dead center, instead of slightly earlier as it would in practice.

The final question answered by this numerical work is: Does the vane cock anytime during the cycle? The resultant moment of all the forces about points A_1 and A_2 was determined

over a complete cycle for all 3 testing conditions. During the first portion of the cycle, the vane can cock about point A_1 if the net moment is positive. As seen in Figure 2.23, that is the case. During the later portion of the cycle, when ΣF_y is positive, the vane can cock about pivot point A_2 only when the net moment about A_2 is positive. This is the case for some part of the cycle. As the vane travels towards top dead center, the cocking effect vanishes. Hence, the vane seems to cock for some portion of the cycle and this will be taken into account in the design of the vane lifting mechanism.

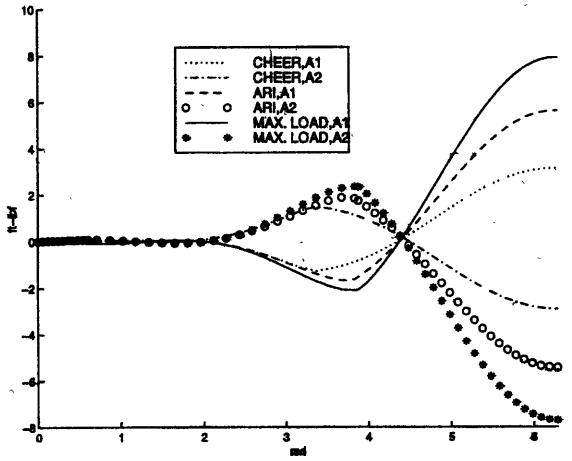

Figure 2.23: Net moment about pivot points A_1 and A_2

2.5 Stress Analysis

2.5.1 Theory and Formulas

The contact between the vane and the rolling piston should remain elastic during operation. If that is not the case, we would expect the softer material (the rolling piston in this system) to fail. Failure would most likely occur due to plastic deformation and subsurface yielding leading to the formation of wear debris.

No hardness test was performed on the samples. The hardness cited on design drawings provided by Carrier are assumed to be accurate and used in the analysis. The vane is M2 tool steel of Rockwell hardness HRC:60-65. The rolling piston is cast iron, HRC:45-55. Obviously, both components must have been subjected to some special heat treatment to achieve those unusually high hardnesses.

The Rockwell Hardness (HRC) can be related to the Brinell Hardness (B) by [3]:

$$B = \left(\frac{C_1}{C_2 - HRC}\right)^2 \tag{2.81}$$

The coefficients C_1 and C_2 were determined empirically by Cowdrey and Adams (1944): C_1=1590 and C_2=122. The Brinell Hardness can be used to estimate the ultimate tensile strength of the material in psi [4]:

$$\sigma_u \cong 500B \tag{2.82}$$

For the purpose of the analysis, the maximum allowable shear stress (before yielding occurs) can be assumed to be:

$$\tau_{max} \approx \frac{1}{2}\sigma_u \tag{2.83}$$

The contact is assumed to be perfectly elastic. It is further idealized as perfect line contact between two cylindrical surfaces. Thus, equations for Hertzian line contact between two parallel axis cylindrical surfaces can be used [5]. The equivalent modulus of elasticity of the system is given in terms of the elastic moduli (E_i) and the Poisson's ratio (υ_i) of the two materials:

$$E_e = \frac{1}{\frac{1-\vartheta_v^2}{E_v} + \frac{1-\vartheta_{rp}^2}{E_{rp}}} \tag{2.84}$$

The area of contact between cylinders is a rectangle of half width b:

$$b = \sqrt{\frac{2Fd_v d_{rp}}{\pi l_v E_e (d_v + d_{rp})}} \tag{2.85}$$

where F/l_v is the load per unit length of contact. The maximum contact pressure is:

$$q = \frac{2F}{\pi b l_v} \tag{2.86}$$

The maximum shear stress occurs at approximately 0.768b below the surface and has the value:

$$\tau \approx 0.3q \tag{2.87}$$

2.5.2 Numerical Simulation

The Rockwell hardness of each material can be converted to the Brinell hardness scale via equation 2.81. The approximate Brinell hardness of the vane ranges from 657.7 to 778.1. That of the rolling piston ranges from 426.4 to 563.2. Hence, the maximum allowable

shear stress can be roughly calculated. For worst case scenario, the vane can take up to 164.4 kips shear stress. The rolling piston can take up to 106.6 kips. Clearly, the rolling piston is the limiting factor.

No data (experimental or company furnished) is available on the values of Young's Modulus and Poisson's ratio for either component. Hence, these values are assumed, after consulting some references [4] & [6]. The Poisson's ratio is taken to be 0.27 and 0.25 for the vane and the rolling piston, respectively. Young's Modulus is considered to be 30 Mpsi and 14.5 Mpsi respectively.

The values assumed are used in conjunction with equations 2.84 through 2.87 to determine the maximum subsurface shear stress. This shear stress varies with crank angle and also with operating conditions, as seen in Figure 2.24. As expected, the trend of the variation in shear stress closely follows that of the contact force. The maximum shear stress encountered under the harshest operating condition is much less than the maximum allowable values calculated previously.

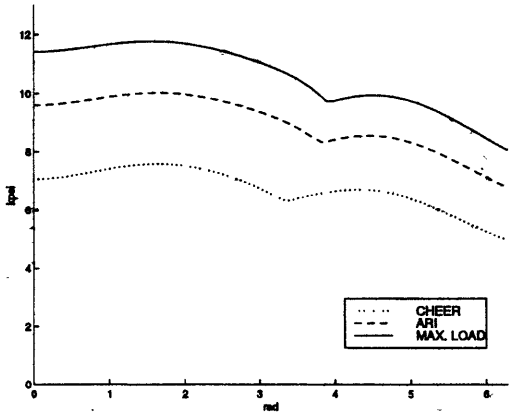

Figure 2.24: subsurface shear stress due to Hertzian contact

2.6 Impact Analysis

This section presents a very simplified model of eccentric impact between the vane and the rolling piston. An approximate method, the Energy Method, is used to estimate the maximum contact force due to impact. Thus, the maximum Hertzian shear stress can be determined using the equations of the previous section.

To simplify the analysis, several assumptions are made, namely:
1. The effect of the oil film between the rolling piston and the eccentric is completely neglected.
2. The piston is assumed to remain rigid during impact.

3. The vane is assumed to be initially stationary.

The first and second assumption lead to an over-estimate of the contact force. The last assumption leads to an under-estimate. Hence, it is hard to predict whether the estimated value of the contact force will be too high or too low; it depends on the relative importance of the assumptions made.

The center of gravity of the rolling piston moves at a constant angular velocity, ω=377 rad/s. Hence, its linear velocity is constant in magnitude ($V=\omega e$), but changes in direction. Because of the geometry of the problem, the line of impact is always along the line of centers CC'.

Along the line of impact, the relative velocity is, by definition:

$$V_{v/rp} = V_v - V_{rp} = 0 - V_{rp} = -V_{rp} \tag{2.88}$$

The worst case impact occurs when the relative velocity of the vane to the rolling piston is highest in magnitude along the line of impact. That is, when the component of velocity of the rolling piston along the line of impact is at its largest value. That occurs when the direction of the rolling piston velocity coincides with the line of centers. In that case, $V_{v/rp}=-V=-\omega e$.

Particle impact theory is based on a coefficient of restitution, e_r. This coefficient compares the relative separation velocity to the relative approach velocity along the line of contact [7].

$$e = -\frac{(V_{v/rp})_f}{(V_{v/rp})_i} \tag{2.89}$$

Subscripts i and f denote the state right before and right after impact, respectively. The value of e_r depends on several factors: the materials of the colliding particles, the geometry of the problem and the impact velocity. e_r can take on any value between 0 and 1. e_r=0 for perfectly plastic impact while e_r=1 represents perfectly elastic impact. In practice, collisions fall somewhere between these two theoretical cases; some energy is always lost.

An attempt will be made to extend the simplified theory of particle impact using a coefficient of restitution to the non-central rigid body impact problem at hand. This is a gross oversimplification of the problem. This analysis only aims to obtain a rough, ballpark figure. The impact is assumed to be perfectly elastic; thus, energy is conserved and simply transformed from elastic strain energy (U) to kinetic energy of the vane (KE). Also, impact occurs in an infinitely small period of time. Hence, the velocity of the center of gravity is assumed to be essentially constant immediately before and after the collision: $(V_{rp})_i=(V_{rp})_f=V$.

Therefore,

$$e = 1 = -\frac{(V_{v,f} - V_{rp,f})}{(V_{v,i} - V_{rp,i})} = -\frac{(V_{v,f} - V_{rp,f})}{(0 - V_{rp,i})} = \frac{(V_{v,f} - V_{rp,f})}{V_{rp,i}} = \frac{(V_{v,f} - V)}{V}$$

$$\therefore V_{v,f} = 2V \tag{2.90}$$

Keep in mind that all this analysis is done along the line of impact. The vane can move significantly only along the X axis.

Consider the vane only for the remainder of this analysis: A contact force develops during impact. This force tends to deform the vane locally through a maximum deformation δ, at which point the contact stress is maximum. As mentioned previously, this model considers the interaction to be perfectly elastic. Thus, no permanent deformation occurs and all the elastic strain energy (U) due to deformation during the collision phase of the impact is converted to kinetic energy (KE) during the restitution phase.

Another assumption is made to simplify the analysis: The instantaneous contact force is assumed to be linearly related to the instantaneous deformation x. The linearity constant is $K=F_{(x)}/x=F/\delta$.

Thus,

$$\Delta KE + \Delta U = (KE_2 - KE_1) + (U_2 - U_1) = (KE_2 - 0) + (0 - U_1) = 0$$

States 1 and 2 are the states immediately before and after the restitution phase. The internal strain energy U_1 is equal to the total work done by the contact force in bringing about the deformation. That is,

$$U_1 = \int_0^{\delta} F_{(x)}dx = \int_0^{\delta} Kxdx = K\left[\frac{1}{2}x^2\Big|_0^{\delta}\right] = \frac{1}{2}K\delta^2 = \frac{1}{2}F\delta$$

Hence,

$$\frac{1}{2}m_v(2V)^2 - \frac{1}{2}F\delta = 0 \tag{2.91}$$

Hertzian stress theory relates the maximum deflection δ to the maximum contact force F [6]:

$$\delta = \frac{2F}{\pi l_v E_e}\left[Log_e\left(4\frac{r_v}{b}\right) - \frac{1}{2}\right] \tag{2.92}$$

Substituting for b from equation 2.85, and then substituting for δ from equation 2.92 into

equation 2.91, we get an equation in one unknown, F:

$$\frac{F^2}{\pi l_v E_e}\left[Log_e\left(2r_v\sqrt{\frac{\pi l_v E_e(r_v + r_{rp})}{F r_v r_{rp}}}\right) - \frac{1}{2}\right] - 2m_v\omega^2 e^2 = 0 \qquad (2.93)$$

This equation can be solved for F numerically. The value of F, the maximum contact force due to impact, is found to be around 5542 lbf. The resulting Hertzian maximum shear stress is then around 85 kips.

It is impossible to predict the error in the value obtained for shear stress: too many assumptions and oversimplifications are involved. If the number is reasonably accurate, then impact might not be a problem. In fact, such impact probably occurs at every compressor start-up. As a further precaution, the area of contact is calculated (bl_v) and compared to the total surface area of the vane tip ($2\Omega r_v l_v$). The ratio of these two areas gives us an idea of how large a portion of the vane tip suffers during impact. Assuming equal probably of impact anywhere on the vane tip surface, then a small ratio implies low probability of failure due to fatigue. That is, a given region does not get hit enough during the life of the compressor to fail. In fact, the ratio is found to be 0.042.

This analysis, however crude it may be, seems to indicate that impact might not be a crucial factor to be taken into account in the design of the vane lifting mechanism.

Chapter 3

Mechanism Design and Construction

This section deals with the design and construction of the vane lifting mechanism. The functional requirements and the constraints of the design are listed first. All components of the mechanism are then described. Design parameters are explained. Design decisions are defended where appropriate. Detailed assembly and part drawings follow. Also included are schematic diagrams that illustrate the operation of the mechanism. Finally, the construction of a prototype mechanism is described.

A word of caution on the vane lifting mechanism design described in this chapter. As stated previously, the aim of this work is twofold: to verify the saneness of the concept and to attempt to practically build a working mechanism. At this stage, no effort was made to design for mass manufacturing or assembly. Additionally, given this understanding that the mechanism will not go into mass production without modifications, no effort was made to carry out a cost analysis of the mechanism.

3.1 Functional Requirements of the Design

The crucial step in the design was to clearly list what is expected of the mechanism. That is, to set the requirements that the design aims at fulfilling. Based on the concept discussed in Chapter 1, the mechanism should be able to cyclically unload and load the compressor. It should do so by lifting the vane and letting it be, respectively. Thus, the first level requirements of the mechanism are:

- It should not interfere with the operation of the compressor when in normal mode.
- It should be able to lift the vane and hold it in place at top dead center for the unloaded mode.

At this stage, it was decided upon a pneumatic mechanism. Such a mechanism would take advantage of the availability of refrigerant at two drastically different pressures: compressor suction (P_s) and discharge pressures (P_d). Another advantage lies in the inherent simplicity of pneumatic devices.

The obvious choice was a piston like mechanism driven to move under the net action of

controlled pressure forces acting on its top and bottom faces. Thus, the two piston faces have to be in contact with two pressure chambers. The pressure in these two chambers should be reversible. One way of achieving that is through the use of a couple of three way valves, one for each chamber. Each valve would also be open to refrigerant at the two working pressure levels. Furthermore, there should be some means of connecting the piston to the vane. A lifting stem somehow attached to the vane seemed like a good choice.

Figure 3.1 illustrates the above design decisions. This is only an over-simplified preliminary design. It lacks many details. However, it served as a starting point as it seems to satisfy the first level functional requirements.

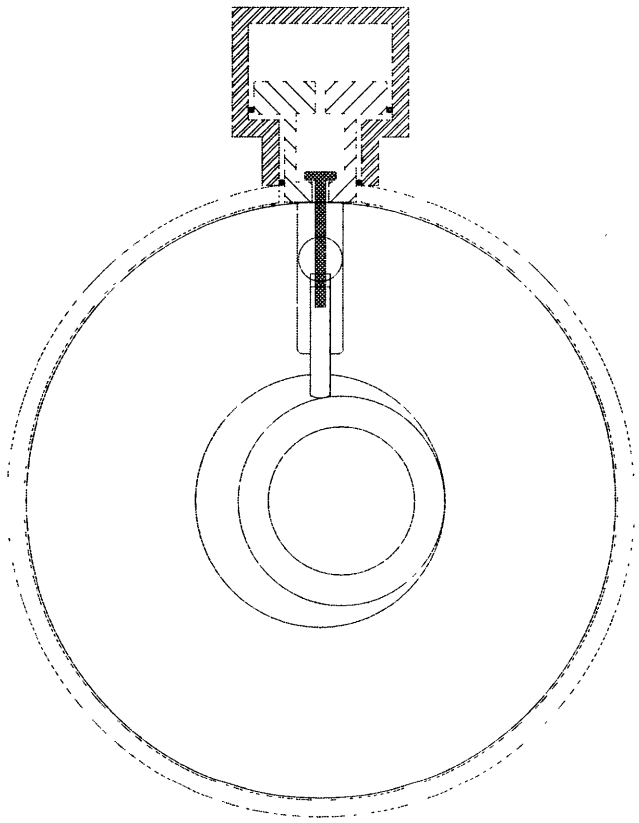

Figure 3.1: Preliminary design of the vane lifting mechanism

Based on the constraints imposed by the aforementioned design decision, each of the first level functional requirements can be decomposed further.

Ideally, the performance of the compressor should be completely unaffected by the modifications under normal operation. Practically, deterioration in performance should be minimized. The addition of the mechanism could affect the system in several ways: First, it could alter the dynamics of the vane. It can do so by changing the inertia of the vane, by changing the spring or pressure forces on it, or by altering the frictional forces opposing its motion. Second, addition of the mechanism could alter system performance by chang-

ing the leakage characteristics of the system. The most obvious site of possible additional leakage is along the sides of the vane. Third, any change in vane lubrication could measurably affect system performance. Thus, to satisfy the first requirement, the mechanism should not significantly alter any of the parameters listed. Finally, to avoid failure, some compliance should exist between the vane and the lifting stem.

In the unloaded mode, the first level functional requirement can be decomposed into several others. The mechanism should be able to hold the vane at top dead center. Thus, the differential pressure force on the piston should be enough to balance the forces on the vane along the X-direction, most notably the pressure force. The mechanism should also be able to lift the vane during one or a fraction of a complete crank revolution. Otherwise, the vane would come in the path of the rolling piston, leading to impact and possible damage. How fast the pneumatic device moves from bottom to top dead center depends on the magnitude of the differential pressure force driving it. What causes the device to move in the first place is either a pressure reversal or variation. Thus, the time delay for pressure reversal to occur also affects the speed of the device. Finally, to prevent damage, impact between the vane and the rolling piston should be minimized. Thus, impact while loading or unlading the vane should be avoided if possible. Also, the vane should not interfere with the motion of the rolling piston when it is unloaded.

One major constraint on the design is size. The mechanism should fit in the small space outside the compressor shell between the vane and the accumulator.

3.2 Details of the Design

The final design evolved after several rounds of iteration, modification and brainstorming. A complete set of design drawings for the vane lifting mechanism is presented at the end of this section. It consists of two assembly drawings (to scale and magnified twice), detailed parts drawings, and schematic diagrams showing the operation of the mechanism.

The function and design of each component will be explained in reverse order of assembly. That is, the part that goes on last will be discussed first. The names of all the parts are indicative of their function.

The *cover plate* (Figure 3.4) covers the mechanism, creating a sealed pressure chamber above the piston. In fact, when the mechanism is mounted on the compressor, the piston will be horizontal. Strictly speaking, above and below the piston are erroneous descriptions. However, below will be used to refer to the side of the piston facing the compressor, while above refers to the side away from the compressor. The shape of the cover plate is dictated by the need for a surface through which bolts can be driven to connect this part to the rest of the assembly. Obviously, a circular plate with diameter larger than that of the cylinder would have worked as well. The square shape was chosen to satisfy the require-

ment of minimizing parts size. Four holes at the four corners of the plate hold the connecting bolts in place. Another hole through the center of the plate connects the pressure chamber above the piston to a 3 way normally open solenoid valve.

The *cylinder* (Figure3.5) forms a smooth surface along which the piston can slide. It also constitutes the walls of the two pressure chambers above and below the piston. The length of the cylinder is designed to allow for the piston to travel a distance of one vane stroke plus an additional ten thousands of an inch (0.010 in.). This clearance length is to make sure that when the vane is lifted, it doesn't contact the rolling piston at zero crank angle every cycle. The circular groove milled at the lower end of the cylinder forms a seat for the circular top part of the piston liner. Circular O'ring grooves are milled on the top and bottom faces of the cylinder. These hold static O'rings that isolate the pressure chambers from atmospheric conditions surrounding the mechanism.

The *piston liner* (Figure 3.6) consists of a brass ring soldered to a steel cylinder at its end. The inner surface of the piston liner is smooth to allow for minimal friction sliding of the piston. The outer surface serves as a sealing surface in conjunction with two O'rings. The function of these two static O'rings is to isolate the chamber above the vane and the space below the piston from surrounding atmospheric conditions. The small part welded to the inner surface of the piston liner holds the spring in place and compresses it. Without this part, the spring would be free floating. The larger hole through the ring is a part of the flow path between the pressure chamber and a normally closed 3 way solenoid valve. The smaller hole is for alignment. It fits a small pin in the mounting base.

The *mounting base* (Figure 3.7) mounts the assembly onto the compressor. The top portion is connected to the cover plate by four long bolts, and thus matches it in shape. The bottom portion is cylindrical to minimize size, leaving room for welding. The step at the end of the mounting base fits it into its seat in the compressor shell. A small pin is inserted in the top surface of the mounting base. It is used to align the piston liner. The groove at the bottom end holds a static O'ring that was previously referred to in conjunction with the piston liner. A flow path is drilled through the mounting base. It connects the 3 way normally closed solenoid valve to the pressure chamber below the piston.

The *piston* (Figure 3.8) is altered from traditional pistons in that it is hollowed out. The reasons are twofold: first, to minimize the weight of the piston, thereby decreasing its inertia. That would increase the speed of the system in loading and unloading, for a given pressure force differential. Also, the inner ledge thus formed at the bottom end of the piston contacts the lifting stem (which will be discussed shortly). The location of the ledge at the bottom end of the piston decreases the length requirement of the stem. The inner surface of the ledge is very smooth to reduce friction on the lifting stem. Two O'ring grooves are drilled into the piston near its top and bottom ends. These hold two dynamic O'rings. The upper O'ring maintains two separate pressure chambers above and below the piston. The lower O'ring seals off the pressure chamber below the piston from the fluid in the

space surrounding the vane. The thin circular recess at the bottom end of the piston has no function. It was end milled to create a seat for the spring. Further thought revealed that for the modified system to be able to start, the spring needs a stationary surface to push against. At start-up, no pressure differential exists to hold the piston in place. Thus, the inner ledge was added to the piston liner, as mentioned earlier.

The steel *lifting stem* (Figure 3.9) is an extension to the vane so it can contact the piston. Thus, the motion of the vane and the piston can be coupled under certain circumstances.[1] Coupling is achieved by means of a washer held by a bolt to the top of the lifting stem. This washer can rest on the inner ledge of the hollow piston, and thus forces the vane to move up with the piston. A notch was cut out in the vane to match the profile of the lifting stem end (Figure 3.10). The shape of the lifting stem end and the corresponding notch is such that the vane and the lifting stem can be assembled inside the cylindrical chamber of the pump. However, the clearance in the vane guide is small enough to prevent disassembly once the compressor is running. Note that the profile in the vane does not exactly match that of the lifting stem. That is to create some compliance in the assembly. In the absence of any compliance, the slightest cocking of either vane or lifting stem would stress the thin section of the stem, possibly leading to failure. The lifting stem is kept cylindrical at the top. The length of the cylindrical portion is slightly larger than the maximum travel of the vane. This is to keep a close fit between the stem and its guide in the piston, to minimize leakage across. The cylindrical portion is very smooth to reduce friction. The bottom part of the stem is made narrower. This is to decrease the mass of the lifting stem, thus making system loading and unloading faster. Additionally, during normal operation, the smaller mass causes smaller mass increase in the vane/stem assembly.

In the unmodified compressor, the space above the vane is in contact with refrigerant at discharge conditions. The pressure force on the top edge of the vane drives the contact force up. The high contact force is not required for proper operation of the pump. Furthermore, the design adopted requires larger differential pressure force on the piston to overcome higher pressure. The opposite is also true.

It was speculated that it might be advantageous to decrease the pressure of the fluid above the vane. That would decrease the contact force. Also, the force requirement on the mechanism decreases, making it faster in unloading for a given set of parameters (pressure differential, flat surface area). Finally, during normal operation with the mechanism installed, high pressure fluid acts on the vane stem and the washer. Fluid at some intermediate pressure acts on the top edge of the vane. Hence, pressure force, albeit much smaller, still acts on the vane ensuring continuous contact with the rolling piston. The only way to vary the pressure on the vane is to isolate the space above the vane from the rest of the system. This idea was implemented on the prototype built. The practical details are discussed in the next section.

1. Strictly speaking, the motion is not always coupled. One component sometimes moves faster than the other, depending on what crank angle piston motion is initiated at.

The *solenoid valves* used are 3 way, 24 Volt DC solenoid valves manufactured by KIP Corp. They were ordered through Minuteman Controls Co.[1], Catalog #189. The part numbers are 241140 and 141150 for the normally closed and the normally open valves, respectively. They were chosen based on functionality, pressure rating, size and response time. Neoprene seals were used for refrigerant compatibility.

The reversal time critically affects the proper functioning of the mechanism. The reversal time of the solenoid valves used ranges from 6 to 12 ms. Assuming that the flow path from the solenoid valves to the chambers does not hinder the reversal process: the piston then has another 6 to 12 ms to compete its motion, while avoiding interference between the vane and the rolling piston. The orifice diameter of the solenoid valves is 1/32 of an inch. The flow paths were made larger, using the next available larger drill size (0.056 in. dia.). Also, the flow paths were made as short as practically possible. The reasons are twofold: to decrease losses in the flow path and to decrease the dead volume. Both effects, if not minimized, lead to an increase in pressure reversal time which should be avoided.

Finally, it is worth noting that the choice of materials for many of the components was somewhat arbitrary. Whatever useful material and stock available in the shop was used. The combination of brass and stainless steel for the piston liner was chosen for ease of silver soldering the parts together.

All components of the mechanism, except for two, are always stationary. The piston and the lifting stem can move, either together as a unit or relative to each other. The lifting stem always moves together with the vane.

Figure 3.12 shows the mechanism when the compressor is loaded (normal operation). In this case, the chamber above the piston is kept at discharge pressure. The other chamber is at suction pressure. Hence, the piston remains at bottom dead center. The lifting stem and vane follow the rolling piston and the compressor operates in its usual manner.

The changes in the system under normal operation are minimal. One apparent alteration is the addition of a small moving mass: the lifting stem. The effects of the lifting stem are twofold. First, the inertia of the vane increases. Second, the frictional forces opposing the motion may also increase. Minimizing the mass of the lifting stem takes care of the first effect as best possible. Ensuring proper lubrication and smooth surfaces remedies the second.

The effect of this additional mass on system normal operation can be roughly predicted by back of the envelope calculations. The approximate volume of the stem is:

---

1. Minuteman Controls Co.: 7 Foster St., P.O. Box 1559, Wakefield, MA 01880. (617)245-9550.

$V_{ms} \approx (1.518 - 0.780)$x area of circular top part + 0.780x area of rectangular part

$$V_{ms} \approx (1.518 - 0.780) \cdot \frac{\pi}{4}(0.25)^2 + 0.780 \cdot (0.094x0.183) \approx 0.05in^3$$

The approximate volume of the vane is:

$$V_v \approx t_v \cdot l_v \cdot w_v \approx 0.313in^3$$

The ratio of volumes is roughly 1/6. Assuming similar densities, the vane mass is about 6 times that of the stem. The corresponding increase in inertia force is roughly 17%, which shouldn't alter system dynamics considerably given that the inertia force is quite small in comparison to other forces.

The original spring was replaced by another, flat end spring. The flat end pushes against the inner ledge of the piston liner. The stiffness of the replacement spring was chosen to match the original; Its length was chosen so that the resulting spring force for a given crank angle is roughly the same as in the original design.

The frequency of the modified system consisting of the spring, the vane and the lifting stem is an important parameter. If it matches the frequency of the motor shaft, resonance problems could ensue. Back of the envelope calculations, assuming the mass of the lifting stem is about 1/6 that of the vane, give the natural frequency of the system as:

$$\omega_n \approx \sqrt{\frac{kJ}{m_v + \frac{1}{6}m_v}} = \sqrt{\frac{6kJ}{7m_v}} = \sqrt{\frac{6 \times 8.29 \times 386.4}{7 \times 0.083}} \sim 181hz$$

Thus, resonance is not expected to be a problem in case the lifted vane does not clear the rolling piston.

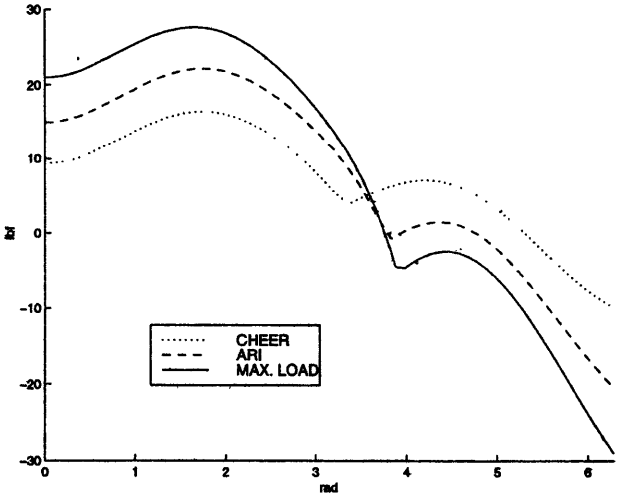

Figure 3.14: Contact force for limiting case when pressure above vane is suction pressure.

The last significant change is the pressure above the vane. Originally, the vane was in contact with refrigerant at discharge pressure. Modifications led to the creation of a closed chamber above the vane. The pressure in the chamber is determined by the extent of leakage flow between it and the suction chamber, the discharge chamber and the pressure chamber above the piston. Thus, the pressure could range anywhere from discharge to suction. In the former case, the resultant pressure force on the vane and the lifting stem would not change significantly. In the latter case, the pressure force would drop significantly. The resultant contact force would then decrease as well. Figure 3.14 is the result of a simulation of the contact force for this worst case under the three operating conditions. It is obvious that the vane would lose contact with the rolling piston during the last part of each cycle. Keep in mind though that this is only a limiting case: It is probably not encountered in practice due to leakage.

Figure 3.13 shows the system unloaded. The pressures in the two chambers are now reversed. As a result, the piston moves to top dead center and stays there. Thus, it holds the lifting stem and the vane up and prevents contact between the vane and the rolling piston. The rolling piston now simply moves fluid around in the pump.

The minimum differential pressure force on the piston can be roughly calculated as:

$$F_{mp,\,min} = (P_d - P_s) \cdot Area$$

$$\text{where Area is:} \quad \frac{\pi}{4}(0.872 - 0.555)^2 \approx 0.079 in^2$$

Hence, F varies from 9.5 lbf to 24.7 lbf for the 3 testing conditions. The effective pressure force is probably higher than the calculated minimum: that is true if the pressure in the chamber above the vane is higher than suction. The approximate volume of the piston is calculated to be approximately: V_{mp}~0.227in^3. This is an overestimate of the volume because the volumes of the oil grooves are not taken into account. Assuming same density as the vane, the mass of the piston can be approximately calculated:

$$m_{mp} \approx \frac{m_v \times 0.227}{0.313} \sim 0.06 lbm$$

The resulting acceleration is constant at:

$$a_{mp} = \frac{F_{mp,\,min}}{m_{mp}} \cdot J \sim \frac{9.5 \times 386.4}{0.06} \sim 61180 in/s^2$$

This is higher than any instantaneous acceleration and almost double the maximum acceleration seen by the vane. Hence, the piston should have no trouble covering half the distance travelled by the vane during a cycle in about a quarter of the time.

A final word: All the calculations done are back of the envelope calculations. They indicate that the chances for success are high, but they should not be considered decisive due to their rough nature. Only tests can prove the success of the mechanism.

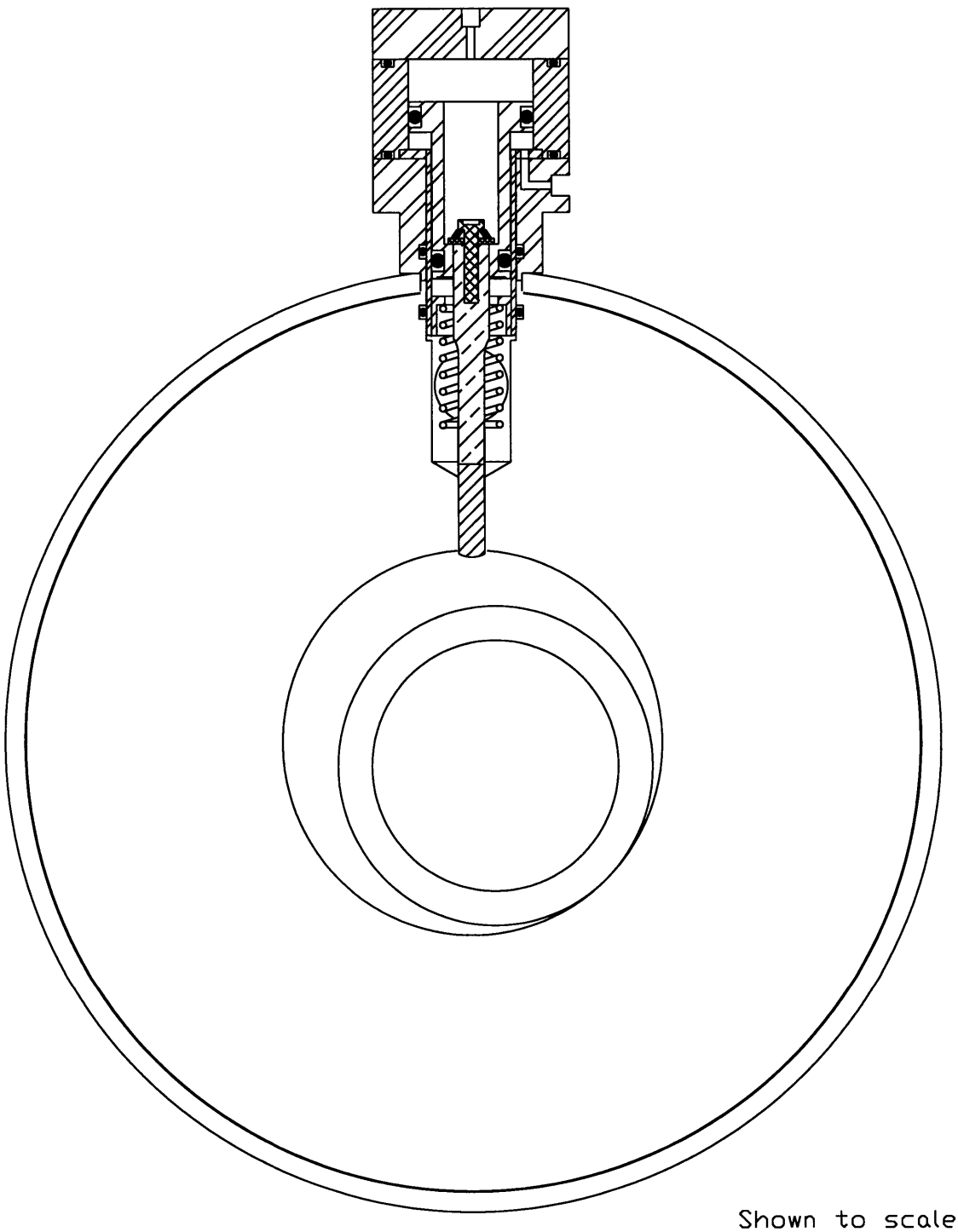

Shown to scale

TITLE: ASSEMBLED MECHANISM		
COMMENTS: Figure 3.2	REVISION: 4	DATE: 6/10/97
MASSACHUSETTS INSTITUTE OF TECHNOLOGY	DRAWN BY: DANIELLE TARRAF	

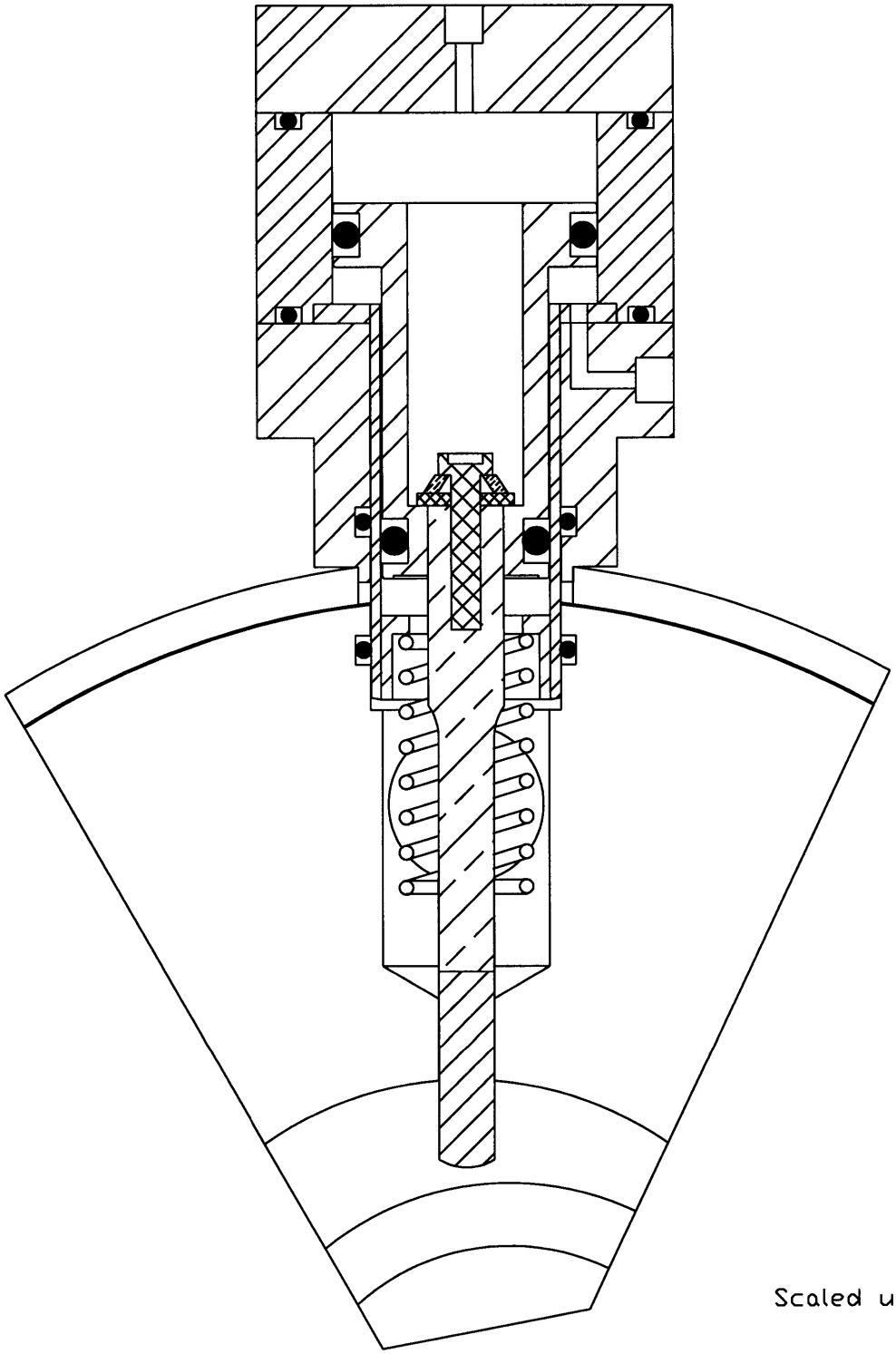

Scaled up 75%

TITLE: ASSEMBLED MECHANISM		
COMMENTS: Figure 3.3	REVISION: 4	DATE: 6/10/97
MASSACHUSETTS INSTITUTE OF TECHNOLOGY	DRAWN BY: DANIELLE TARRAF	

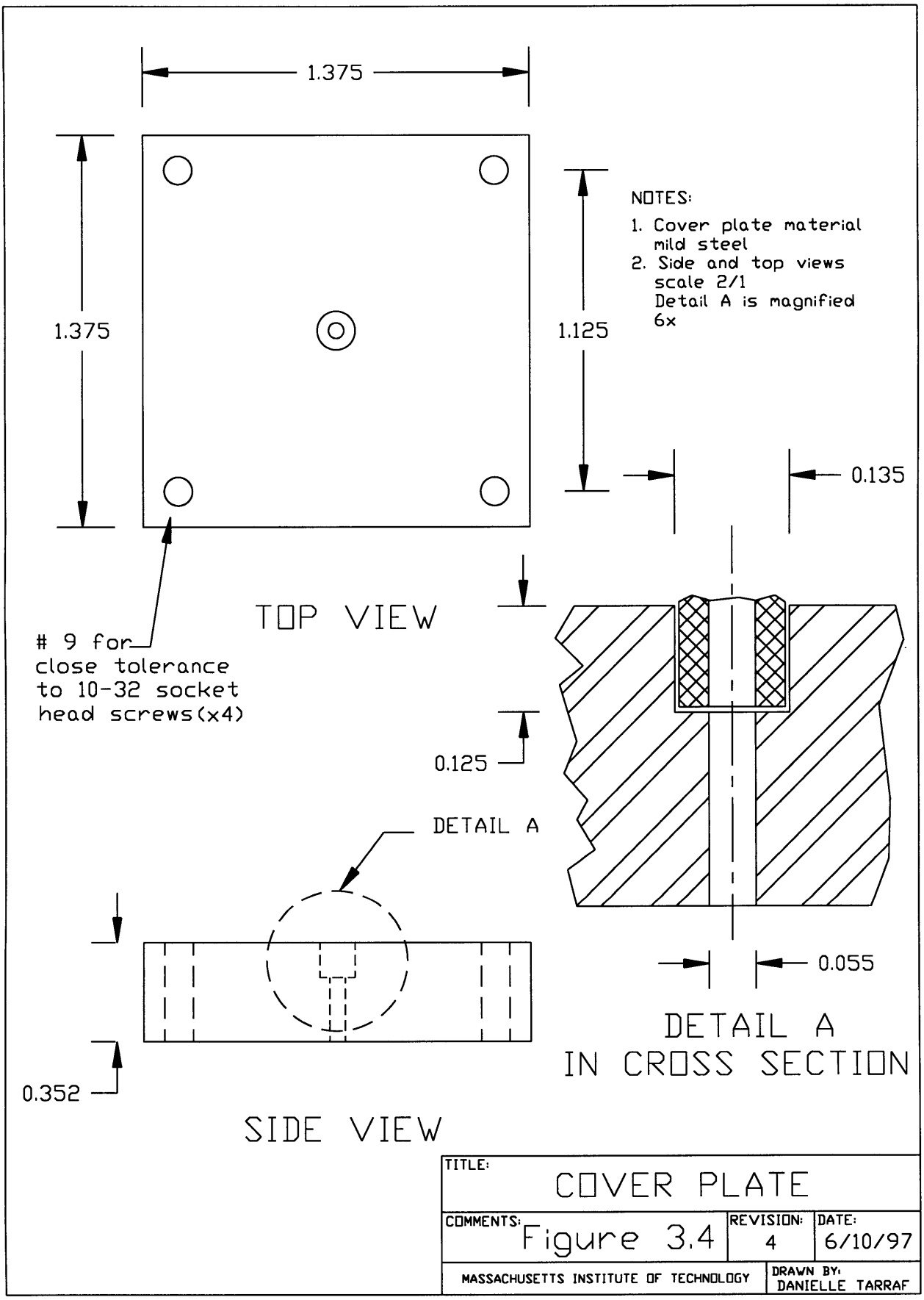
1.375
1.375
1.125
NOTES:
1. Cover plate material mild steel
2. Side and top views scale 2/1 Detail A is magnified 6x
0.135
TOP VIEW
9 for close tolerance to 10-32 socket head screws(x4)
0.125
DETAIL A
0.055
DETAIL A IN CROSS SECTION
0.352
SIDE VIEW
TITLE:
COVER PLATE
COMMENTS:
Figure 3.4
REVISION:
4
DATE:
6/10/97
MASSACHUSETTS INSTITUTE OF TECHNOLOGY
DRAWN BY:
DANIELLE TARRAF

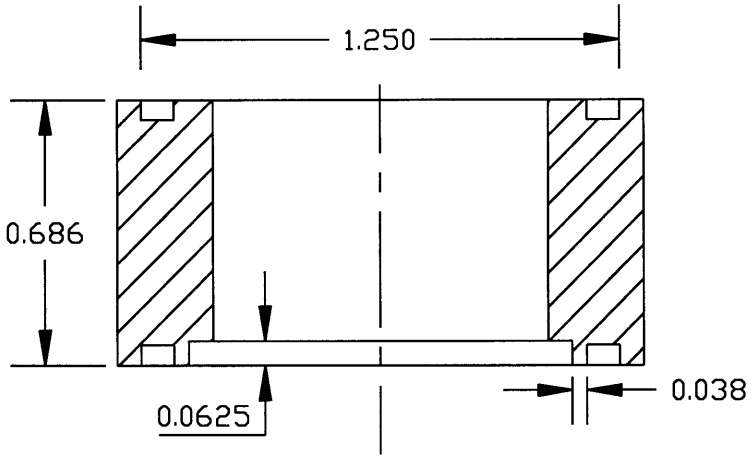

SECTION A-A

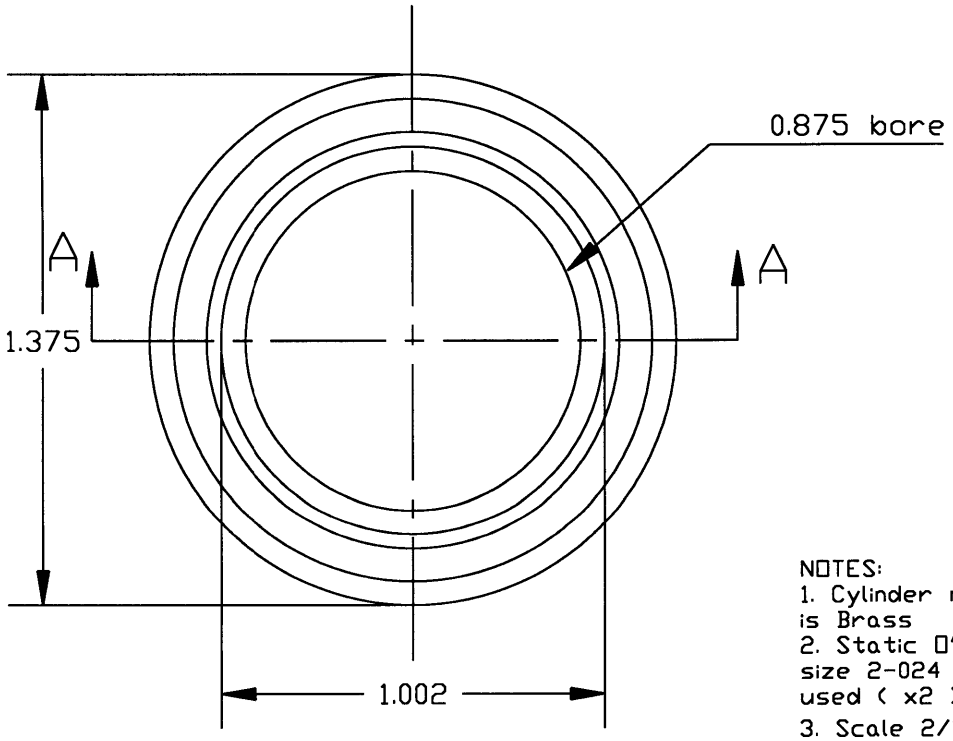

NOTES:
1. Cylinder material is Brass
2. Static O'rings size 2-024 are used (x2)
3. Scale 2/1

BOTTOM VIEW

TITLE: CYLINDER		
COMMENTS: Figure 3.5	REVISION: 4	DATE: 6/10/97
MASSACHUSETTS INSTITUTE OF TECHNOLOGY	DRAWN BY: DANIELLE TARRAF	

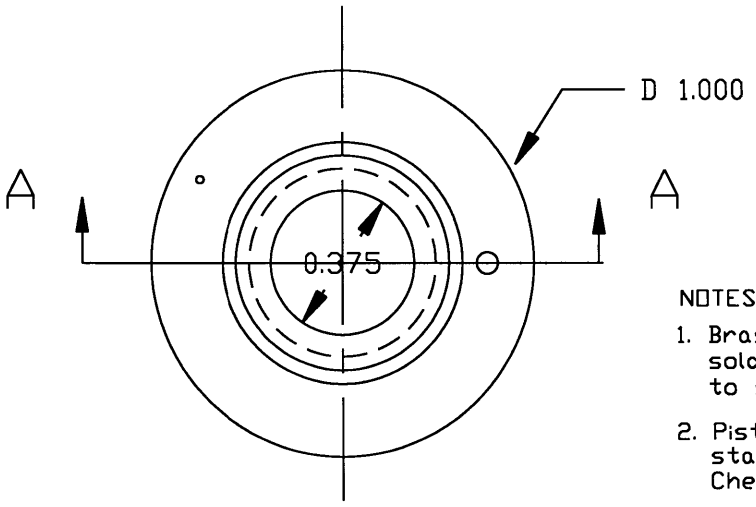

TOP VIEW

NOTES :

1. Brass ring, silver soldered and turned to size
2. Piston liner tube stainless steel,5/8" O.D. Check and turn to fit
3. Scale 2/1
4. Brass fitting silver soldered

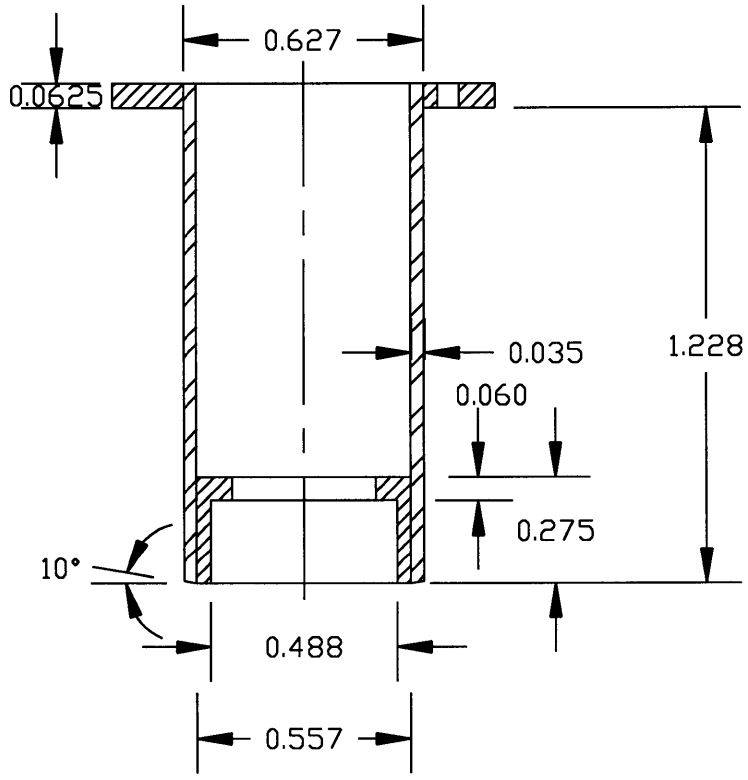

SECTION A-A

TITLE: PISTON LINER			
COMMENTS: Figure 3.6		REVISION: 4	DATE: 6/10/97
MASSACHUSETTS INSTITUTE OF TECHNOLOGY		DRAWN BY: DANIELLE TARRAF	

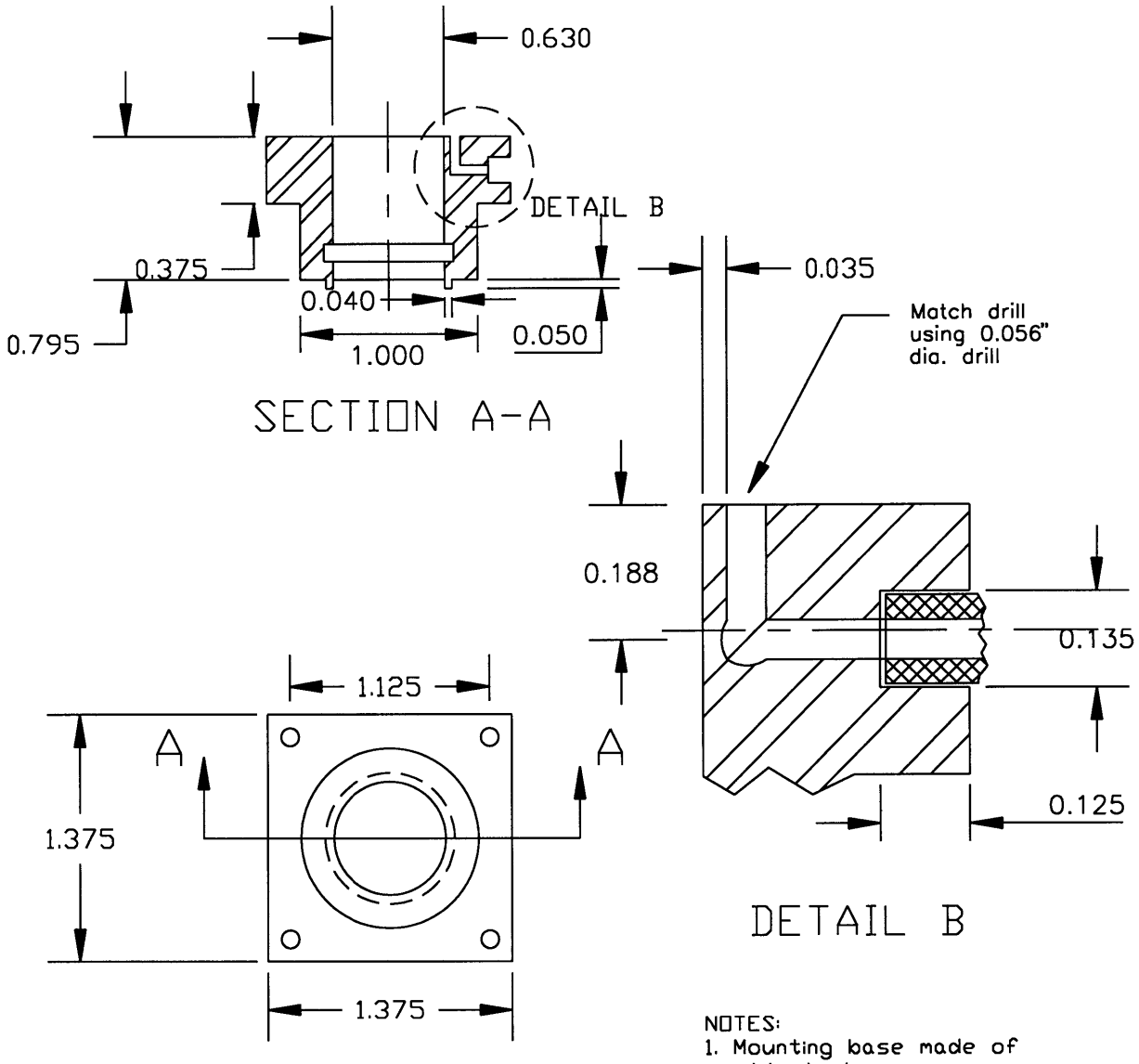

NOTES:
1. Mounting base made of mild steel
2. Bolt holes (x4): Drill and tap using #21 tap drill
3. Valve fitting: Stainless steel tube, 1/8" O.D., 0.035" wall thickness
4. Bottom and sectional views shown to scale. Detail B shown magnified 4x

TITLE: MOUNTING BASE		
COMMENTS: Figure 3.7	REVISION: 4	DATE: 6/10/97
MASSACHUSETTS INSTITUTE OF TECHNOLOGY	DRAWN BY: DANIELLE TARRAF	

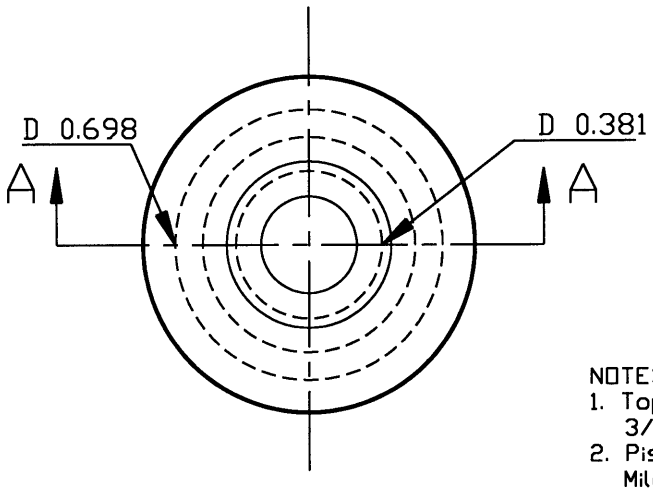

TOP VIEW

NOTES:
1. Top bore: ream to 3/8 "
2. Piston material: Mild steel
3. Piston O'ring sizes: 2-115 (Top) 2-110 (Bottom)
4. Scale 2/1

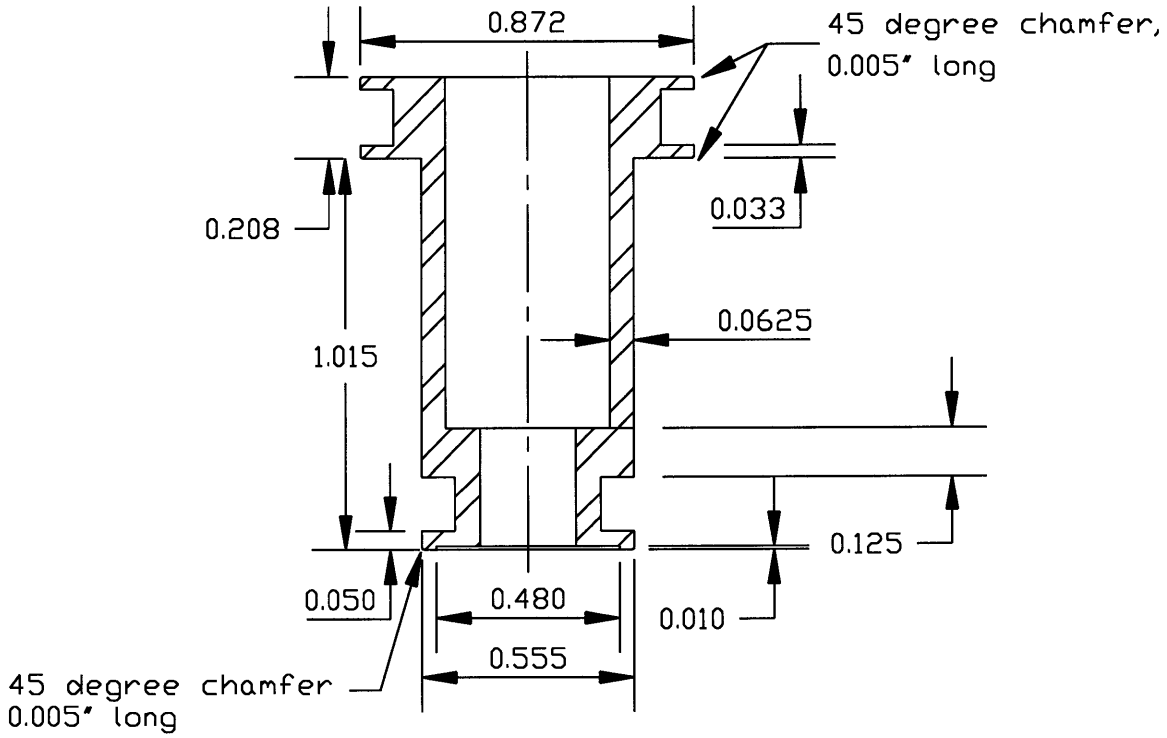

SECTION A-A

TITLE: PISTON		
COMMENTS: Figure 3.8	REVISION: 4	DATE: 6/10/97
MASSACHUSETTS INSTITUTE OF TECHNOLOGY	DRAWN BY: DANIELLE TARRAF	

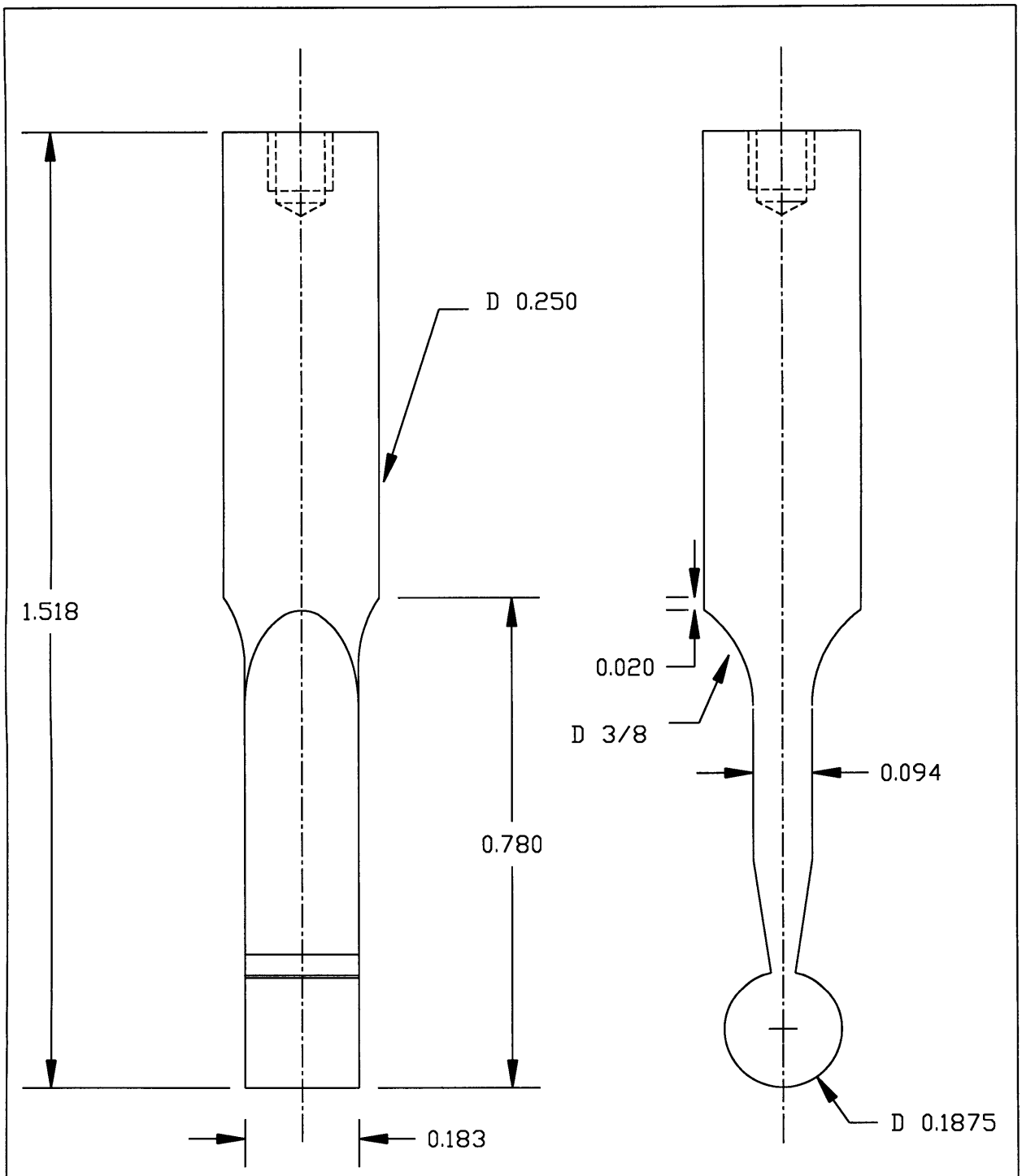

NOTES:
1. Scale is 4/1
2. All dimensions in inches, angle in degrees
3. x depends on the height of the Belleville washer

TITLE: LIFTING STEM		
COMMENTS: Figure 3.9	REVISION: 4	DATE: 6/10/97
MASSACHUSETTS INSTITUTE OF TECHNOLOGY	DRAWN BY: DANIELLE TARRAF	

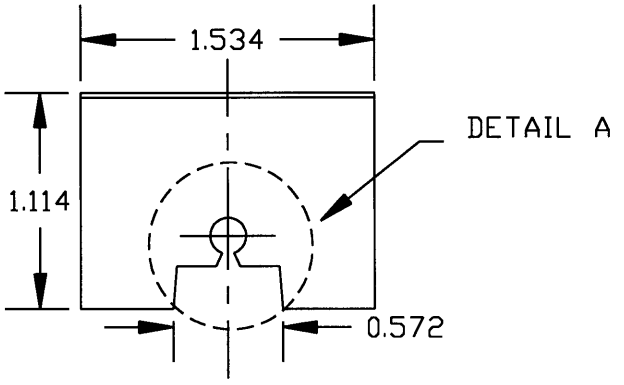

FRONT VIEW

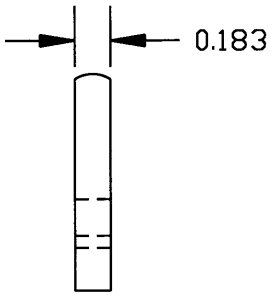

SIDE VIEW

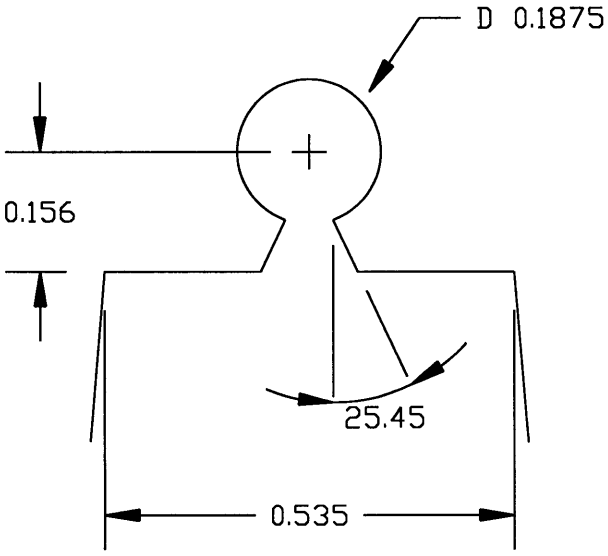

DETAIL A

NOTES:

1. Front and side views drawn to scale. Detail A scale 4/1
2. All dimensions in inches, angle in degrees

TITLE: VANE MODIFICATIONS		
COMMENTS: Figure 3.10	REVISION: 4	DATE: 6/10/97
MASSACHUSETTS INSTITUTE OF TECHNOLOGY	DRAWN BY: DANIELLE TARRAF	

NOTES:
1. Weld preparation: cut 0.044" radially into bolted shell to get a 1" diameter flat circular surface
2. Use size 2-016 static O'ring

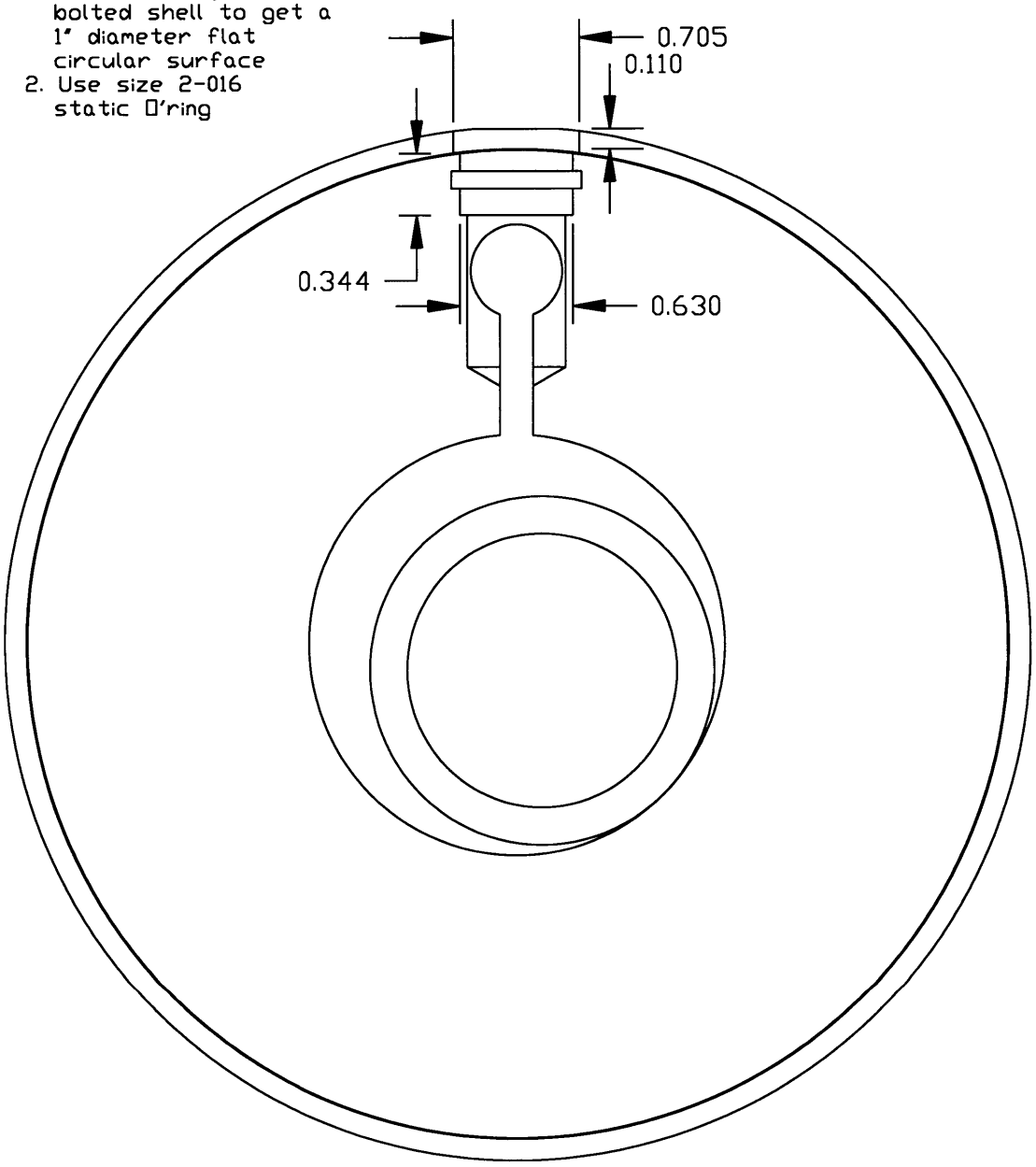

Shown to scale

TITLE: COMPRESSOR MODIFICATIONS		
COMMENTS: Figure 3.11	REVISION: 3	DATE: 6/5/97
MASSACHUSETTS INSTITUTE OF TECHNOLOGY	DRAWN BY: DANIELLE TARRAF	

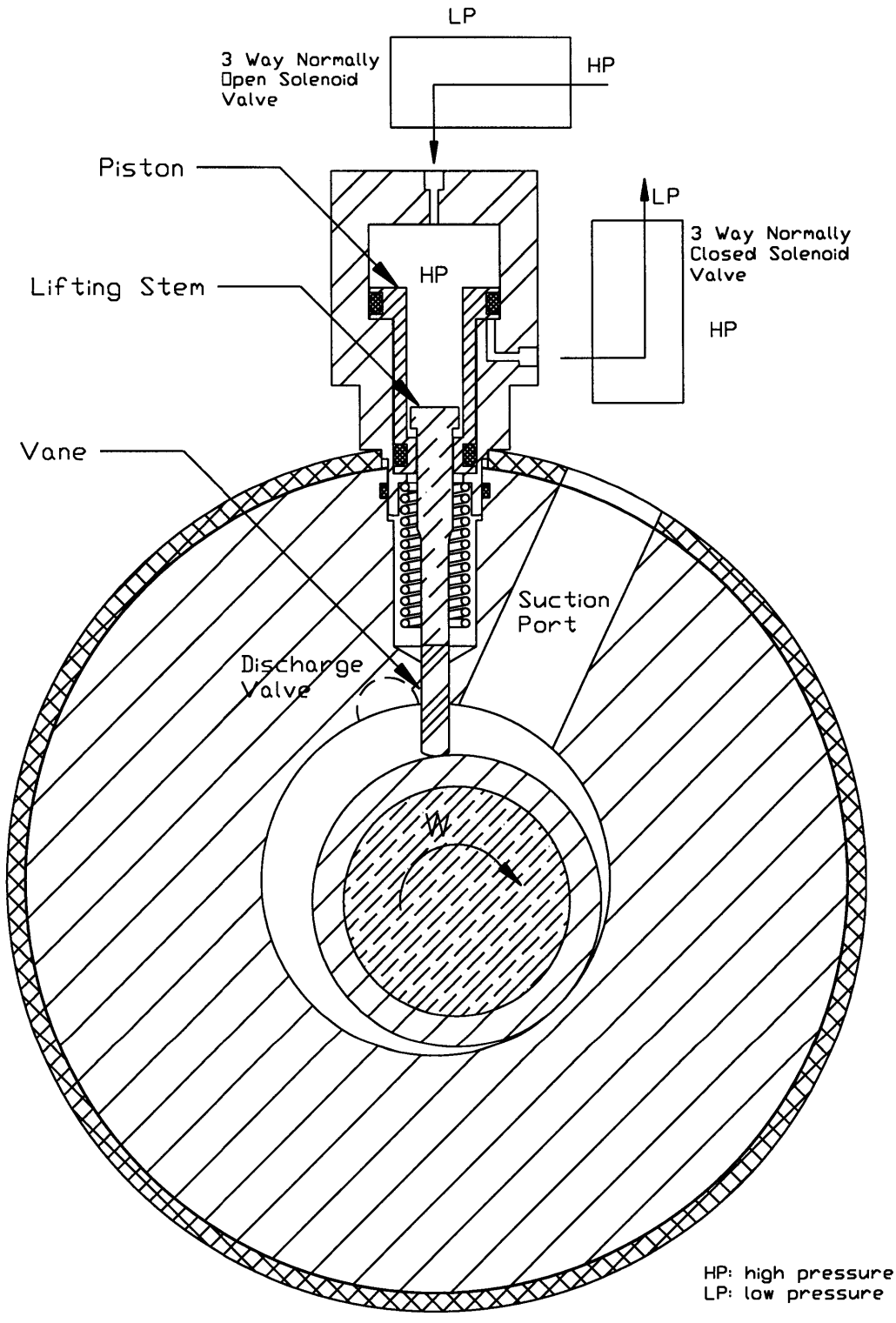

Figure 3.12

SHOWN:
Normal Operation

VARIABLE CAPACITY COMPRESSOR

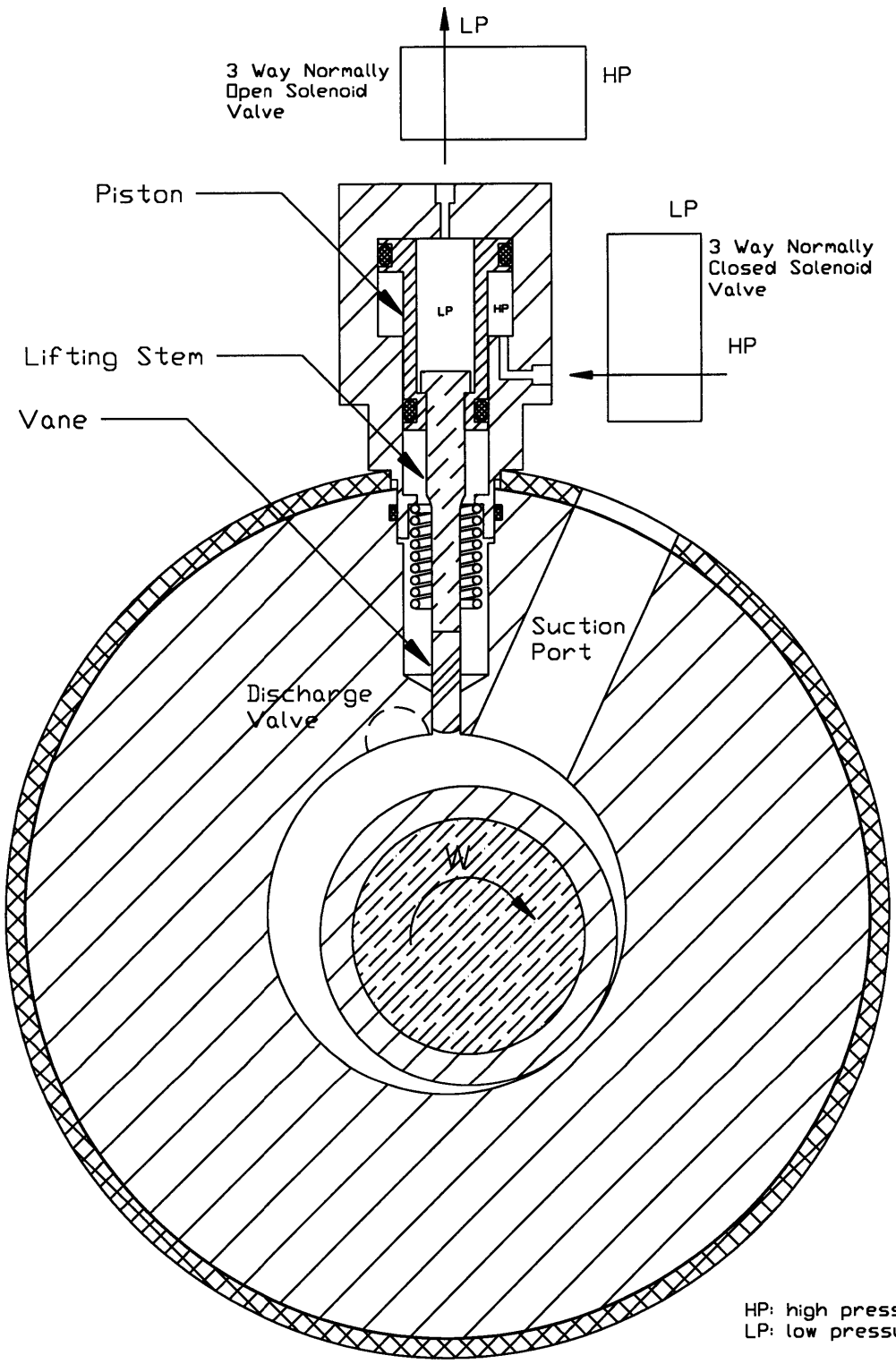

Figure 3.13

SHOWN:
Unloaded with Vane Lifted

VARIABLE CAPACITY COMPRESSOR

3.3 Construction of a Prototype Mechanism

In a real system, the pump and the driving motor are placed in a hermetically sealed shell. For the purpose of building a prototype, a bolted shell compressor was provided by Carrier. Essentially, the bolted shell is very similar to the hermetically sealed shell design shown in Figure 1.1. The main difference lies in that the shell consists of two flanged parts, almost equal in size. The top and bottom parts can be bolted together along a horizontal plane at about shell mid-height. Thus, such a compressor is easy to take apart and modify.

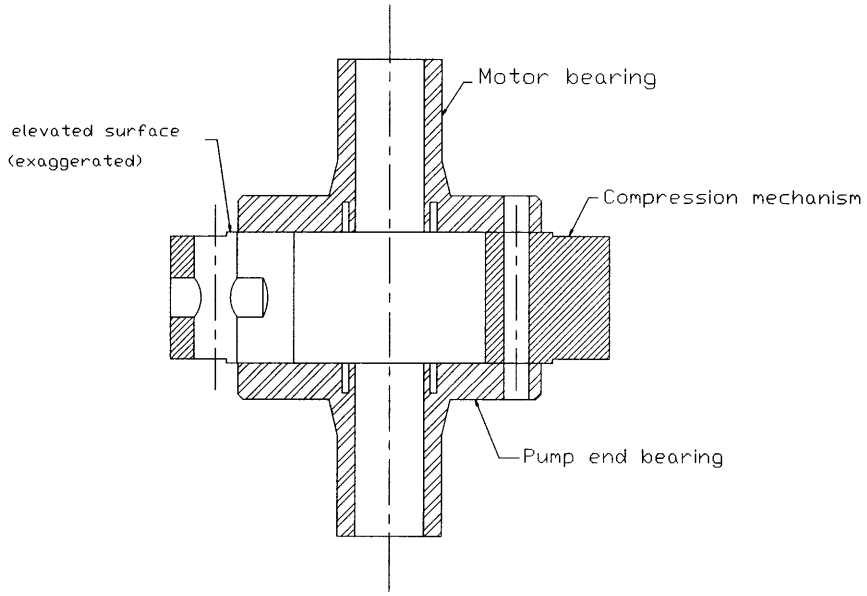

Figure 3.15: Sectional view of the compression mechanism and bearings (some details omitted)

As shown in Figure 3.15, the top and bottom faces of the pump are not flat. A concentric circular part rises slightly above the rest of the surface on either side of the pump. This elevated surface is precision machined to mount the pump and motor end bearings via screws. The rest of the surface is rough. The vane guide extends beyond the bearings, and thus comes into contact with fluid at discharge conditions.

In order to seal off the space behind the vane from the rest of the system, some work had to be done on the pump surfaces and the two bearings. The top and bottom faces were end milled to form a flat surface. The top and bottom bearings were correspondingly milled to form a flat edge along a chord (Figure 3.16). Two rectangular pieces of steel were cut to appropriate size and their surfaces were milled flat. Each piece was then attached to the pump by four vertical screws and to the bearing by two long horizontal screws.

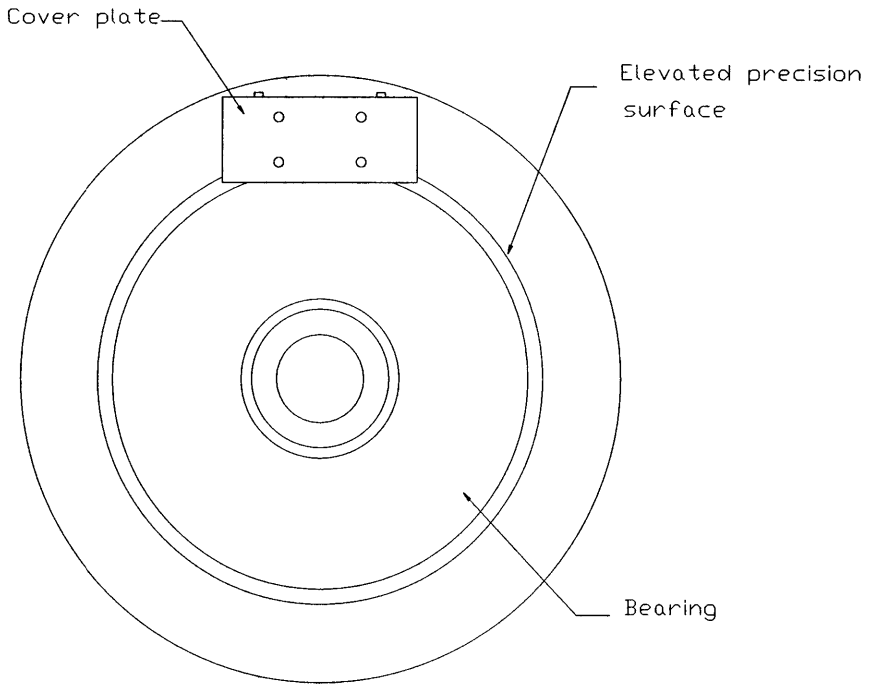

Figure 3.16: Top view of pump and one bearing after addition of sealing cover plate (some details omitted)

Further work was done on the pump before it was repositioned in its shell. As shown in Figure 3.11, the cylindrical space above the vane was drilled out to match the outside diameter of the piston liner. An O'ring groove was then cut into this new surface with a boring head in the milling machine.

The next step was to make the components. As mentioned earlier, whatever material available in the shop were used. All parts were made using traditional cutting tools (milling machines, drills, etc...). The only exception was the vane, because of its hardness. A CNC abrasive water jet cutter was used. No manual programming was required. Instead, the .dxf format version of the vane AutoCAD drawing was fed into the CNC computer.

To mount the mechanism on the compressor, a hole was cut in the shell. Some problems were encountered with the radial and horizontal alignment of the drill bit with respect to the compressor. Alignment was done manually. Then, a flat surface was machined into the shell, to mount the mounting base (see Figure 3.11). The base was carefully welded to the compressor shell at its top and bottom contact points with the flat surface and seal welded on the inside diameter to the shell. The mechanism was then assembled in reverse order in which the components were described. The prototype was now ready for testing.

Chapter 4

Prototype Testing

The variable capacity concept that was implemented and the prototype mechanism that was constructed were experimentally evaluated. A series of tests were carried out over a span of several months. Each test or group of tests aimed at answering a particular set of questions. These tests are the subject of this chapter.

The format of the chapter is simple; All the questions requiring answers are listed. The tests done are discussed in chronological order. For each test group, the experimental setup is described and the test procedure is explained. Relevant data is presented and conclusions are drawn.

4.1 Purpose of the Experiments

A variety of tests were performed on different levels, ranging from component tests to system tests. Each experiment was designed and carried out with one or several goals in mind. The most prominent questions that the experiments aimed at answering are:

- Can the solenoid valves reverse the pressure as anticipated?
- Can the mechanism load and unload the vane as designed?
- Does the mechanism affect the performance of the compressor under normal operation?
- For a given set of operating conditions, how bad is impact during loading? Unloading?
- When placed in a system, can the modified compressor achieve variable capacity operation?
- What system parameters constitute the determining factors in setting cycle times during variable capacity operation?
- What is the viable range of cycle times, based on these parameters?
- What is system performance like under various variable capacity operation modes?
- How can system performance be improved?

The tests were designed to answer the questions in the order listed. However, no perfect

mapping exists between the questions and the experiments. Most tests tackled more than one question. Some overlap occurred in the sense that some questions were tackled by more than one experiment.

4.2 Preliminary Testing of the Components

Before the solenoid valves were mounted on the prototype, they were tested to make sure they function. They were connected to a small air cylinder. The high pressure fluid was provided by a shop compressed air line while the low pressure fluid used was atmospheric air. A 24 volt DC power supply was used for power. The piston could be seen to move when the power supply switch was turned on and off. Both solenoids could be heard clicking.

It was decided to use a simple solid state electronics timer to control the operation of the solenoid valves. The on and off times of the timer can be manually set by means of two dials. The timer acts as a switch in the power circuit between the solenoid valves and the 24 V DC power supply. The solenoid valves were wired to the timer such that in the default setting (timer off), the circuit is broken. Hence, the solenoids are de-energized. When the timer is on, the circuit is closed, thus energizing the solenoid valves.

The timer was tested alone and in conjunction with the solenoid valves. It was observed that as cycle times became shorter, timer repeatability suffered. For instance, cycle times of the order of 5 seconds were found to be repeatable within a 10% margin.

Finally, the solenoid valves were mounted on the modified compressor. They were connected to the timer and the power supply. The compressor shell was left open. A mock test was done using pressurized Freon and atmospheric air in the high and low pressure lines to the solenoid valves. The mechanism seemed to be working properly, cyclically holding up and letting go of the vane.

After these preliminary tests, the compressor was ready for the next stage of testing on a de-superheater loop test stand.

4.3 Compressor Test Stand Experiments

4.3.1 Experimental Setup

The de-superheater loop compressor test stand used is shown in Figure 4.1. The flow of refrigerant (and entrapped oil) in the system is indicated by the sense of the arrows. The relative elevation and size of the components is preserved intact in this schematic, as this would prove to be of importance later on. Thus, the heat exchanger, the liquid receiver

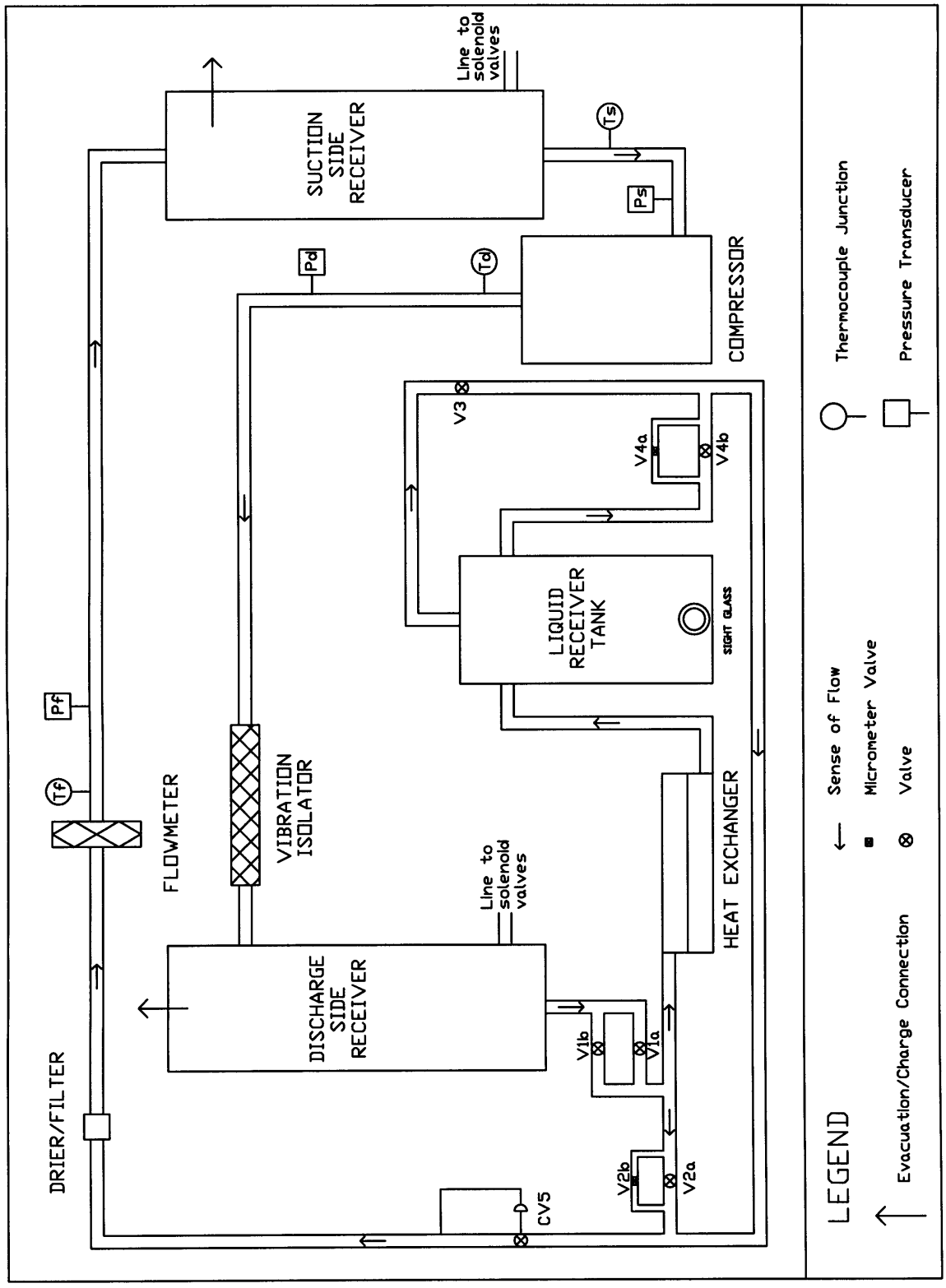

Figure 4.1: Schematic diagram of the compressor test stand

tank and the compressor are all seated at the same level on the test stand. Valves V1a and V1b are adjustment valves in the high pressure line. Closing either or both of them causes the pressure in the discharge line to increase and vice versa. Two valves are used for coarse and fine adjustment, as is the case with other valve pairs in this circuit. Valves V2a and V2b are the heat exchanger bypass valves. Valve V3 is the vapor valve out of the receiver tank. Valves V4a and V4b are the liquid line valves out of the receiver tank. A siphon system is used to retrieve liquid (refrigerant mixed with oil) from the bottom of the tank. CV5 is the suction pressure regulator valve. Most of the throttling takes place across this valve.

The test stand is equipped with a flowmeter to measure flow rate upstream of the compressor suction side. Three thermocouple junctions are used to indirectly monitor the temperature of refrigerant at suction, discharge and near the flowmeter. Voltage readings from the thermocouple circuit are displayed and need to be converted manually to temperature measurements. Pressure transducers allow pressure to be monitored at similar locations. Finally, a digital meter is hooked up to the compressor power supply line. It measures instantaneous current and voltage as well as power consumed by the compressor.

4.3.2 Experimental Procedure

The modified compressor was filled with 668 ml of oil, bolted shut, and placed in the test stand. The system was charged with 5 lb. and 2 oz. of refrigerant. The compressor was then turned on, along with the required water pump for water flow in the heat exchanger. The valves were adjusted to bring the system to near ARI operating conditions. A set of data readings were taken. During this time, the system was running stable and only required minor fine adjustments.

A complete set of data readings consists of the following measurements:

- Ambient conditions (temperature and pressure).
- Temperature and pressure of refrigerant at suction and discharge from the compressor.
- Voltage and current in the power line and power consumed by the compressor.
- Flowmeter data consisting of pressure (P_f) and temperature (T_f) of fluid at the flowmeter, in addition to a frequency reading by the flowmeter (F).

The ultimate aim of these readings is to determine the system EER. EER is a performance evaluation parameter commonly used for air-conditioning systems. EER compares the cooling capacity of the system in BTU/hr to its power consumption in Watt. Essentially, the EER is thus a dimensional coefficient of performance.

$$EER = \frac{Q_{cooling}}{P_{in}} \tag{4.1}$$

Due to the modesty of the test apparatus used, system conditions cannot be accurately

controlled. Hence, some discrepancy always exists between the actual testing conditions (denoted by the subscript 'test') and the desired testing conditions (denoted by the subscript 'des'). Hence, before any comparison can be made, the measured EER at the test conditions has to be corrected to its corresponding value at the nearby desired testing conditions.

The test condition is expected to be close to the desired condition. Thus, the compressor efficiency, η, can be assumed constant.

$$\eta_{test} = \eta_{des} \Rightarrow \left(\frac{\dot{W}}{\dot{W}_{rev}}\right)_{test} = \left(\frac{\dot{W}}{\dot{W}_{rev}}\right)_{des}$$

$$\left(\frac{\dot{W}/m}{\dot{W}_{rev}/m}\right)_{test} = \left(\frac{\dot{W}/m}{\dot{W}_{rev}/m}\right)_{des} \tag{4.2}$$

W stands for the rate at which work is done to drive the compressor. m is the refrigerant mass flow rate. The subscript 'rev' refers to a reversible process.

Consider a vapor compression refrigeration cycle. Let subscripts 1 and 2 refer to compressor suction and discharge, respectively. Subscript 3 denotes conditions at exit from the condenser. Subscript 4 denotes conditions at evaporator inlet. The First Law of Thermodynamics applied to a control volume is:

$$\frac{dE}{dt} = Q - \dot{W} + m_{in}h_{in} - m_{out}h_{out} \tag{4.3}$$

dE/dt is the time rate of change of energy of the system. Q is the rate of heat transfer, and $\dot{W}$ is the rate of work done. The sign convention adopted is such that the heat transferred into the system and the work done by the system are positive. m is the mass flow rate and h is the enthalpy. Subscripts in and out refer to the mass flow into and out of the system, respectively.

First Law applied to the evaporator at steady state gives:

$$Q_{cool} = m(h_1 - h_4) \tag{4.4}$$

Starting from the definition of EER, and keeping in mind that power is the rate of doing work:

$$(EER)_{des} = \frac{(Q_{cool})_{des}}{(P_{in})_{des}} = \frac{m_{des}(h_1 - h_4)_{des}}{(P_{in})_{des}} = \frac{m_{des}(h_1 - h_4)_{des}}{\dot{W}_{des}}$$

$$(EER)_{des} = \frac{(h_1 - h_4)_{des}}{(\dot{W}/m)_{des}} \tag{4.5}$$

Based on the assumption of constant compressor efficiency, and making use of equation 4.2, we get:

$$(EER)_{des} = \frac{(h_1 - h_4)_{des}}{(\dot{W}/m)_{test}} \cdot \frac{(\dot{W}_{rev}/m)_{test}}{(\dot{W}_{rev}/m)_{des}}$$

$$(EER)_{des} = m_{test} \cdot \frac{(h_1 - h_4)_{des}}{(P_{in})_{test}} \cdot \frac{(\dot{W}_{rev}/m)_{test}}{(\dot{W}_{rev}/m)_{des}} \tag{4.6}$$

Applying the First Law of Thermodynamics to the compressor at steady state, assuming adiabatic reversible (isentropic) compression process, gives the magnitude of reversible work done per unit mass:

$$\frac{\dot{W}_{rev}}{m} = (h_{2,s} - h_1) \tag{4.7}$$

Replacing equation 4.7 in equation 4.5:

$$(EER)_{des} = m_{test} \cdot \frac{(h_1 - h_4)_{des}}{(P_{in})_{test}} \cdot \frac{(h_{2,s} - h_1)_{test}}{(h_{2,s} - h_1)_{des}}$$

$$(EER)_{des} = \left(\frac{h_1 - h_4}{h_{2,s} - h_1}\right)_{des} \cdot \left[\frac{m(h_{2,s} - h_1)}{P_{in}}\right]_{test} \tag{4.8}$$

Let G be a correction factor for a given desired state:

$$G = \left(\frac{h_1 - h_4}{h_1 - h_{2,s}}\right)_{des} \tag{4.9}$$

Thus, the EER at any desired condition can be calculated based on test data of some other close operating condition, using the equation:

$$(EER)_{des} = G \cdot \frac{m_{test}(h_{2,s} - h_1)_{test}}{(P_{in})_{test}} \tag{4.10}$$

Obviously, the value of G depends on the desired condition. In particular, G was calculated for the ARI and CHEER testing conditions to be 4.829 and 8.166 respectively.

The measured properties of the fluid at the flowmeter are input into a computer program,

REFPROP. REFPROP can calculate the thermodynamic properties of a number of refrigerants at any thermodynamic state within a given range. The dynamic viscosity (μ) and the density (ρ) of the refrigerant are read off from this program; The ratio μ/ρ determines the kinematic viscosity of the fluid (ν). The mass flow rate of the refrigerant (m) can be calculated from the frequency measurement (F), the density, and a calibration factor K which depends on the ratio (F/ν). REFPROP is used once again to determine the enthalpy of fluid at suction (h_1) and at discharge assuming the compression process to be isentropic ($h_{2,s}$). Thus, the EER of the system can be determined by equation 4.10, using the appropriate value of G.

4.3.3 First Set of Experimental Data

The purpose of this experiment was to evaluate the extent of the detrimental effect, if any, that the mechanism has on the compressor. Four sets of test data were taken at ARI conditions. The data was compared to data from a similar set of tests dine earlier on the same compressor at Carrier testing facilities. Table 4.1 summarizes the results of the four tests done. The data provided by Carrier is also shown for the sake of comparison. A sample data sheet, showing the calculations done, is found in Appendix C.

Table 4.1: Pre and Post modification test results at ARI conditions

The standard deviation is the square root of the 'n-1' sample variance, given by: $SD = \sqrt{\frac{1}{n-1}\sum_{i=1}^{n}(x_i - \bar{x})^2}$: x is the i^{th} sample value, $\bar{x}$ sample mean and n number of samples

	Test 1	Test 2	Test 3	Test 4	Average	Std. Dev
pre-modification tests (Carrier)						
m (lbm/hr)	340.2	337.2	337.2	338.4	338.3	1.4
Pin (Watt)	2182	2181	2179	2180.8	2180.8	1.3
EER (BTU/W-hr)	10.53	10.45	10.44	10.48	10.48	< 0.1
post-modification tests (MIT)						
m (lbm/hr)	345.6	347.0	349.6	346.5	347.2	2.6
Pin (Watt)	2288	2287	2292	2305	2293	5.1
EER (BTU/W-hr)	10.54	10.58	10.65	11.57	10.84	0.5

The standard deviation of the data taken at MIT is clearly higher than the corresponding

Carrier tests. This inferior repeatability is probably due to the use of less sophisticated instrumentation and coarser controls.

The compressor EER is slightly higher after modifications. At first glance, compressor performance seemed to improve. However, positive conclusions shouldn't be drawn too fast because the testing conditions were not exactly replicated: The mass flow rate and input power were slightly different in the pre and post modification tests. The suction and discharge conditions were probably different as well. The location of the pressure and temperature transducers in the test stand was somehow arbitrary; It did not match exactly the locations in the pre-modification test.

In view of the above uncertainties, and owing to the modesty of the test stand and instrumentation used, only a very conservative conclusion can be drawn based on these test results: The presence of the mechanism does not seem to significantly degrade the performance of the compressor, as reflected by the EER.

After this first set of data was taken, the compressor was left running at ARI conditions for approximately 90 hours. Minor adjustments were required to keep it at the same operating conditions. The purpose was to run in the compressor prior to taking another set of data readings under similar conditions. Unfortunately, the planned set of measurements wasn't taken as planned. The compressor stopped and refused to start up. Disassembly revealed that the compressor had run dry of oil; only about 3/8 in. deep oil was left in the oil sump. The rolling piston was jammed on its bearing and score marks could be distinguished all around its surface near one end. Small metal chips were found in the compressor, and additional score marks could be seen on the inner cylinder wall and on the surfaces of the pump and motor end bearings.

A very crude calculation was done to determine how long it would take the compressor to empty of oil, assuming that all the oil leaving the compressor is not returned. The mass flow rate of oil entrained is assumed to be 1% that of the refrigerant. The average mass flow rate of fluid, 347.2 lbm/hr, is used. Hence, the oil mass flow rate is around 3.5 lbm/hr. The compressor was filled with 668 ml of oil, equivalent to 0.0236 ft.^{3}. No data was available for oil density. An unopened container, holding 3.78 liters of oil, was weighed to be 7.3 lbm. Neglecting container weight (the container is made of very thin plastic), the density was estimated to be around 54.7 lbm/ft.^{3}. The time required is then:

$$\Delta T = \frac{V_{oil}}{\dot{V}_{oil}} = \frac{V_{oil}}{\dot{m}_{oil}}\rho_{oil} = \frac{0.0236 ft^3}{3.5 lb/hr} \times 54.7 lb/ft^3 \approx 0.37 hours \approx 22 minutes$$

Given how small this number is, it is not at all surprising that the compressor ran out of oil after a relatively long time, if provisions were not adequately made to ensure that oil entrained with the refrigerant is returned to the compressor.

The compressor required some repairs. All its components were disassembled and carefully inspected for marks. Any high points found on the sliding surfaces were scraped and polished minutely by hand and then tested manually to make sure everything was running smoothly. The compressor was now ready for re-assembly.

4.3.4 Modified Experimental Setup

The de-superheater loop used for the first series of tests was unable to ensure proper oil return for long term trouble free operation. The major pitfalls of the test stand were predicted to be the following:

- The heat exchanger was placed on the table, at the same level as the liquid receiver tank. The fluid exiting the heat exchanger had to rise up about 1 foot to reach the top of the liquid receiver tank. Thus, it is expected that some liquid refrigerant, and hence some oil, collects in the heat exchanger.
- A siphon system was used to collect liquid refrigerant from the bottom of the liquid receiver tank. Hence, proper flow of liquid through the liquid line out of the receiver requires that a minimum pressure difference be maintained, in addition to a sufficient amount of liquid at the bottom of the receiver. A large temperature drop could be felt across valve CV5, which meant that a lot of throttling occurred there, and only a small pressure drop occurred across valves V4a and V4b. The lack of sufficiently low downstream pressure could have impaired the functioning of the siphon. Additionally, it could be observed through the sight glass on the side of the liquid receiver tank that the liquid level sometimes fell dangerously low.

Minimal adjustments were made to the test stand, based on the above guidelines and the need to minimize liquid presence anywhere in the system except in the liquid receiver tank. The resulting modified test stand is shown in Figure 4.2. As in the previous schematic, the relative elevation of system components is relevant. The heat exchanger was placed on a stand, elevated above all other components. This ensures that all the liquid refrigerant and oil dribble back into the liquid receiver tank. The liquid valves, V4a and V4b, were also elevated. The hot gas bypass line was connected as close as physically possible to the liquid valves and the throttling valve (CV5) was placed just downstream. This ensures better siphoning action by forcing lower pressures at valve outlets. A fourth pressure transducer was placed upstream of CV5, to monitor the pressure drop across the valve. The system can be adjusted such as to split the throttling effect between valves V4 and CV5. Practically, the pressure upstream of the low pressure regulator was kept 20 to 30 psi above suction. The filter/drier was replaced by a new one with bigger O.D. (5.8 in.). The test stand was now run with valve V3 fully closed at all times.

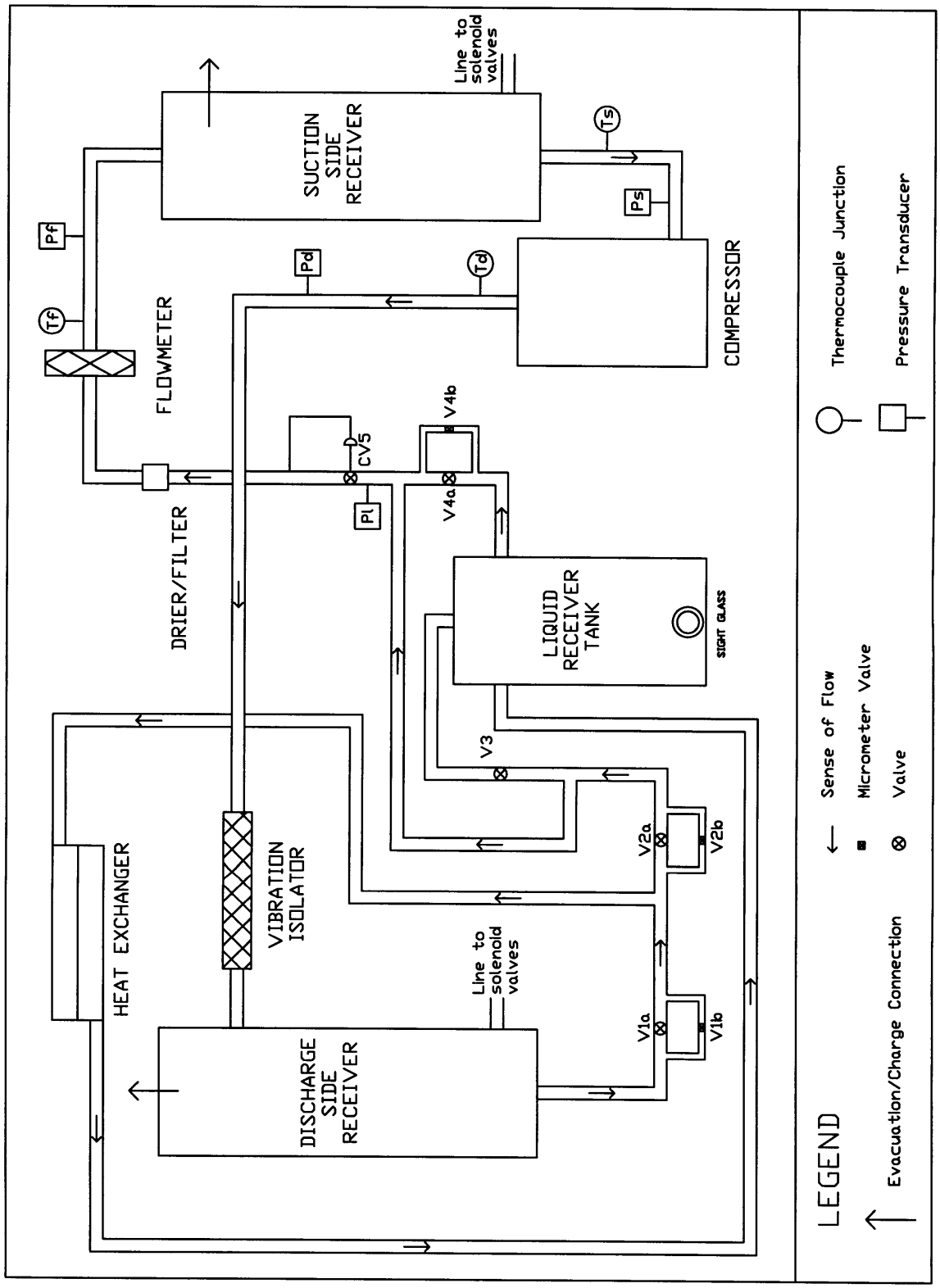

Figure 4.2: Schematic diagram of the compressor test stand after modifications

4.3.5 Second Set of Experimental Data

The compressor was installed in the modified de-superheater loop and the system was charged with 4 lb., 1 oz. of refrigerant. The valves were adjusted to bring the system to ARI conditions. As before, a set of four data readings were taken. The results are summarized in Table 4.2.

Table 4.2: Modified compressor test results at ARI conditions, modified test stand used

	Test 1	Test 2	Test 3	Test 4	Average	Std. Dev.
m (lbm/hr)	347.8	347.0	345.3	345.5	346.4	1.2
Pin (Watt)	2306	2297	2301	2298	2300.5	4.0
EER (BTU/W-hr)	10.47	10.49	10.43	10.45	10.46	<0.1

A slight improvement in repeatability is observed in comparison with the first series of tests. The calculated EER values are quite close to their pre-modification values. Again here, the only safe conclusion that can be drawn is that system performance does not significantly suffer because of the addition of the mechanism. Also, the compressor did not seem to be negatively affected by the "oil loss accident".

4.3.6 Variable Capacity Tests

The next step was to check whether the mechanism can perform the function for which it was designed: to unload the vane thus decreasing compressor capacity. The system was brought to CHEER operating conditions. The timer was set to cycle at approximately 30 seconds on and 30 seconds off. The timer was then powered. The vane could be heard rattling while it loaded and unloaded. Various parameters could be observed to vary between loaded and unloaded operation. The power consumption, for instance, dropped from around 1600 Watts during normal operation to around 425 Watts when the system was unloaded. The frequency reading of the flowmeter dropped by a factor of 20 or more. Correspondingly, the mass flow rate, which goes in proportion to F^2, must have dropped by a factor of 400 at least. The general trend observed during the unloaded phase was that suction pressure continuously rose while discharge pressure continuously dropped. Suction temperature was observed to increase during the unloaded phase.

A crude attempt was made to quantitatively measure and record the impact that occurs upon transition between loaded and unloaded operation. An oscilloscope was hooked up to an accelerometer. The accelerometer was attached to the outer wall of the bolted shell, next to the vane lifting mechanism. Thus, it could pick up vibrations of the compressor housing. The signal on the oscilloscope display showed small amplitude vibrations due to

the running motor. Additionally, five spikes could be seen upon loading and seven upon unloading. The natural frequency of the signal seemed to be around 3.8 kHz. The spikes definitely represented impact. The impact was most likely between the vane and the rolling piston. However, it could have also been between the mechanism piston and its housing. The measurement method used could not distinguish between the two. This rough experiment seemed to indicate that impact was not a big problem, except maybe for fatigue considerations and external noise from the compressor.

The compressor test stand is designed to test the steady state operation of a compressor. It cannot be used in modeling or predicting the interaction of the compressor with a system. Hence, the compressor was removed from the test stand and placed in a system. Further tests were performed, and that is the subject matter of the next section.

4.4 System Experiments

4.4.1 Experimental Setup

A 3 ton Carrier air -conditioning unit was used for the system experiments. The original scroll compressor was removed from the unit. It was replaced by the modified compressor with prototype mechanism. Obviously, the system was oversized for the compressor.

A schematic of the system and its setup is shown in Figure 4.3. Each of the rooms shown is a 9' x 7.5' x 7.5' cubicle with dry walls and wooden doors.

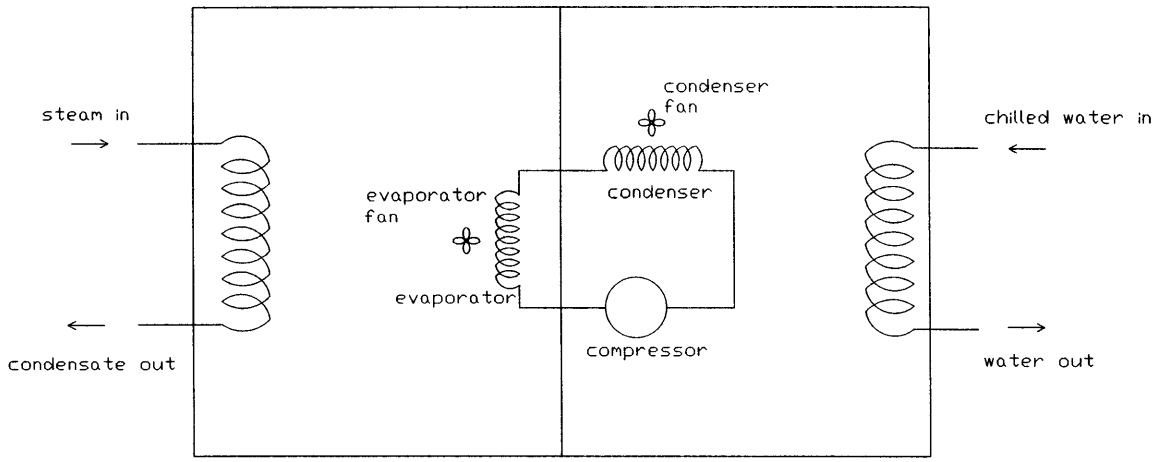

Figure 4.3: Experimental system setup

The compressor is found in the warm room, along with the condenser and the condenser fan. Chilled water is passed through a heat exchanger in the room. Its function is to absorb heat dumped by the system into the room. In the absence of chilled water, the temperature

of the room would rise very quickly, due to its small thermal capacity. The rate of flow of chilled water can be monitored and manually regulated by a flowmeter and valve placed outside the room.

The room containing the evaporator and the evaporator fan is the cold room. Steam is passed through a heat exchanger in the room to warm it up. The steam flow rate can be adjusted by a series of control valves mounted on the steam line outside the room. The steam, having lost heat to the room, exits as liquid condensate. The amount of condensate can be used as an approximate measure of system cooling capacity once steady state operation has been reached.

Four thermocouple junctions were installed in the two rooms. One thermocouple measures the temperature of the air at evaporator inlet. This value is a good measure of the air temperature in the cold room. Another thermocouple measures the temperature of the air exiting the evaporator, downstream of the evaporator fan. The remaining two thermocouples measure the same quantities on the condenser side. The thermocouples were hooked up to four channels of an Omega bench thermometer. Thus, the temperatures could be read off the display, one at a time. At this stage, no means were available to track the four temperatures simultaneously, or to record the data.

4.4.2 First Set of Experiments and Results

During the initial phase of system experiments, it wasn't quite obvious what to expect. For that reason, the first few experiments were quite coarse and somewhat ad hoc. As tests proceeded, the instrumentation and procedures were refined, based on feedback from the experiments.

The first experiment done was to verify that system capacity drops when the compressor is run in variable capacity operation mode. This experiment also gave some insight about system behavior.

The compressor was first run at full capacity (normal operation). The steam and chilled water flows were regulated to reach a given operating point. Once steady state was reached, the four thermocouple readings were recorded. Steam condensate was collected in a bucket over a period of time. The bucket was weighed. The weight of the empty bucket was subtracted from this number to get the weight of water. Water was assumed to have a latent heat of vaporization of 1000 BTU/lbm. Thus, the amount of heat absorbed by the steam in the heat exchanger could be approximated. The ratio of heat energy absorbed to the time taken to absorb it gives an estimate of system capacity. The same procedure was followed with the compressor cycling at equally long loaded/unloaded cycles.

During the first test, the cold room temperature was maintained at around 67°F. The air exiting the evaporator was around 56.5°F. The warm room temperature was around 82°F,

while the air exiting the condenser was at 98°F approximately. Note that all these temperatures are just approximate. Some fluctuations were observed throughout the experiment. The system capacity was estimated to be around 14,682 BTU/hr. This figure is significantly lower than the compressor nominal capacity (24,000 BTU/hr). This is due to several factors; The operating conditions affect the system capacity. The nominal capacity is only achievable for a given operating condition which was not matched in this experiment. Also, the mismatch between the sizing of the compressor and the system heat exchangers (condenser/evaporator) could have played a role.

For the variable capacity test, the timer was adjusted to load the vane for 29.5 seconds and unload it for 29.9 seconds. The basis for choosing these cycle times was simple. The evaporator and condenser time constants were guessed to be around 30 seconds. Thus, the cycle times were matched to that initial guess. The calculated system capacity seemed to drop to 4982 BTU/hr. During the experiment, the cold room air temperature seemed to cyclically vary between 60°F and 64.5°F. The warm room temperature seemed to vary between 83.6°F and 88.2°F. The air temperatures at exit from the evaporator and condenser varied between 53.7°F and 63.6°F for the former and 86.4°F and 99.4°F for the latter.

A considerable drop in measured system capacity seemed to accompany variable capacity operation. However, the capacity didn't drop by 50%, as would be expected given that the on time is equal to the off time. The average operating conditions were not identical. Also, the temperature fluctuations were significant. This could explain the discrepancy.

The bench thermometer used could only display the instantaneous measurement from one channel. Hence, the four temperatures couldn't be simultaneously monitored. Once steady state was reached, each channel was monitored over a few system cycles to determine the temperature range. Some effort was also made to manually monitor and record the instantaneous temperature data every two seconds. The approximate temperature profile could then be constructed. Obviously, that kind of measurement is plagued by various human errors. Thus it became quite obvious that some data acquisition system had to be used before the experiments could go any further.

By putting a hand downstream of the condenser fan, the air temperature could be felt to change during the second experiment. The air was perceivably getting cooler during the unloaded cycle and vice versa. Interestingly, the temperature of the air seemed to equalize before the end of a given phase. That is, a steep change could be felt during the first part of an unloaded phase. The change seemed to taper off during the remainder of the phase. The same observation was made during each loaded phase. A possible explanation would be that the heat exchanger characteristic times were shorter than the 30 seconds originally predicted.

The last relevant observation made during this experiment deals with noise. Every time the

vane was loaded or unloaded, it rattled, producing some noise. Both the previous tests and the analysis in Chapter 2 seemed to agree that the impact anticipated should not cause failure (Fatigue failure was not analyzed and is a valid possibility). However, the accompanying noise was quite annoying. Such noise level would probably be deemed unacceptable for domestic air-conditioning units.

An attempt was made to repeat the variable capacity test with slightly longer cycle times, of the order of 45 seconds per phase. During the last few seconds of each unloaded phase, the vane seemed to chatter significantly longer than usual (the noise would last around 7 or 8 seconds). As the experiment progressed, the chatter seemed to be getting longer in duration. The longest "chatter phase" recorded lasted around 12 seconds. After that, the system was shut of.

One possible explanation is the following: As the pressures in the condenser and the evaporator equalized during the unloaded phase, the pressure difference holding the mechanism piston dropped. Once the pressure difference plunged below some critical value, it wasn't enough to hold the piston, and thus the vane, lifted all the way. The vane probably bounced on the rolling piston until it was loaded again. This problem was not observed during the second test. The unloaded phase was probably too short to allow the pressure to equalize sufficiently to produce this effect.

The pressures were not monitored during this set of tests. Thus, there was no way to prove or disprove the above theory. However, one important observation was made: The air temperatures in the warm and cold rooms equalized at around 80°F towards the end of each unloaded phase.

4.4.3 Second Set of Experiments and Results

For the next two tests, the system setup was kept the same. However, the instrumentation was considerably altered. A data acquisition program developed by Dave Otten of the MIT Electromechanical Systems Lab. was used. It employs an RS-232 interface. It tracks and records compressor power consumption. It also measures the temperature and pressure of fluid at two locations. The first thermocouple/pressure transducer pair is found at condenser outlet. The conditions there are approximated to be compressor discharge conditions. The second pair is located at compressor inlet, upstream of the accumulator. The conditions approximate suction. The unmodified program could not measure room temperatures. Thus, it was decided to use the bench thermometer used previously to manually monitor and record the air temperatures in the cold room. Data readings were taken every 5 seconds, to make sure the system operates within a certain range.

Ultimately, the setup just described is not the optimal for our purposes. The fluid pressure transducers and thermocouples could have been better positioned. This setup had been used previously to test a scroll compressor. For lack of time, the same setup was used.

Two variable capacity tests were done. In one test, the cycle times were approximately 57s/48s loaded/unloaded. In the second test, the cycle times were approximately 29s/30s for the loaded and unloaded phases, respectively. The choice of cycle times is similar to the first set of tests.The aim was to experiment with different cycle durations and to observe how the system behaves. A summary of the relevant data is shown in Table 4.3 below. The average value cited is the time average.

Table 4.3: Test data for variable capacity tests, 57s/48s and 29s/30s loaded and unloaded cycles

	57s/48s			29s/30s		
	Minimum	Maximum	Average	Minimum	Maximum	Average
Compressor power (Watts)	353.07	1645.49	998.12	351.01	1698.23	970.71
Compressor suction pressure (psia)	73.8	133.1	97.9	82.3	144.4	111.8
Compressor discharge pressure(psia)	152.6	218.1	187.3	169.0	228.4	200.0
Compressor suction temperature (F)	47.1	104	56.9	66.0	73.1	68.3
Compressor discharge temperature (F)	81.3	91.3	87.0	88.3	94.0	91.0
Evaporator inlet air temperature (F)	60.91	67.20	63.64	60.95	65.25	63.24
Evaporator outlet air temperature (F)	53.65	66.47	58.93	54.10	63.98	58.47
Evaporator air temperature difference (F)	0.10	7.95	4.71	0.77	7.99	4.77

In the discussion that follows, the 57s loaded 48s unloaded will be referred to as the first test; the 29s loaded, 30s unloaded experiment will be referred to as the second test.

Water condensate was collected and measured as before to estimate system capacity. The estimated values for the two tests were 4967 BTU/hr and 12,450 BTU/hr for the first and second tests, respectively. The first value seems to agree with earlier tests. The second value is suspicious. It is probably due to some experimental error.

The rate of heat transfer from the cold room to the system, Q_{evap}, is given by: $m_{air}C_p\Delta T_{air,evap}$, where m_{air} is the mass flow rate of air across the evaporator and C_p is the constant pressure heat capacity. m_{air} is set by the evaporator fan, which runs continuously at constant speed in this setup. Also, the change in room temperature is small enough that C_p can be considered constant. Thus, the average temperature difference of air across the evaporator ($\Delta T_{air,evap}$) is a good measure of the refrigeration capacity of the system.

Based on the data collected, it seems that the system capacity was comparable in the two tests, within experimental error. This result is somewhat surprising, given the different proportion of load to unload times in the two experiments.

Four parameters characterize a load/unload cycle: time duration of the loaded phase (t_{on}), time duration of the unloaded phase (t_{off}), cycle time $t_{cycle}=t_{on}+t_{off}$, and ratio of loaded to unloaded time, $R=t_{on}/t_{off}$. Of these four parameters, only two are independent. Therefore, R and t_{cycle} will be chosen to characterize a given cycle. The values of the characteristic cycle parameters for the two tests done are given in Table 4.4 below.

Table 4.4: Characteristic cycle parameters for the two tests

	57s/48s test	29s/30s test
$R=t_{on}/t_{off}$	1.18	0.97
t_{cycle} (s)	105	59

A very simple model can be used to analyze system behavior: The system is assumed to operate at full capacity during the loaded phase. The capacity is assumed to drop to zero during the unloaded phase. In this case, the percentage system capacity (relative to full load) is given by:

$$\% \text{ Cap.} = \frac{R}{1+R} \times 100 \tag{4.11}$$

Based on this model, the percentage of normal operation capacity for the two experiments would be 54% for the first test and 49% for the second test. If the experimental data is correct, the results conflict with the model. The average air temperature across the evaporator is lower for the first test, indicating lower system capacity.

This discrepancy may be due to experimental errors. It may also indicate that the model is too simplified to correctly predict system behavior. The ratio of on/off time is certainly a significant parameter. But it may not be the only one. The heat transfer coefficient of the evaporator depends on the state of the heat exchanger. The state of the heat exchanger

changes during each phase. Thus, the heat exchanger transient may play an important role in determining its heat transfer characteristic during the course of a cycle, and ultimately system capacity. Hence, knowledge of the transient could be beneficial in determining optimal cycle times.

These two tests are not sufficient to draw a conclusion about the effect of cycle times on system capacity. The reason is that other parameters, namely R and the operating conditions, are not identical. However, the results seem to indicate that cycle times, if they are too long, could possibly have a negative effect on the operation of the system. In the first test, slightly lower system capacity seems to have been achieved while consuming more power.

The compressor pressure, temperature and power consumption transients are plotted over two cycles in Figures 4.4, 4.5 and 4.6, respectively for the first test. The corresponding graphs for the second test are shown in Figures 4.7, 4.8 and 4.9.

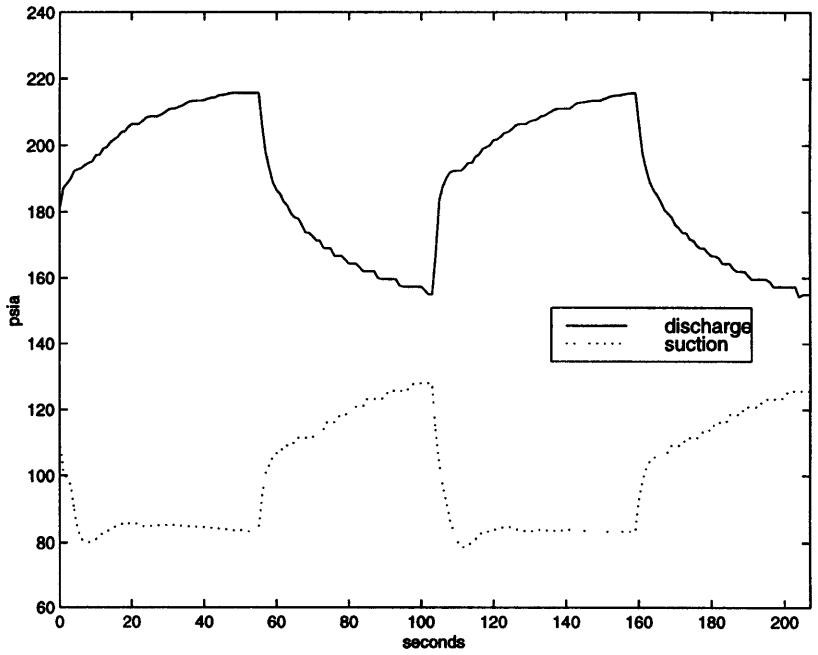

Figure 4.4: Compressor suction and discharge pressure variation over two cycles (t_{cycle}=105s, R=1.18)

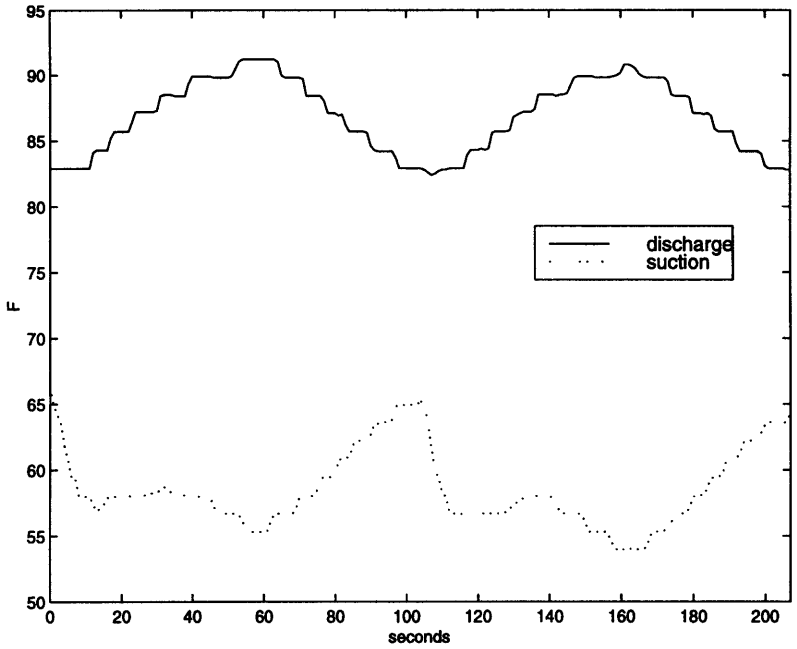

Figure 4.5: Compressor suction and discharge temperature variation over two cycles (t_{cycle}=105s, R=1.18)

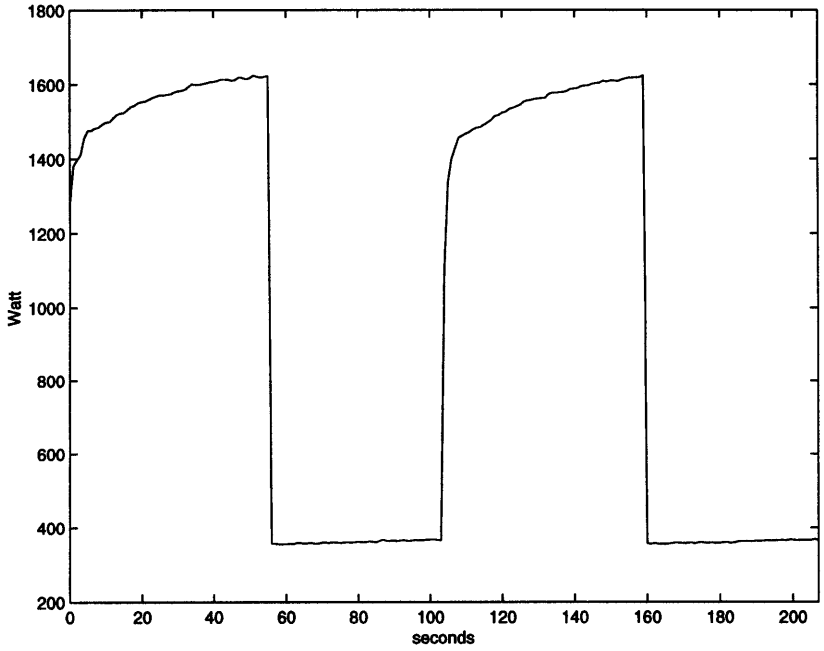

Figure 4.6: Compressor instantaneous power consumption over two cycles (t_{cycle}=105s, R=1.18)

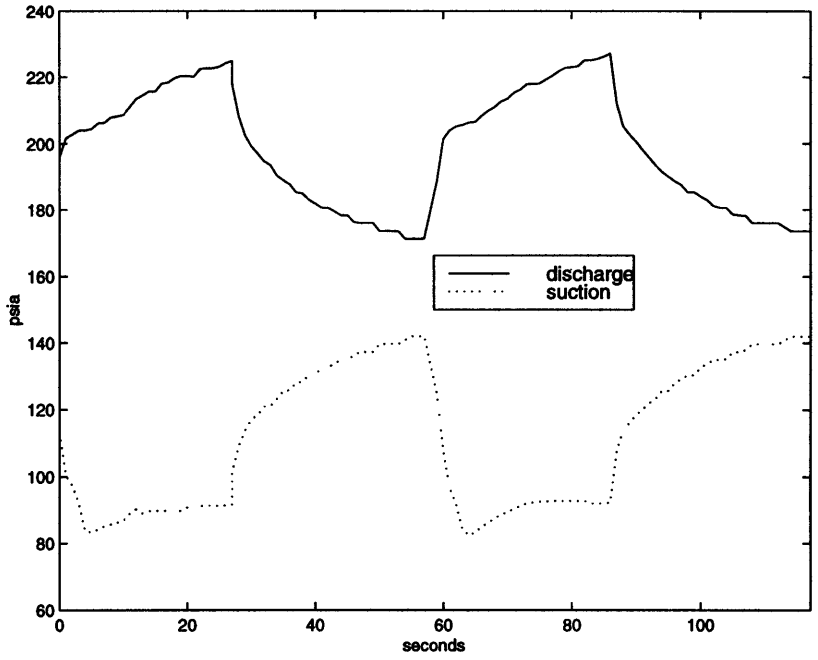

Figure 4.7: Compressor suction and discharge pressure variation over two cycles (t_{cycle}=59s, R=0.97)

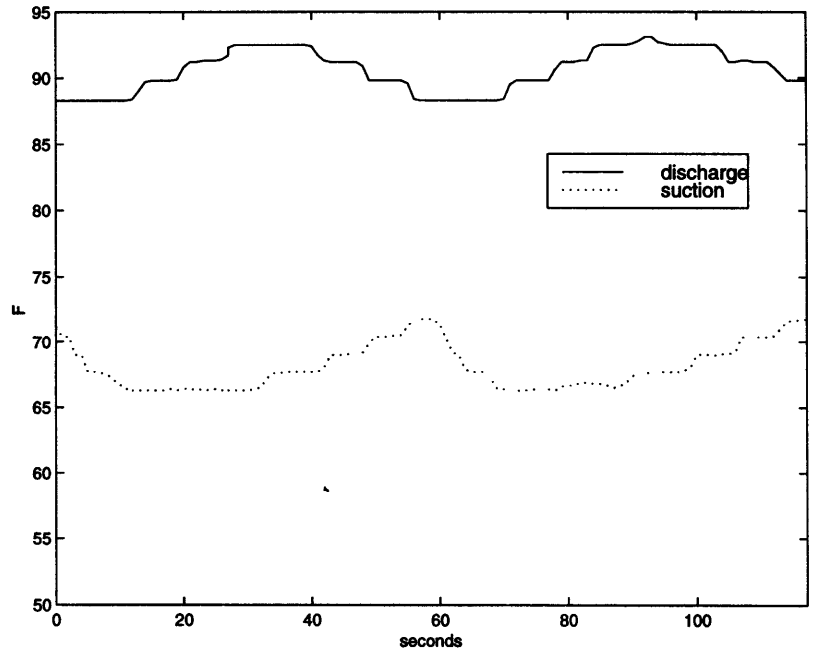

Figure 4.8: Compressor suction and discharge temperature variation over two cycles (t_{cycle}=59s, R=0.97)

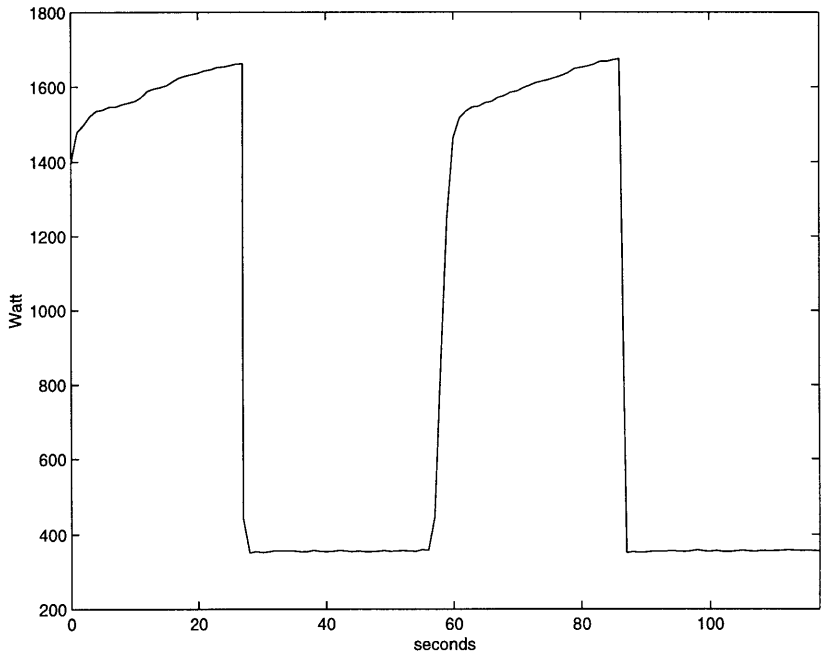

Figure 4.9: Compressor instantaneous power consumption over two cycles (t_{cycle}=59s, R=0.97)

In both experiments, the power is seen to drop to a nearly constant value during the unloaded phase. This is expected since power is consumed in overcoming friction at various locations in the motor, the compressor, and the bearings. These frictional effects are not related to the state of the rest of the system. During the loaded phase, the power consumption varies. As the pressure difference between suction and discharge increases, and as suction temperature drops, more power is consumed. In short, power consumption during the loaded phase depends on the state of the fluid at compressor inlet and exit.

Comparing the pressure and temperature graphs of each of the two experiments, we notice that the pressure transients seem to be much faster than the temperature transients. In Figure 4.4 for instance, the discharge pressure seems to vary by 60 psia about an average of 185 psia or so. The variation is then about 30% of the average value. In Figure 4.5, the variation in discharge temperature is of the order of 10°F about an average of approximately 87°F. This corresponds to an approximate percentage variation of 12% only. A similar trend is also observed in the second test.

The above may suggest that the pressure transient is the main system parameter to be taken into account in determining optimal cycle times. This is especially true because the temperatures tracked are fluid temperatures. Thus, the heat exchanger walls would be even slower in responding to temperature changes. Wall temperatures may not change significantly, especially for shorter cycle times.

The last interesting observation deals with pressure changes when the compressor is loaded. The pressure drop in the evaporator when the compressor is loaded seems much steeper than the corresponding pressure rise in the condenser. This is probably due to the sudden removal of a large amount of vapor from the evaporator.

4.4.4 Third Set of Experiments and Results

The previous two sets of experiments seemed to indicate that relatively long cycle times, of the order of 50 seconds for each phase, may be unfavorable for various reasons. It seemed interesting to experiment with shorter cycle times.

The plan was to carry out several tests, all with R=1. The cycle times decided upon were t_{cycle}=60s, t_{cycle}=40s, t_{cycle}=20s and t_{cycle}=10s. The approach would be to set the timer for a given cycle and run the system. The steam and chilled water flow rates can be adjusted until a steady, or quasi-steady state is reached[1]. Various system parameters would then be monitored and recorded.

The next task was to decide upon the significant system parameters that need to be monitored. Previous tests seemed to indicate that compressor suction and discharge pressures were the most important system parameters. This is especially true as the system pressure transients were the fastest and thus the most significant. The other important parameter is the cold room air temperature. Ultimately, this is what the customer feels. Customer comfort and satisfaction is best achieved when the air temperature remains at a comfortable level with minimal fluctuations. The fourth important parameter is air temperature leaving the evaporator. The reason being that the temperature difference of the air across the evaporator is, at worst, a measure of the system capacity relative to normal operation. If the mass flow rate of air can be measured, the actual system capacity may be approximated.

A Hewlett Packard data acquisition system was used. It was connected and programmed to monitor the four thermocouples set up previously to measure air temperatures across the evaporator and the condenser. A fifth channel monitored voltage to the timer. This was to track timer cycling times. Two other current channels were used to record pressure transducer readings. They were hooked up to the two pressure transducers already installed in the system, at condenser exit and compressor inlet. The readings are approximate because the current and pressure were assumed to vary linearly within the transducer range.

The evaporator inlet and exit temperatures were plotted for the four tests in Figures 4.10 through 4.13. The temperature axis has the same scale and range in all four graphs for ease of comparison. For each test, data is plotted over four load/unload cycles. Hence, the time axis is necessarily different for the four graphs, to accommodate different cycle lengths.

---

1. It wasn't clear at this point whether steady state can be reached with the elementary thermal control setup of the system.

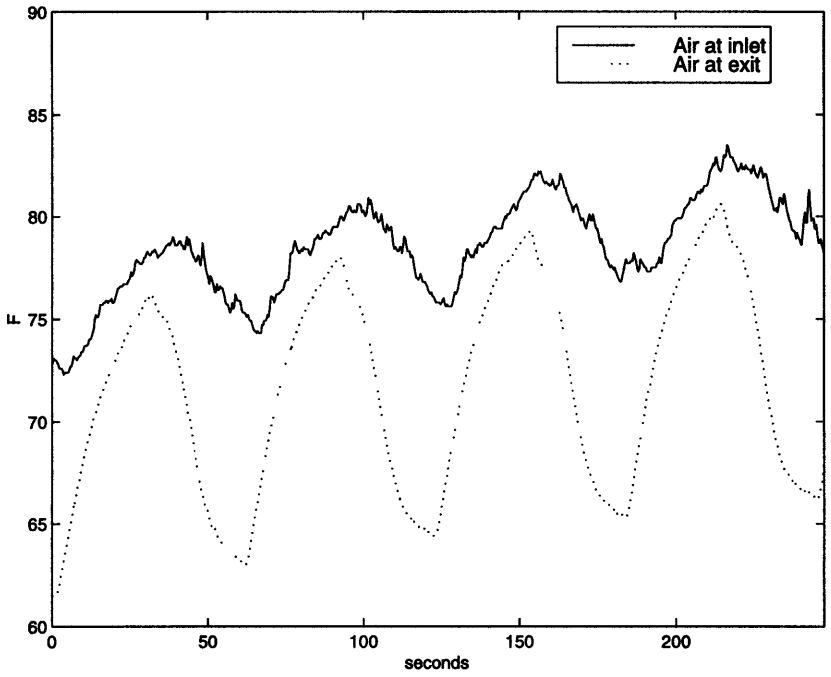

Figure 4.10: Air temperatures at evaporator inlet and outlet (R=1, t_{cycle}=60s)

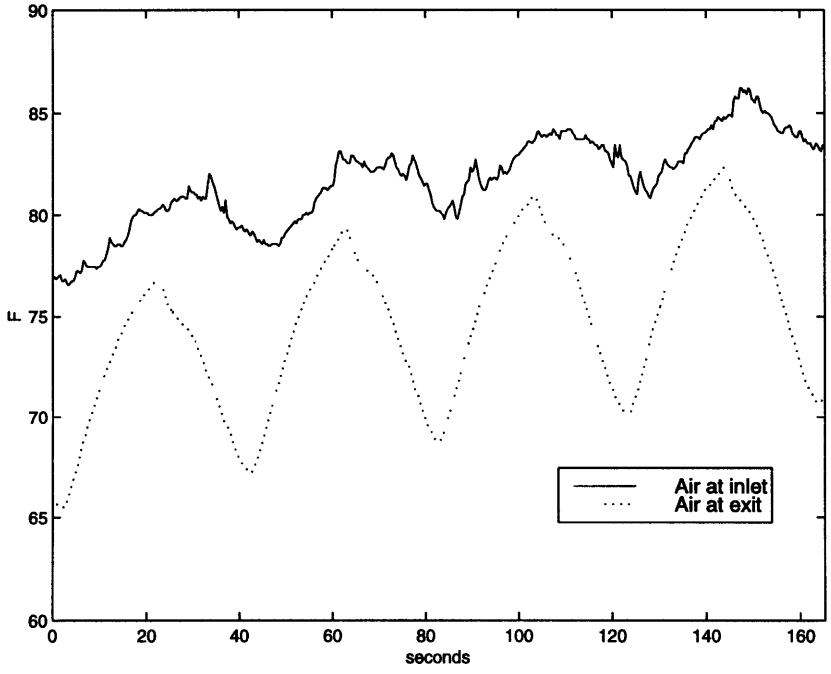

Figure 4.11: Air temperatures at evaporator inlet and outlet (R=1, t_{cycle}=40s)

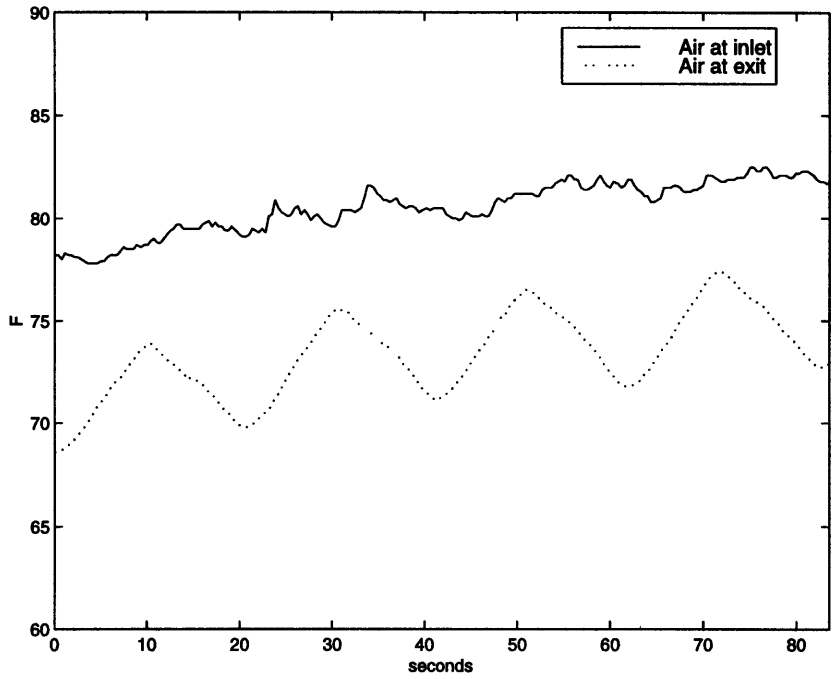

Figure 4.12: Air temperatures at evaporator inlet and outlet (R=1, t_{cycle}=20s)

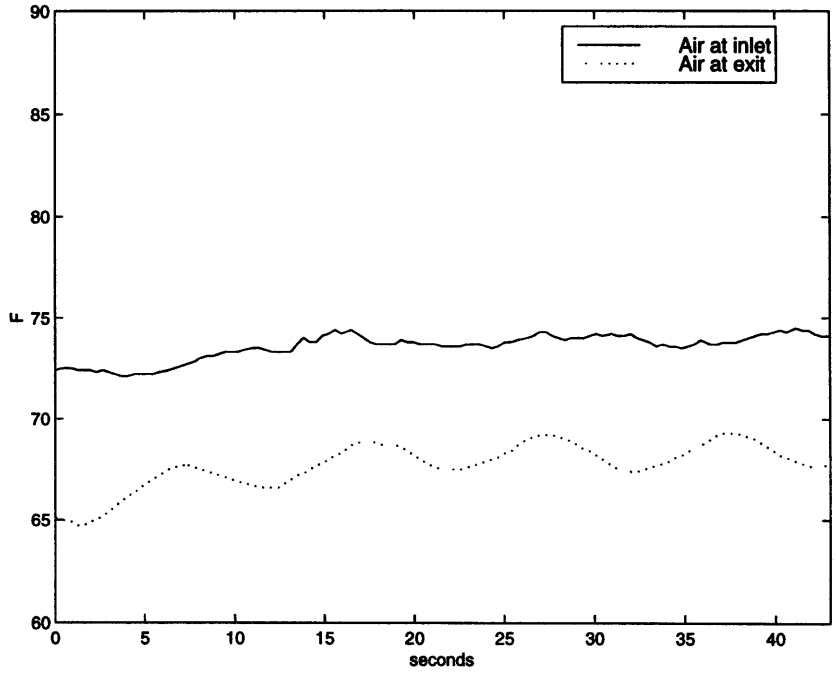

Figure 4.13: Air temperatures at evaporator inlet and outlet (R=1, t_{cycle}=10s)

Two transient behaviors are apparent in these graphs. The longer temperature transient is the response of the room as it warms up due to decreased cooling capacity. This response is observable during the experiment because of the insufficient thermal capacity of the small room and its contents.

The shorter transient is the air temperature response to the cyclic loading and unloading of the compressor. The first observation is that the peaks of the two plots representing the temperatures of air at inlet and at exit are non-synchronized. The "air temperature at inlet" plot lags behind the "air temperature at exit" plot. This is expected, since any change in evaporator conditions affects first the air that comes in contact with it. This air then circulates in the room and causes the room temperature to vary.

The temperature of air at evaporator inlet is a good indication of room temperature. For t_{cycle}=60s, the fluctuations are of the order of 8°F. The fluctuations decrease with cycle time, and approach 2°F for t_{cycle}=10s. Human comfort requires minimal fluctuations in room air temperature. Hence, shorter cycle times seem to be favorable from this aspect.

Let $\Delta T_{evap,\ avg}$ represent the average temperature difference of air across the evaporator, during a given test. That is, $\Delta T_{evap,\ avg}$ =Average($T_{air,inlet}$-$T_{air,exit}$). As described previously, this parameter is a good indication of the system cooling capacity. Its value was approximately 6.8°F, 6.8°F, 6.9°F and 5.8°F for the longest to shortest cycle time tests. The values for the tests with t_{cycle}=60s, t_{cycle}=40s and t_{cycle}=20s are equal, within experimental error. This is anticipated, because R is kept constant (R=1) for all the tests. The seemingly lower capacity of the last test (t_{cycle}=10s) is probably due to cycle timing errors: Both human errors in manually setting the timer on and off times, and decreased timer repeatability at shorter cycle times. These errors probably drove the value of R below its nominal value of 1.

The heat exchanger pressures for the four tests are plotted in Figures 4.14 through 4.17. The "evaporator" pressure is measured at compressor suction, upstream of the accumulator. The "condenser" pressure is measured downstream of condenser outlet. As before, the scale and range of the pressure axis is the same in all four graphs. The time axis is different to accommodate four cycles. During the tests, data was taken at nearly fixed intervals of 0.35s. Hence, data points are equally spaced in time.

The evaporator pressure graph consists of individual data points. This is done on purpose, to emphasize the fast transients encountered when the compressor is loaded. Evaporator pressures are observed to suddenly plunge. No such fast transients are observed in the condenser (and thus it is plotted as a continuous curve). Note the glitch observed in the condenser pressure plot, immediately following compressor loading.

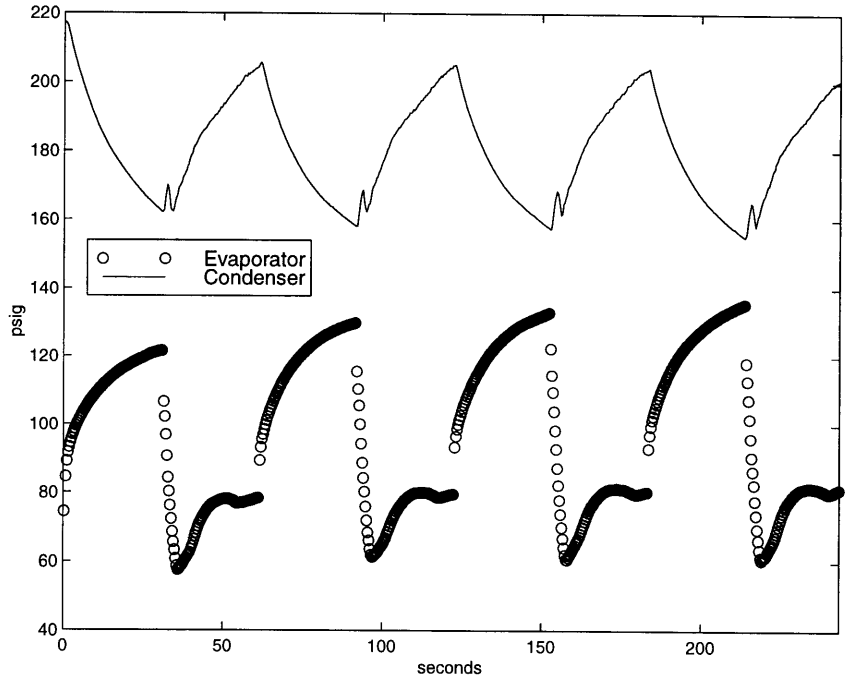

Figure 4.14: Evaporator and condenser pressures (R=1, t_{cycle}=60s)

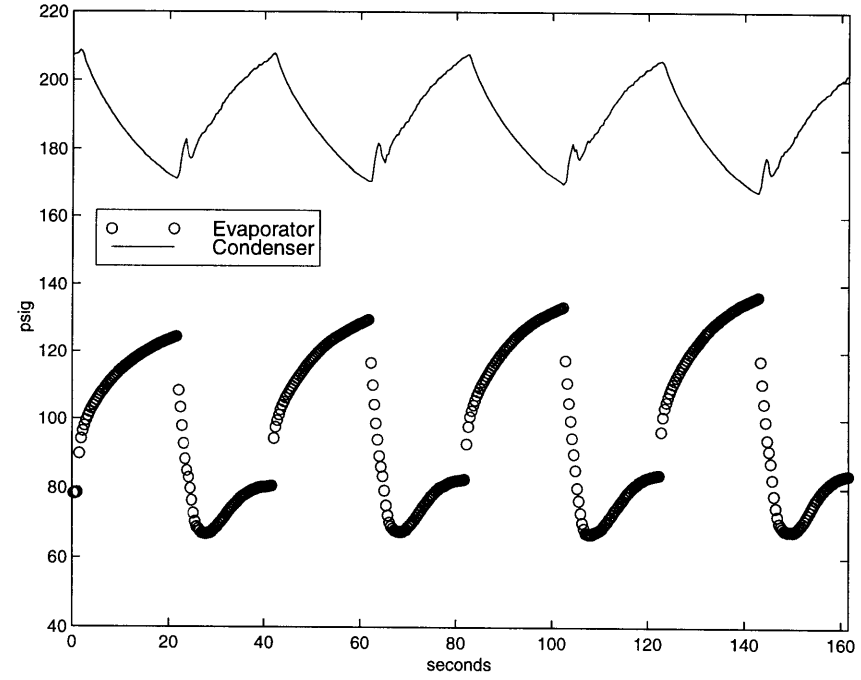

Figure 4.15: Evaporator and condenser pressures (R=1, t_{cycle}=40s)

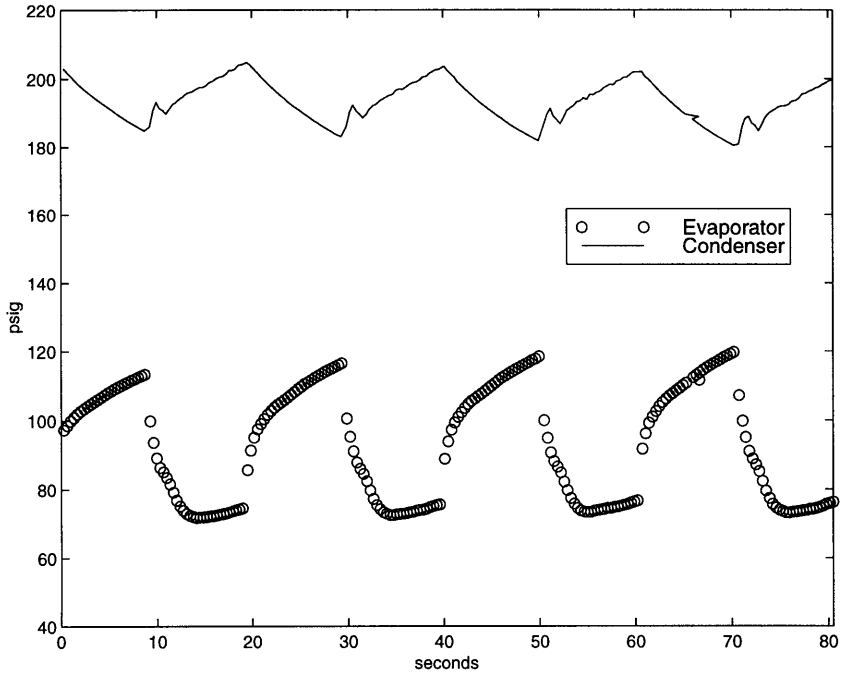

Figure 4.16: Evaporator and condenser pressures (R=1, t_{cycle}=20s)

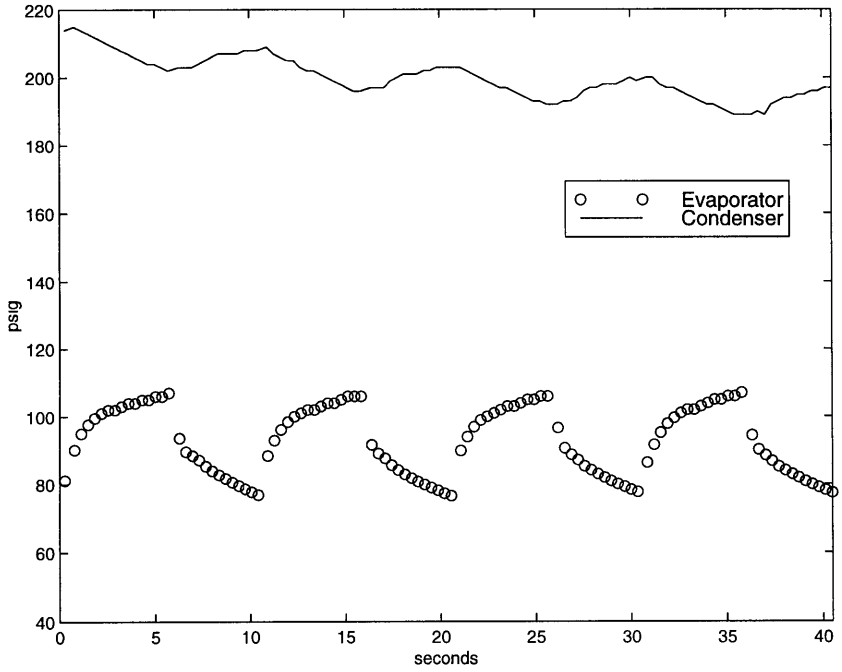

Figure 4.17: Evaporator and condenser pressures (R=1, t_{cycle}=10s)

One plausible explanation for this observed behavior is the following: When the compressor is unloaded, the Freon mass flow rate is zero through the compressor. Some fluid continues moving from the condenser to the evaporator as long as a pressure difference exists between the two. Refrigerant is just sitting in the heat exchangers. A large amount of vapor exists at the discharge end of the evaporator. When the compressor is loaded, a quantity of refrigerant, mostly in the vapor state, is removed from the evaporator. It is replenished by an equal quantity of liquid from the condenser. The specific volume of liquid is much smaller than that of vapor, and hence the vapor left in the evaporator can now occupy a much larger volume. Thus, the evaporator pressure drops. As heat is transferred to the evaporator, more vapor starts to form thus making the pressure drop much slower and eventually causing a gradual rise in pressure. Finally, steady state is reached when the liquid and vapor concentrations in the evaporator reach their "normal" levels. The direct opposite happens in the condenser. When the compressor is loaded, liquid refrigerant leaves the condenser and is replaced by vapor. The pressure starts to rise rapidly, but is stopped from doing so by the TXV valve in the system. This is probably the cause of the glitch. As a result, the condenser pressure now continues to rise gradually.

In Figure 4.14, the whole process described above can be observed in the evaporator. Sharp pressure drop is observed first, followed by a less steep drop, a gradual rise and a steady state. In Figure 4.15, the loaded phase is cut down to 20 seconds. As a result, the compressor is unloaded just as evaporator pressure reaches steady state. For the shortest cycle (Figure 4.17), the first transient phase seems to be cut short. The resulting system pressure drop is lower. Figure 4.16 is perplexing. The first, sharp transient has sufficient time to occur (10 seconds); for some unknown reason, the pressure starts rising before the transient phase, as observed in the longer cycles, is completed.

The pressure transients observed in the system heat exchangers, especially the evaporator, are very interesting and perplexing. The different trends observed seem to indicate that various physical phenomena are interacting. The evaporator pressure transient during the loaded phase seems to go through four different regimes. Each of the regimes is probably driven by one dominant physical process. An attempt was made (in the previous paragraphs) to identify some of the phenomena involved. A rigorous physical model of the system might provide some insight on this complex problem.

The average system pressures during these four tests are shown in Table 4.5. Obviously, the system operating conditions in the four tests do not match. Also, note that the prevailing room conditions were quite different during the four tests. This difficulty in setting the operating conditions was remedied for the following set of experiments, as described in the next section.

Table 4.5: Average evaporator and condenser pressures

	Test: R=1, t_{cycle}=60s	Test: R=1, t_{cycle}=40s	Test: R=1, t_{cycle}=20s	Test: R=1, t_{cycle}=10s
Average evaporator pressure	101.3	104.1	95.3	93.2
Average condenser pressure	200.6	186.1	190.0	194.9

The response of system pressures and room air temperature to the different cycle times seems to indicate that the shorter cycle times (t_{cycle}=10s) are preferable to the longer ones experimented. The resulting room air temperature is more stable. Additionally, the system pressure swings are attenuated by the shorter cycle times. Optimally, a system performs best when the variations are so small they can hardly be detected.

4.4.5 Fourth Set of Experiments and Results

This set consists of four experiments. The first experiment ("test a") is just normal operation of the compressor. The data from this experiment serves as a basis for reference. The second ("test b") and third ("test c") experiment shared an R value of 1, but different cycle times, t_{cycle}=10s and t_{cycle}=4s. R was 1/3 and t_{cycle} was 8s for the last experiment ("test d"). Naturally, the system capacity is expected to be lower in this last experiment (nominally at 25% of normal operation capacity). No further attempt was made to experiment with longer cycle times. This is because previous tests had clearly implied that shorter cycle times are preferable.

The aim of these experiments was to observe system behavior and measure system power consumption over a range of capacities. Data collected from these experiments would then prove useful in:

- evaluating system performance under variable capacity operation, relative to normal operation.
- determining some of the optimization criteria that set optimal cycle times for a given capacity

One problem encountered during the previous set of experiments was keeping the average room air temperature constant throughout the experiment. The cause of this problem was twofold. First, the thermal capacity of the experimental room was too low. Second, no feedback was used in controlling the steam and chilled water flow rates. To remedy this situation, a pneumatic bulb thermostat was used to control the action of a pneumatic valve

already installed in the chilled water line. A pneumatic valve actuator was added to the steam inlet flow line. It was used in conjunction with another thermostat to control the cold room temperature. This setup managed to keep the average room temperatures stable, when averaged over long periods of time. However, the cold room average air temperature over a cycle fluctuated significantly. This was probably because of the low thermal capacity of the small room, and the relatively slow feedback of the setup. Three wooden boxes, with mesh screen bottom, were constructed. The boxes were filled with 8 pounds of small (0.5 in.) gravel and stone. The boxes were placed on the steam heat exchanger, downstream of the fan. In addition to increasing the room thermal capacity, the stones served as thermal dampers. They prevented the high cyclic fluctuations of heat transferred from the steam into the room.

A watt-hour meter was installed to measure total system power. Power is consumed in the system by the evaporator fan, the condenser fan and the compressor. The power consumption of the two fans should remain nearly constant as they operate at constant speed, regardless of what is happening in the system. The evaporator and condenser fans were run individually. Their average power consumption was measured to be around 530 Watt and 145 Watt, respectively. Thus, compressor average power consumption in KW is approximately $P_{avg,c}=P_{avg,system} - 0.68$.

As before, air temperature at inlet and exit to the condenser and the evaporator were monitored. Condenser and evaporator pressures were also monitored at the same locations as in the previous set of experiments.

The new control scheme seemed successful in keeping the average room air temperature constant; of course, the instantaneous room air temperature still fluctuated cyclically with the loading and unloading of the compressor. The fluctuations in room air temperature were found to be around 2°F for tests a and b, around 1.5°F for test c and slightly less than 1°F for test d.

Figure 4.18 shows the variation in condenser and evaporator pressures over a 20 second interval for all four tests. The average condenser pressure is nearly the same for all three reduced capacity tests, and is lower than its normal operation value. The average evaporator pressure is similar for tests b and c and visibly higher for test d. In all variable capacity tests, it is significantly higher than its normal operation value.

The pressure difference between the evaporator and the condenser, $\Delta P=P_c-P_e$, among other factors, determines the power consumption of the motor. ΔP is seen to drop with system capacity. Thus, motor power consumption is also expected to drop. The extent of this drop is crucial in determining resulting system coefficient of performance (COP).

Table 4.6 summarizes the system performance during all four tests. Power consumption and average air temperature across the evaporator are normalized with respect to their nor-

mal operation value. The ratio of normalized capacity to normalized power consumption is a normalized system coefficient of performance. A significant improvement in system performance is noted for tests b and c; The system seems to function satisfactorily at a nominal half capacity. However, a large deterioration in system performance is observed when the nominal capacity is lower.

A final word of caution: The evaporator room conditions were different for the four tests. The average room air temperature was roughly 65°F, 68°F, 68°F and 70.5°F for tests a, b, c and d respectively. Hence, no concrete quantitative conclusions can be made in comparing the different cycling schemes tested based on the above measurements: only qualitative trends can be observed.

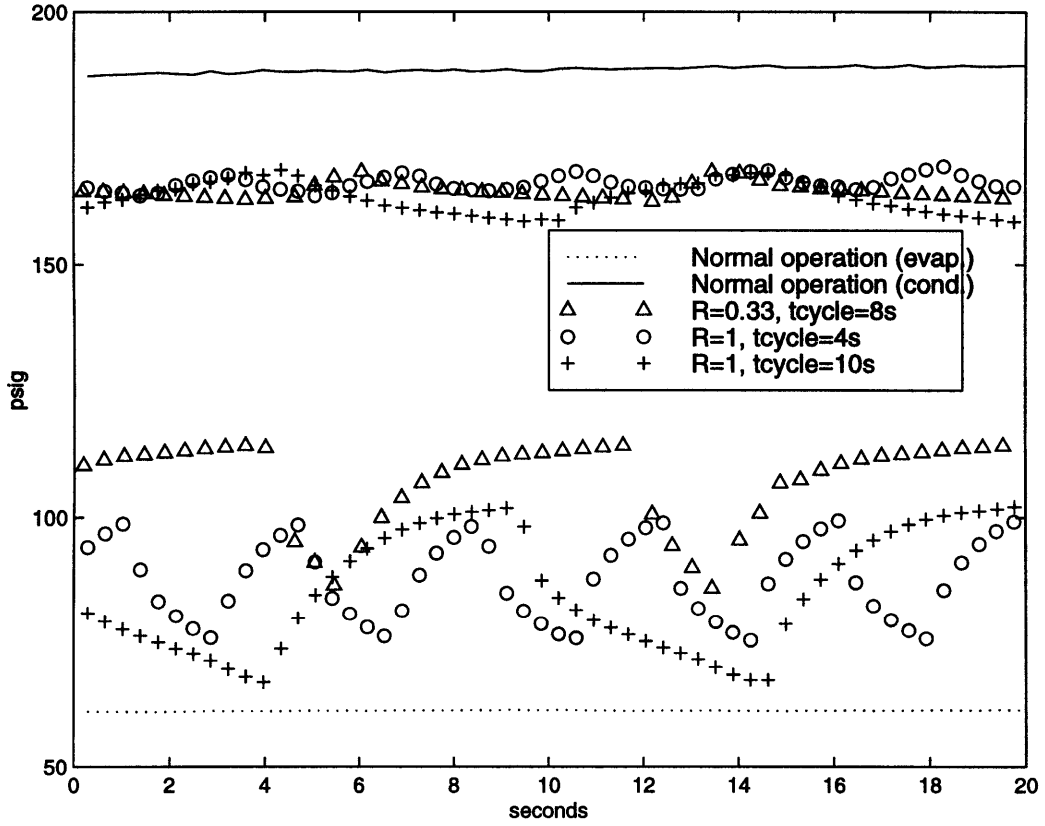

Figure 4.18: Evaporator and condenser pressure variation over 40 seconds for 4 tests: Normal operation; R=1, tcycle=10s; R=1, tcycle=4s; R=0.33, tcycle=8s

Table 4.6: Summary of system performance

	Test: Normal operation	Test: R=1, t_{cycle}=10s	Test: R=1, t_{cycle}=4s	Test: R=0.33, t_{cycle}=8s
$P_{avg,system}$	2.53	1.60	1.52	1.35
$P_{avg,c}$	1.85	0.92	0.84	0.67
Normalized power consumption	1	0.5	0.45	0.36
$\Delta T_{evap,avg}$ (°F)	7.43	4.34	4.32	1.76
Normalized capacity	1	0.58	0.58	0.24
Normalized COP	1	1.16	1.29	0.67

A simple model of the system can be used to explain the variation of system performance with capacity. Let P_l be the average power consumed by the compressor during one loaded phase. Let C_l be the corresponding average system capacity during this phase. Assume that the loaded phase is short. As a result, the changes in system operating conditions are small. Then, the ratio C_l/P_l is approximately the system coefficient of performance under normal operation at similar average operating conditions (COP_n). Let P_u be the average power consumed by the compressor during one unloaded phase. This power is used to overcome friction in the bearings, and viscous friction between the rolling piston and the surrounding fluid. Thus, P_u should be (nearly) constant and independent of operating conditions, assuming the temperature does not vary enough to significantly affect friction. System capacity during this phase, C_u, should drop to 0. This is because the mass flow rate of refrigerant through the compressor is 0. Let x represent the fraction of time the system is loaded, $x=t_{on}/t_{cycle}$. The fraction of time the system is unloaded is then: $(1-x)=t_{off}/t_{cycle}$. As before, R is the ratio of loaded phase duration to unloaded phase duration.

$$R = \frac{t_{on}}{t_{off}} = \frac{t_{on}/t_{cycle}}{t_{off}/t_{cycle}}$$

$$R = \frac{x}{1-x} \tag{4.12}$$

Based on this model, the average power consumed by the compressor during one load/ unload cycle is:

$$P_{cycle} = x \cdot P_l + (1-x) \cdot P_u \tag{4.13}$$

The system capacity during this cycle is:

$$C_{cycle} = x \cdot C_l \tag{4.14}$$

The system coefficient of performance is then:

$$COP = \frac{C_{cycle}}{P_{cycle}} = \frac{x \cdot C_l}{x \cdot P_l + (1-x) \cdot P_u}$$

$$= \frac{1}{\frac{P_l}{C_l} + \left(\frac{1-x}{x}\right)\frac{P_u}{P_l}} = \frac{1}{\left(\frac{1}{COP_n}\right) + \frac{1}{R} \cdot \frac{P_u}{C_l}}$$

$$\therefore \frac{1}{COP} = \frac{1}{COP_n} + \frac{1}{\frac{RC_l}{P_u}} \tag{4.15}$$

If R->infinity, RC_l/P_u->infinity and $(RC_l/P_u)^{-1}=0$, in which case COP reduces to COP_n, as expected. This is because R->infinity signifies that $t_{off}=0$, or equivalently the system is constantly loaded.
In general[1],

$$COP < COP_n \tag{4.16a}$$

and

$$COP < \frac{RC_l}{P_u} \tag{4.16b}$$

Based on this model, system performance under cyclic loading is expected to be lower than its normal operation value, when operating at the average operating conditions during the loaded phase.

The term RC_l/P_u varies when R or C_l vary. P_u is assumed to be constant for the reasons previously cited. If the average operating conditions are maintained constant, and if the cycle times are kept short, C_l should not vary considerably. Hence, the change in the

1. Mathematically, if 1/a=1/b+1/c and a, b and c are all positive, then a<b and a<c.

RC_l/P_u term is mainly due to a change in R (0<R<infinity).

As long as R remains high, the term RC_l/P_u is large and hence $(RC_l/P_u)^{-1}$ is small. Thus, the COP is expected to be only slightly lower than the corresponding value under normal operation at the average loaded phase conditions. As R decreases, however, RC_l/P_u decreases and its impact on decreasing system COP increases. Hence, system performance suffers.

This analysis is only approximate, as the model is over-simplified. The major assumption made is that the power when system is loaded is constant. In fact, compressor power consumption depends on the fluid conditions at suction and discharge and on the volumetric efficiency of the compressor. Hence, this model cannot be used to predict system COP. However, it is useful in studying the general trend of system behavior as capacity varies.

4.4.6 Fifth Set of Experiments and Results

The model developed in the previous section predicts that the system COP drops as the ratio of time off to total cycle time increases. This drop is sharper as the ratio of P_u/P_l is higher. Thus, the extent of system COP deterioration with lower capacity can be decreased by decreasing the ratio P_u/P_l. P_l depends on the system operating conditions. Hence, it cannot be increased while maintaining same operating conditions. P_u, on the other hand, may be decreased; the simplest technique is by turning the motor off during the unloaded phase. Moreover, the model predicts that system performance improves as the ratio of RP_u/C_l drops (see equation 4.5). Thus, decreasing the average compressor power consumption during the unloaded phase might be beneficial at all capacities.

This idea was investigated by running two series of tests. These tests will be referred to as series A and B. Each series consists of 7 tests. The tests are described in Table 4.7.

The compressor was run under normal operation for test 1. For tests 2, 3 and 4, the motor was kept constantly running. The vane was loaded and unloaded intermittently at the cycle times cited. For tests 5,6 and 7, the motor was turned off as the vane was unloaded. It was turned on again before the vane was loaded, to give the motor some time to start-up. This was achieved by the use of a time delay circuit timer. The setup is shown in Appendix A.

Table 4.7: Test characteristics

Test #	t_{on}(s)	t_{off} (s)	**R**	t_{cycle}(s)	**motor**
1	NA	NA	∞	∞	on constantly

Test #	t_{on}(s)	t_{off} (s)	R	t_{cycle}(s)	motor
2	5	5	1	10	on constantly
3	2	2	1	4	on constantly
4	2	6	0.33	8	on constantly
5	5	5	1	10	off intermittently
6	2	2	1	4	off intermittently
7	2	6	0.33	8	off intermittently

Figure 4.19 is a simplified schematic of compressor motor power consumption for different states of the vane. For tests 2 through 4, the model is kept the same as in the previous section. The motor is assumed to consume an average power P_l while in the loaded phase and a much lower power P_u in the unloaded phase. For tests 5 through 7, the motor is assumed to consume P_l during the loaded phase as before. However, motor state and hence power consumption can vary during the unloaded phase. At first, the motor is completely shut off, so it consumes no power. The motor then consumes some average start-up power P_{start} during the start-up phase, after which its average power consumption drops to P_u again until the vane is loaded.

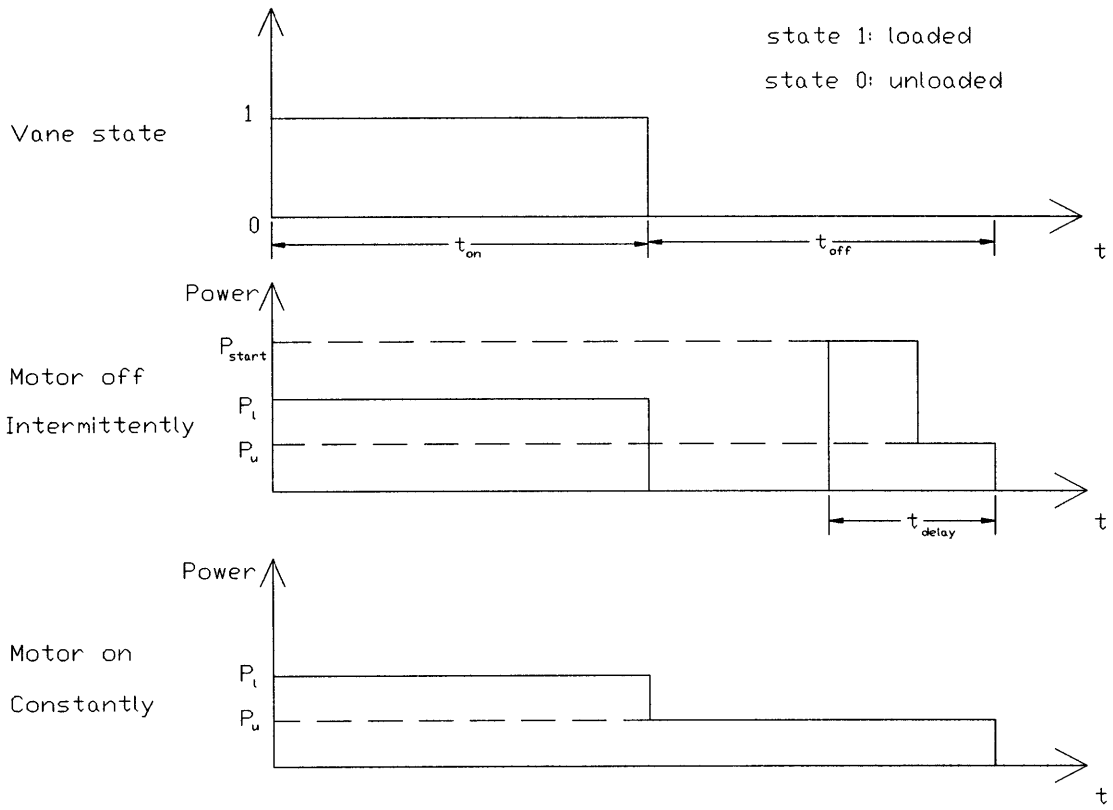

Figure 4.19: Compressor power consumption for various vane states

The time delay differed between setups A and B. In the former, the time delay (t_{delay}) was arbitrarily set at approximately 1 second. After series A tests were completed, a current probe and an oscilloscope were used to measure motor current. As expected, current surge was observed during motor start-up. This surge lasted about 200ms. Thus, t_{delay} was set at approximately 200ms for the B series tests. Note that the timer used lacked sophistication and hence precision. Thus, the values given for time delay are only approximate, average values.

The power measurements were made slightly differently in the two series of tests. The watt-hour meter was hooked up to measure total system power for series A. The motor power consumption was then approximately calculated by subtracting fan power consumption. For series B, the watt-hour meter was directly hooked up to measure compressor power consumption.

Finally, note that cycle times cited in Table 4.7 are only nominal values. Actual cycle times may vary slightly due to mediocre timer quality.

Relevant data from the two series of tests are shown in Table 4.8. Turning the motor off

during the unloaded phase seems to significantly benefit system performance at the lowest nominal capacity tested. For the tests at 50% nominal capacity (R=1), the opposite seems to be true.

Table 4.8: Test data and performance parameters

Test #	$P_{avg,system}$ (kWatt)	$P_{avg,c}$ (kWatt)	Normalized power	$\Delta T_{evap,avg}$ (°F)	Normalized capacity	Normalized COP
1A	2.31	1.63	1	7.07	1	1
2A	1.58	0.90	0.55	3.96	0.56	1.01
3A	1.62	0.94	0.58	3.91	0.55	0.96
4A	1.28	0.60	0.37	2.04	0.29	0.78
5A	1.67	0.99	0.61	3.76	0.53	0.88
6A	1.63	0.95	0.58	3.92	0.55	0.95
7A	1.09	0.41	0.25	1.85	0.26	1.04
1B	NA	1.52	1	6.98	1	1
2B	NA	0.86	0.57	4.00	0.57	1
3B	NA	0.87	0.57	3.96	0.57	1
4B	NA	0.55	0.36	1.96	0.28	1
5B	NA	0.87	0.57	3.65	0.52	0.91
6B	NA	0.95	0.63	3.61	0.52	0.83
7B	NA	0.40	0.26	1.78	0.26	1

The model described in Figure 4.19 can be used to successfully predict some trends in system performance for the various cycles tested. Let P_U be the average power consumed during the unloaded phase. P_U is the total area underneath the power graph (in the unloaded phase) divided by the time duration of the phase. As cycle times become shorter, the start-up energy, which should be constant, takes its toll in increasing P_U. At some limiting time t_{off}, the start-up energy consumed just balances the energy saved during the time when the motor is off. As t_{off} becomes longer, a definite advantage starts to appear in reducing P_U by shutting off the motor. Recall that as P_U drops, the COP is expected to increase.

The trend just described is observable in the data. For shorter off times (tests 2, 3, 5 and 6),

the motor shut-off scheme yields lower COP values. Whereas for tests 4 and 7, where t_{off} is longer, the COP improves when the motor is shut off.

Following similar reasoning, as t_{delay} is shortened, system COP should improve. This trend is observed for test 4. Series B COP is higher than its series A counterpart. However, COP is seen to deteriorate with shorter t_{delay} for shorter cycle times (test 6). One possible explanation is that in test 6A, the motor only had 1 second to shut off. Thus, it was unable to do so and was started again from some non-zero speed. Hence, the power consumed during start-up was significantly lower. This would improve system COP. Unfortunately, no data on motor shutdown could be obtained using the available resources. Hence, this hypothesis could not be experimentally verified or struck down.

4.4.7 Sixth Set of Experiments and Results

The aim of this last experiment was to determine the critical duration of the unloaded phase, t_{off}, beyond which it becomes more energy efficient to shut the motor off.

An oscilloscope was used to monitor the voltage across the compressor and the current drawn by the compressor. A sampling rate of 10,000 samples/s was used. This ensures that a sufficient number of data readings are made every motor cycle ($16.\overline{6}$ ms for no slip case). Instantaneous current and voltage were thus measured and recorded at equally spaced time intervals of 0.1 ms. Their product gave the instantaneous power. The instantaneous power could then be integrated over a motor cycle to get the average power consumption over that cycle.

The average evaporator room temperature was kept around 72.2°F. The average condenser room temperature was kept around 88.3°F. The system was then cycled and measurements were made. In the first experiment, the motor was kept on during the unloaded phase. Oscilloscope measurements were made during both the loaded and the unloaded phase. The average power consumption per cycle was calculated and averaged over a number of cycles for each phase. The compressor average power consumption during the loaded phase was approximately 1696 W. The power consumed by the motor during the unloaded phase averaged 373W. These values are close to the average power consumption values measured during the compressor test stand experiments discussed in Section 4.3. The small variation is possibly due to slightly different system conditions (refrigerant temperatures and pressures).

In the second experiment, the motor was turned off during the unloaded phase. The motor current and voltage transients were measured during the start-up phase. They are shown in Figures 4.20 and 4.21. The corresponding instantaneous power consumption is shown in Figure 4.22. As expected, the voltage across the compressor is not affected by motor start-up. It remains unaltered. However, the amplitude of the current shoots up, driving the power consumption to a value several times higher than its normal operation value. The

start-up phase seems to last a little over 200 ms. The total energy consumed during this time is about 1525 Joules.

If the motor is kept running unloaded, the time it requires to consume this much energy is 4.1 seconds, based on the measurements made. Hence, the critical t_{off} beyond which it becomes advantageous to turn the motor off is approximately $t_{off,critical}$=4.1 s.

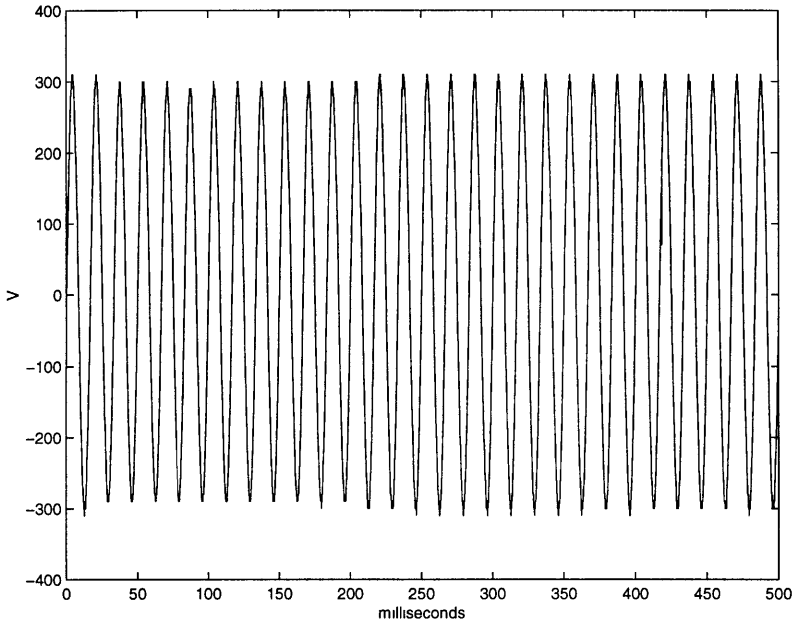

Figure 4.20 : Voltage across the motor during start-up

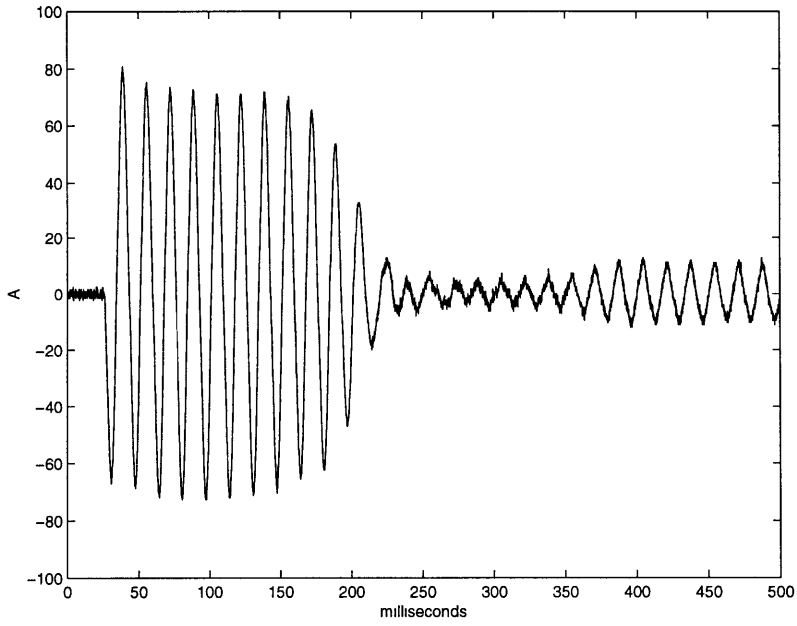

Figure 4.21 : Current transient during motor start-up

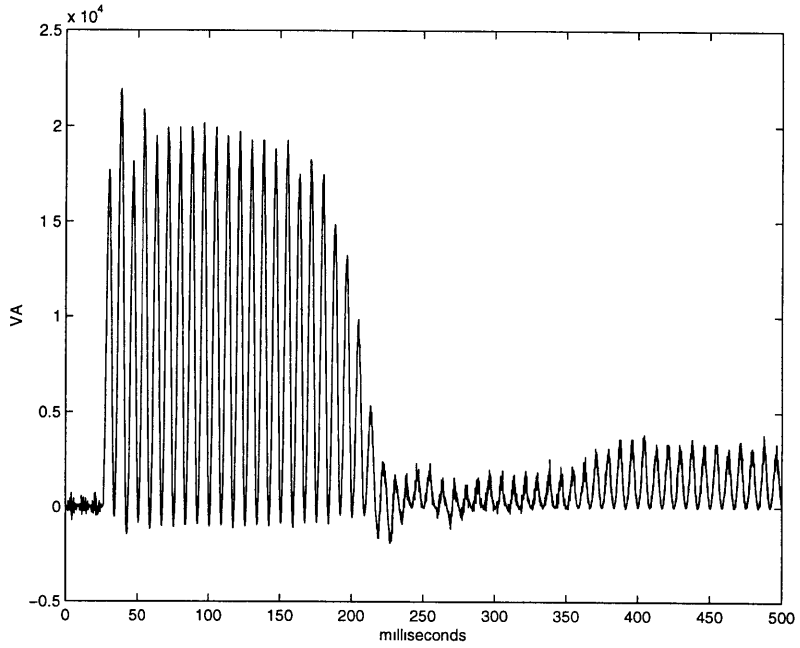

Figure 4.22 : Instantaneous power transient during motor start-up

The experiment was set up so that the motor starts and runs unloaded for a short period of time (~100 ms), after which it is loaded. This is obvious in the variation in current amplitude seen in Figure 4.21. Some interesting observations were made: Immediately after the power surge during the start-up phase, the average power per cycle drops abruptly to about 217W. After that, it rises sharply to a near steady value averaging slightly above 500W. When the motor is loaded, the power rises steadily over 3 or 4 motor cycles. After that, it maintains a near steady value, averaging 1440W.

The lower average power consumption during the loaded phase could be due to the drop in pressure difference across the compressor during the unloaded phase. The cause of the other observations is not as obvious.

4.5 Summary of Findings and Results

The main findings and conclusions of the experiments done are summarized in this section. The success of the project depends on the success of the vane lifting mechanism and on the success of the operating scheme. Hence, both aspects are discussed.

4.5.1 Mechanism Design

The prototype vane lifting mechanism was successfully run in a system, thus experimentally demonstrating the feasibility of the concept. Throughout the experiments, sets of

operating data were recorded and analyzed. The major characteristics of a rotary compressor employing a vane lifting mechanism were determined.

Although it functioned satisfactorily, the prototype mechanism was not optimally designed. It was found to have several weaknesses that can be eliminated by further design work:

- The activation and deactivation of the vane lifting mechanism is not synchronized with the position of the rolling piston. This leads to vane and rolling piston impact upon transition between loaded and unloaded operation. In worst cases, fatigue failure of the rolling piston could ensue. At best, it is a source of noise.
- If the pressure difference between compressor suction and discharge goes too low, the mechanism is unable to hold up the pneumatic piston at top dead center. As a result, the vane tip hangs too low and impacts the rolling piston at every shaft revolution. Needless to say, if the pressure difference ceases to exist or goes negative, the mechanism fails to preform its function.
  In a practical situation, problems of this nature may arise if the customer turns the system on when atmospheric temperature is lower than indoor temperature (such as to dehumidify the internal space).
- The mechanism seems to be unable to complete reversal in one cycle. As a result, the vane can be heard bouncing on the rolling piston at every transition.

4.5.2 Operating Scheme

Several independent parameters are involved and should be accounted for in optimizing cycle times. The experiments helped determine some of the optimization criteria involved. Additionally, a few general observations were made on system performance under varying cycling conditions. These results form the basis for future work on the design and optimization of the system employing the variable capacity compressor.

Only qualitative guidelines are presented. There is no sense in giving numbers and quantitative comments at this stage: the quantities are very much system dependent.

- The upper limit on cycle times seems to be set by system parameters, most notably pressure. Pressure transients are faster in the evaporator. Thus, the cycle should be short enough to limit the pressure swings in the evaporator.
- The lower limit on cycle times was not explored. Experiments seemed to indicate a trend of improved system performance with decreased cycle times. The lower bound could possibly be set by the time for one motor cycle (~$16.\overline{6}$ ms here) or the response time of the mechanism to a load/unload control signal, whichever is shorter.
- For cycles where the unloaded phase is relatively long compared to the loaded phase, the system COP seems to suffer. The power consumed in overcoming frictional losses outweighs the drop in capacity achieved. A possible remedy is to shut off the motor when the vane is unloaded. The motor is then turned on and given just enough time to reach full speed before the vane is reloaded. Average system pressure is not affected

by shutting the motor off.

- Shutting off the motor is not always a favorable scheme. The motor has to be off long enough so that the power savings achieved offset the motor start-up power surge. If that is not the case, the system COP suffers.
- Some cases arise when the motor is not given enough time to go down to 0 speed before it is turned on again. The resulting motor power consumption was not quite understood in this case. Hence it is hard to explain or predict the effect of such a situation on system COP. Further work is required in this direction.
- The compressor was observed to vibrate significantly at motor start-up and shut-off, due to torsion about its vertical axis. Apparently, the mounting base was not designed for frequent start-up and shut-off.

Chapter 5

Conclusion

5.1 Project Achievements

The work done for this thesis proves the soundness of the proposed concept: The capacity of a rolling piston type rotary compressor can be continuously varied by cyclically loading and unloading the vane.

- A first generation prototype vane lifting mechanism was successfully designed and built. It consists of a pneumatic device that is activated by the pressure difference between refrigerant at suction and at discharge. A crude control scheme was applied.

- Experiments seemed to indicate that the prototype mechanism does not affect the normal operation of the compressor.

- Experimentally, the prototype system was able to operate at reduced capacities (50% and 25% of normal operating capacity).

- At 50% capacity level, the calculated system COP seemed to remain constant or even to slightly improve, given that cycle times are kept sufficiently short.

- At 25% capacity level, system COP seemed to deteriorate unless the motor is shut off at the beginning of the unloaded phase and restarted near the end of the same phase.

- The optimal operating scheme seemed to favor shorter cycle times. The evaporator pressure swings seemed to be the fastest system transients, and hence possibly one of the critical parameters in designing a suitable operating scheme.

5.2 Recommendations

The two crucial elements in determining concept success and competitiveness are the vane

lifting mechanism and the operating scheme. Refinements are in order in both these areas to improve the effectiveness of this method.

- The mechanism should be redesigned such as to synchronize its operation with the position of the motor shaft. The main tangible result would be decreased system noise.

- Another requirement for the next generation of mechanisms is the ability to operate under a wider range of operating and system conditions (i.e. the operation of the mechanism should be made independent of system pressures if possible).

- The market success of this concept depends on the production cost of the mechanism to a large extent. This should be taken into account in the next generation of designs.

- The optimal operating scheme has yet to be identified. For that purpose, different parameters and their effect on system COP should be studied.

- Further experiments are needed on three time scales:
  •The shortest time scale arises from the motor response to changing loads and input power. This time scale is of the order of a few hundred milliseconds, at most.
  •The second time scale deals with the system response to loading and unloading the compressor. This time scale obviously depends on the system and probably varies between 2 and 10 seconds.
  •The longest time scale has to do with averaged system parameters over some operating time, of the order of several minutes or hours.

- A predictive system model, applicable for short time scales (to model system transients) might be helpful in understanding system effects and system interaction with the compressor.

- One major goal of further work would be to be able to predict system performance under different loading schemes at given operating conditions, based on the average value of some parameter to be determined (possibly the average evaporator pressure). Thus, the optimal loading scheme can then be singled out and applied in a practical situation.

References

1. T. Natsuzaka and S. Nagatomo, "Rolling Piston Type Rotary Compressor Performance Analysis", Proceedings of the 1982 Purdue Compressor Technology Conference, **1**:149, (1982).

2. G.F. Nellis internal report (1997).

3. F. McClintock and A. Argon, Mechanical Behavior of Materials, Addison-Wesley Publishing Co., Reading, MA, 1966, p.448.

4. Shigley and Mitchell, Mechanical Engineering Design,4th ed., McGraw-Hill, Inc.,1983, p.176, p.800.

5. A.H. Slocum, Precision Machine Design, Prentice-Hall, Inc., Englewood Cliffs, NJ, 1992, pp.228,233-234.

6. R. Roark and W. Young, Formulas for Stress and Strain, 5th ed., McGraw-Hill, Inc., 1975, p.607.

7. J. Meriam and L. Kraige, Engineering Mechanics, Volume Two, Dynamics, 3rd ed., John Wiley & Sons, Inc., 1992, pp.218-220.

Appendix A

Timer and Time Delay Circuits

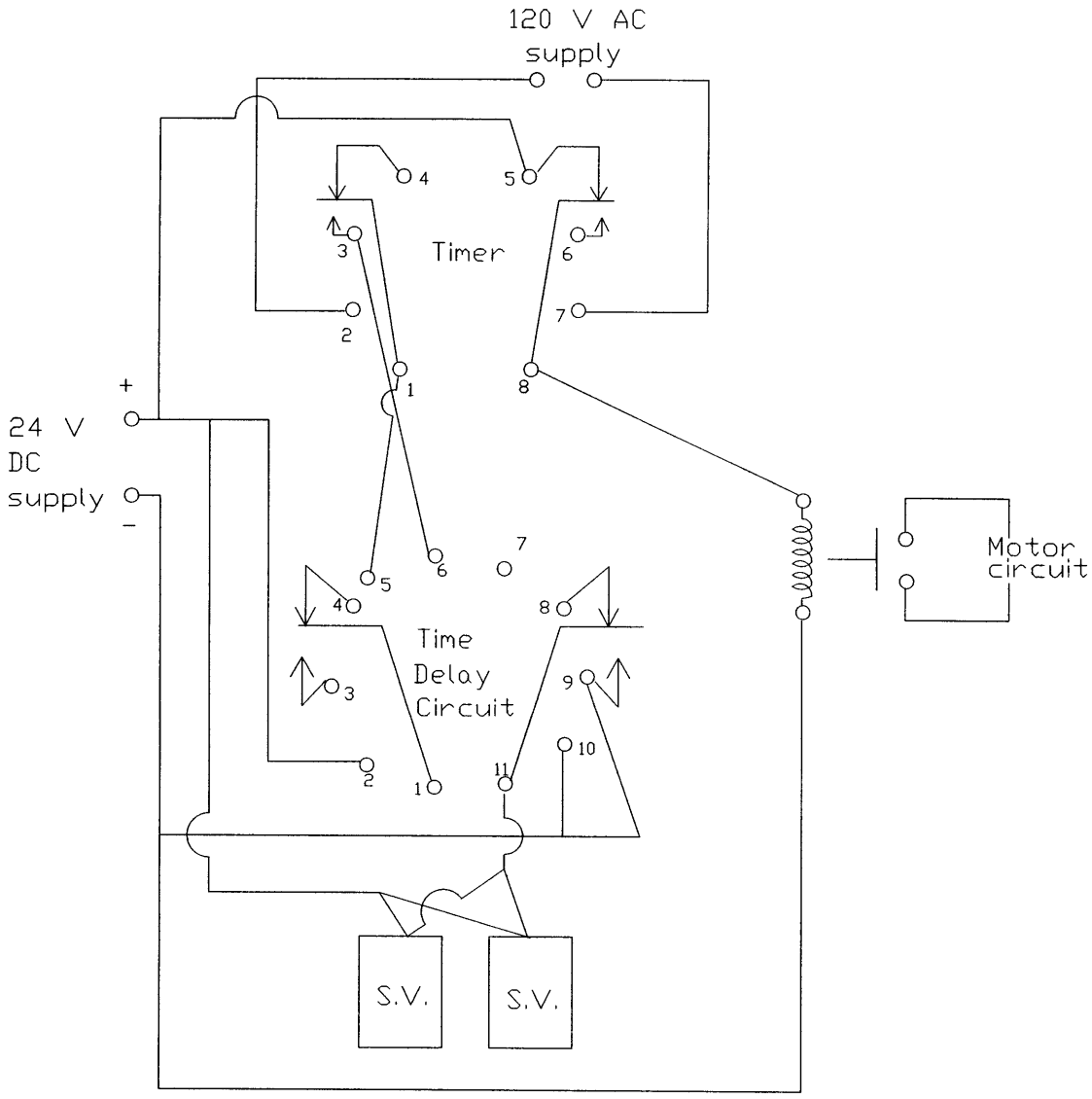

Appendix B

B.1 Matlab Parameters File

```
% PARAMETERS FILE
%  This file holds the values of all the geometric parameters

% Rp : Rolling piston outside radius [in.]
Rp=0.963;

% e : shaft eccentricity [in.]
e=0.199;

% Rc : cylinder inner radius [in.]
Rc=1.162;

% Hc : cylinder height [in.]
Hc=1.535;

% Wv : vane width [in.]
Wv=1.114;

% Lv : vane length [in.]
Lv=1.534;

% Tv : vane thickness [in.]
Tv=0.183;

% Rv : vane tip radius [in.]
Rv=0.177;

% Wn : notch width [in.]
Wn=0.375;

% Hn : notch depth [in.]
Hn=0.119;

% Mv : vane mass [lb]
Mv=0.083;

% J : conversion factor [32.2 lbm.ft/lbf.s2] = [386.4 lbm.in/lbf.s2]
J=386.4;

% k : vane spring constant [lbf/in.]
k=8.29;
```

```
% a : Vector of discretized crank angle values [rad]
a=[0:0.061:0.61 0.714 0.8701 1.0262 1.1822 1.3383 1.4943 1.6504 1.8065 1.9625];
a=[a 2.1186 2.2746 2.4307 2.5868 2.7428 2.8989 3.055 3.211 3.3671 3.5231];
a=[a 3.6792 3.8353 3.8832:0.1:2*pi 2*pi];

% T: Thickness of the pump wall [in.]
T=1.580;

% lo : minimum spring length ( measured ) [in.]
lo=1.417;

% L : distance between center of rolling piston and center of curvature of vane [in.]
L=Rp+Rv;

% w : angular speed of rotation of crank [rad/s]
w=377;
```

B.2 Matlab code that simulates vane motion

```
% MOTION OF THE VANE AS A FUNCTION OF THE CRANK ANGLE
%  Matlab program to evaluate and plot the displacement, velocity and
%  acceleration of the vane as a function of the crank angle


% g : a dummy variable

  clear g;
  g=sqrt( L^2-(e*sin(a)).^2);


%  X : vane displacement from top dead center (in.)
%  V : vane velocity (in./s)
%  A : vane acceleration (in./s2)
%  x : crank angle ( Matrix x was defined previously in file 'variables.m' )

  X=e+L-e*cos(a)-g;
  V=e*w*sin(a)+0.5*e^2*w*sin(2*a)./g;
  A=e*w^2*cos(a)+(e*w)^2*cos(2*a)./g+(e^2*w*sin(2*a)).^2./(4*g.^3);


  figure(1);
  plot(a,X);
  axis([0 2*pi 0 0.4]);
  xlabel('Crank angle (rad)');
  ylabel('Vane displacement from top dead position (in.)');
  print -deps fig2-5.eps

  figure(2);
  plot(a,V);
  axis([0 2*pi -80 80]);
  xlabel('Crank angle (rad)');
  ylabel('Vane velocity (in./s)');
  print -deps fig2-6.eps
```

```
figure(3);
plot(a,A);
axis([0 2*pi -3e4 4e4]);
xlabel('Crank angle (rad)');
ylabel('Vane acceleration (in./sq.s)');
print -deps fig2-7.eps
```

B.3 Matlab code that models the compression process

```
% MODEL OF THE COMPRESSION PROCESS
% Matlab program that:
% 1) Calculates and plots the volume of the compression chamber as a function
%    of crank angle
% 2) Models the compression as an ideal gas isentropic process and determines
%    the pressure within the compression chamber as a function of crank angle
% 3) Takes into account various suction and discharge pressure values


% E, B, C, D : dummy variables
  clear E;
  E=(pi-0.5*a)*(Rc^2-Rp^2);
  clear B;
  B=0.25*e^2*sin(2*a);
  clear C;
  C=0.5*e^2*sin(a).*sqrt((Rp/e)^2-(sin(a)).^2);
  clear D;
  D=0.5*Rp^2*asin(e*sin(a)/Rp);

% Vd : volume of compression (discharge) chamber [cubic in.]
  Vd=Hc*(E+B+C+D);

% Vmax : maximum volume of compression chamber, corresponds to start of
% the compression process when rolling piston has just crossed suction
% port [cubic in.]

  Vmax=Vd(11);

% P : pressure within the compression chamber
  P=Ps*(Vd/Vmax).^(-1.187);

% before the suction port is sealed off...
  for i=1:1:11
  P(i)=Ps;
  end;

% after the discharge valve opens...
  for i=11:1:57
  if P(i)-Pd>0,P(i)=Pd;
  end;

  P(57)=Pd;

 hold off;
 plot(a,P);
```

```
 axis([0 2*pi Ps-20 Pd+20]);
 xlabel('Crank angle (rad)');
 ylabel('Pressure in compression chamber (psig)');

end;
```

B4. Matlab code that simulates vane dynamics

```
% DYNAMIC ANALYSIS OF THE VANE
% Matlab program that calculates and plots:
% 1) The forces that act on the vane
% 2) The moments about pivot point A1 and A2 due to these forces

% g, j, i, z, h, o, f, m: dummy variables
  clear g;
  clear j;
  clear i;
  clear z;
  clear h;
  clear o;
  clear f;
  clear m;
  g=sqrt(L^2-(e*sin(a)).^2);
  j=0.5*Tv/Rv;
  i=e*sin(a)/L;
  z=sqrt(Rv^2-(Tv/2)^2);
  h=e*cos(a)+g;
  o=sqrt(1-(e/L*sin(a)).^2);
  f=0.5*Tv/Rv+e/L*sin(a);
  m=e/L*sin(a)-0.5*Tv/Rv;

% FI : angle giving location of point of contact
% OM : angle giving edge of curved vane tip
  clear FI;
  clear OM;
  FI=asin(e/L*sin(a));
  OM=asin(0.5*Tv/Rv);

% Fs : Spring force on top edge of vane (only x component) [lbf]
  Fs=k*(lo-T-Hn+Wv-e-L+e*cos(a)+g);

% Fi : Inertia force on vane (only x component) [lbf]
  Fi=-Mv/J*A;

  figure(1);
  plot(a,Fs,'-',a,Fi,'--');
  axis([0 2*pi -8 8]);
  legend('Spring force','Inertia force',0);
  xlabel('radians');
  ylabel('lbf');
  print -deps fig2-19.eps

% F1 : Pressure force on top edge of vane (only x component) [lbf]
  F1=Pd*Lv*Tv;
```

```
% La : Length of vane side facing guide [in.]
% Lb : Length of vane side facind suction/discharge chambers [in.]
  for q=1:1:57
  if X(q)>z, Lb(q)=X(q)-z;
  elseif X(q)<z, Lb(q)=0;
  end;
  end;

  La=Wv-z-Lb;

% F2 : Pressure force on side facing guide/discharge (only y component) [lbf]
% F3 : Pressure force on side facing guide/suction (only y component) [lbf]
  F2=0.5*Lv*(P+Pd).*La;
  F3=-0.5*Lv*(Ps+Pd)*La;

% F4 : Pressure force on side facing discharge chamber (only y component) [lbf]
% F5 : Pressure force on side facing suction chamber (only y component) [lbf]
  F4=Lv*P.*Lb;
  F5=-Lv*Ps*Lb;

% F6 : Pressure force on curved tip contacting discharge chamber (x/y) [lbf]
% F7 : Pressure force on curved tip contacting suction chamber (x/y) [lbf]
  F6x=-Lv*Rv*P.*(j+i);
  F6y=Lv*Rv*P.*(g/L.^2-sqrt(1-j^2));
  F7x=Ps*Lv*Rv*(i-j);
  F7y=Ps*Lv*Rv*(sqrt(1-j^2)-g/L.^2);

% Fp : Net pressure force on vane ( Sum of F1 through F7) (x/y) [lbf]
  Fpx=F1+F6x+F7x;
  Fpy=F2+F3+F4+F5+F6y+F7y;

% Fc: MAGNITUDE of the contact force (Fcx/Fcy) [lbf]
  Fc=L^2*(Fs+Fi+Fpx)./g;
  figure(2);
  hold on;
  axis([0 2*pi 0 120]);
  plot(a,Fc,s);
  xlabel('rad');
  ylabel('lbf');

  Fcy=-Fc.*i;

% Fy : Net force on vane along y direction [lbf]
  Fy=Fpy+Fcy;
  figure (3);
  hold on;
  axis([0 2*pi -50 300]);
  plot(a,Fy,s);
  xlabel('rad');
  ylabel('lbf');

% Ms_1, Ms_2 : moment of spring force about pivot points A1 and A2
  Ms_1=0.5*Tv*Fs;
  Ms_2=0.5*Tv*Fs;
```

```
% Mi_1, Mi_2 : moment of inertia force about pivot points A1 and A2
  Mi_1=-Mv/J*Tv*0.5*A;
  Mi_2=-Mv/J*Tv*0.5*A;

% Mc_1, Mc_2 : moment of contact force about pivot points A1 and A2
  Mc_1=Fc.*(-0.5*Tv*o+(X-Rv)*e/L.*sin(a));
  Mc_2=Fc.*(-0.5*Tv*o+(Rv-X)*e/L.*sin(a));

% M1_1, M1_2 : moment of pressure force F1 about pivot points A1 and A2
  M1_1=0.5*Pd*Lv*Tv^2;
  M1_2=0.5*Pd*Lv*Tv^2;

% M2_1, M2_2 : moment of pressure force F2 about pivot points A1 and A2
  M2_1=1/6*Lv*(P+2*Pd).*(Wv-e-L+h);
  M2_2=-1/6*Lv*(P+2*Pd).*(Wv-e-L+h);

% M3_1, M3_2 : moment of pressure force F3 about pivot points A1 an A2
  M3_1=-1/6*Lv*(Ps+2*Pd)*(Wv-e-L+h);
  M3_2=1/6*Lv*(Ps+2*Pd)*(Wv-e-L+h);

% M4_1, M4_2 : moment of pressure force F4 about pivot points A1 and A2
  M4_1=-0.5*P*Lv.*(e+L-Rv+z-h);
  M4_2=0.5*P*Lv.*(e+L-Rv+z-h);

% M5_1, M5_2 : moment of pressure force F5 about points A1 and A2
  M5_1=0.5*Ps*Lv*(e+L-Rv+z-h);
  M5_2=-0.5*Ps*Lv*(e+L-Rv+z-h);

% M6_1, M6_2 : moment of pressure force F6 about points A1 and A2
  M6_1=-Lv*Rv*P.*(f.*(0.5*Tv-Rv*sin(0.5*(FI-OM)))+(o-z/Rv).*(X+Rv*(cos(0.5*(FI-OM))-1)));
  M6_2=Lv*Rv*P.*((o-z/Rv).*(X+Rv*(cos(0.5*(FI-OM))-1))-f.*(0.5*Tv+Rv*sin(0.5*(FI-OM))));

% M7_1, M7_2 : moment of pressure force F7 about points A1 and A2
  M7_1=Ps*Lv*Rv*((z/Rv-o).*(X+Rv*(cos(0.5*(FI+OM))-1))-m.*(0.5*Tv+Rv*sin(0.5*(FI+OM))));
  M7_2=-Ps*Lv*Rv*(f.*(0.5*Tv+Rv*sin(0.5*(FI-OM)))+(z/Rv-o).*(X+Rv*(cos(0.5*(FI+OM))-1)));

% M_1, M_2 : resultant moment about pivot points A1 and A2
  M_1=Ms_1+Mi_1+Mc_1+M1_1+M2_1+M3_1+M4_1+M5_1+M6_1+M7_1;
  M_2=Ms_2+Mi_2+Mc_2+M1_2+M2_2+M3_2+M4_2+M5_2+M6_2+M7_2;

% Converting from in-lbf to ft-lbf
  M_1=M_1/12;
  M_2=M_2/12;

  figure(5);
  hold on;
  plot(a,M_1,s);
  plot(a,M_2,ss);
  xlabel('rad');
  ylabel('ft-lbf');
  axis([0 2*pi -8 10]);
```

B5. Matlab code that calculates Hertzian shear stresses

```
% HERTZIAN STRESSES
% Matlab file that calculates the maximum subsurface shear stress in the vane
% or the rolling piston due to contact


% nv : Poisson's Ratio of the vane
% np : Poisson's ratio of the roller
  nv= 0.27;
  np= 0.25;

% Ev : Young's modulus of the vane (psi)
% Ep : Young's modulus of the roller (psi)
  Ev=30e6;
  Ep=14.5e6;

% Dv : diameter of curvature of vane tip (in.)
% Dp : outer diameter of rolling piston (in.)
  Dv=2*Rv;
  Dp=2*Rp;

% pl : load per unit length (lbf/in.)
  pl=Fc/Lv;

% Ee : equivalent Young's Modulus for the system (psi)
  Ee=1/((1-nv^2)/Ev+(1-np^2)/Ep);

% b : half width of the rectangular area of contact (in.)
  b=sqrt((2*pl*Dv*Dp)/(pi*Ee*(Dv+Dp)));

% Sc : maximum compressive stress (psi)
  Sc=2*pl./(pi*b);

% Sy : maximum shear stress (psi)
  Sy=0.3*Sc;
  Sy=Sy/1000;

  figure(6);
  hold on;
  plot(a,Sy,s);
  axis([0 2*pi 0 13]);
  xlabel('rad');
  ylabel('kpsi');
```

Appendix C

TEST #: 1-A
TESTING CONDITION: ARI

DATE: 6/20/97
TIME: 11:55 am

I. AMBIENT CONDITIONS:

Tambient: 72 °F
Pambient: 1021 mbar

1.45 x 10^{-2} Pambient = Pa: 14.8 psi

II. COMPRESSOR DATA:

SUCTION (1) *P1,gage:* 76.5 psig
T1: 1090 mV

P1,gage + Pa = P1: 91.3 psia
T1: 65.0 °F

DISCHARGE (2): *P2,gage:* 296.5 psig
T2: 6114 mV

P2,gage + Pa = P2: 311.3 psia
T2: 206.6 °F

III. ELECTRICAL DATA:

VOLTAGE: Vin: 226.2 V
CURRENT: Iin: 10.69 A
POWER: Pin: 2288.0 W

IV. FLOWMETER DATA:

Pf,gage: 77.5 psig
Tf: 1085 mV
FREQUENCY F: 1861 Hz

Pf,gage + Pa = Pf: 92.3 psia
Tf: 64.8 °F

From REFPROP, for measured values of Pf and Tf, get:
DYNAMIC VISCOSITY μ: 124.4 micro poise

DENSITY ρ: 1.586 lbm/ft^3

Calculate KINEMATIC VISCOSITY ν=6.246 x 10^{-3} μ/ρ: 1.491 CST

Calculate F/ν: 3798.0

From chart, calculate K-Factor: 2.7116 (c

Calculate Mass Flow Rate m = 3600 ρ F / K: 345.6 lbm/hr

Use REFPROP to calculate enthalpy/entropy at suction and discharge conditions:
h1: 112.47 BTU/lbm

s1: 0.227 BTU/lbm R
Isentropic compression s2,*s*=s1
h2,*s*: 126.92 BTU/lbm

Performance parameter is EER = G m (h2,*s* - h1) / Pin
EER: 10.54 BTU/W-hr

Note: G = 4.829 for ARI operating conditions
G = 8.166 for CHEER operating conditions

Parameters in italics are experimentally measured, all other parameters are calculated.